Low-Frequency Uniaxial Stress Reversal Fatigue Behavior of Plain Concrete

By

Raza Nasir

A Thesis

Submitted to the Faculty of Graduate Studies of

The University of Manitoba

In partial fulfillment of the requirements for the degree of

Master of Science

Department of Civil Engineering

University of Manitoba

Winnipeg, Manitoba, Canada

Abstract

This thesis investigates the uniaxial stress reversal fatigue behavior of plain concrete under low-frequency cyclic loading, with a focus on frequencies below 1 Hz. The research aims to enhance the understanding of the fatigue life of concrete structures, particularly in infrastructure subjected to repeated loading such as dams and bridges. The specimens were tested at three specific frequencies: 0.2 Hz, 0.5 Hz, and 0.75 Hz. These tests were performed under a constant stress range of 11.4 MPa, replicating the stress conditions identified through Finite Element Analysis of a spillway from an existing gravity dam in northern Manitoba. The testing regime set the maximum stress level at 90% of the tensile strength of the concrete and the minimum stress level at 20% of the compressive strength of the concrete.

The analysis concentrated on evaluating the fatigue life of concrete, examining maximum strain curves, stiffness degradation, and energy dissipation under stress reversal conditions. The analysis revealed that higher frequencies generally resulted in a longer fatigue life. The maximum strain and stiffness degradation curves exhibited typical S-shaped patterns, indicating progressive damage accumulation in the concrete specimens, and increasing strain at failure. Additionally, stiffness degradation showed negligible differences in deterioration indices between 0.5 Hz and 0.75 Hz, with slightly higher deterioration observed at 0.2 Hz. Energy analysis indicated that higher frequencies result in increased energy dissipation per fatigue cycle.

The application of the Weibull distribution effectively modeled the variability in fatigue life data, providing insights into the probabilistic nature of concrete's fatigue behavior under stress reversal loading. Furthermore, the research included a validation of the stress reversal fatigue model proposed by Ferreira et al. (2024). The model's applicability across different frequencies was

assessed, demonstrating its potential for broader application in predicting the fatigue behavior of concrete under uniaxial stress reversal loading.

Acknowledgments

First and foremost, I would like to extend my deepest gratitude to my advisor, Dr. Dagmar Svecova, for her unwavering support and guidance throughout the course of this research. Her insights and encouragement were invaluable in navigating the challenges of this study.

I am also deeply thankful to Dr. Payam Sotoudeh Foumani, who provided crucial assistance and guidance throughout the work. His expertise and continuous support were essential to the progress and completion of this research.

I would also like to acknowledge the significant technical expertise and tireless efforts contributed by Dr. Chad Klowak, Daniel Szara, and Samuel Abraha. Their hands-on support and valuable recommendations greatly enhanced the efficiency and success of the experimental program.

My sincere thanks also go to Dr. Graziano Fiorillo and Dr. Mohamed T. Bassuoni for their thoughtful feedback and ongoing support as members of my advisory committee.

A special mention goes to Dr. Huma Khalid, who has been a motherly figure to me throughout my course of study, offering invaluable support and care.

Lastly, I would like to express my special thanks to Manitoba Hydro for their valuable feedback and financial support provided to the University of Manitoba research team throughout the project.

Table of Contents

List of Tables

List of Figures

Chapter 1 Introduction

1.1 Overview and Background

The integrity of structures and the materials from which they are constructed has long been a concern in engineering and industrial development. The concept of material fatigue—where structures fail under cyclic loading—has been particularly critical. This phenomenon first gained widespread attention in the 19th century following catastrophic failures such as the Versailles rail accident in 1842. These early incidents, along with later disasters such as the Comet airliner crash in 1954 and the Los Angeles B767 crash in 2006, highlighted the deadly consequences of fatigue-related failures in engineering structures (Bathias & Pineau, 2013). Fatigue, the progressive weakening of a material due to repeated loading, was first observed in the 1800s by European engineers who noticed cracks forming in bridges and railroads under repetitive loads. This discovery encouraged extensive research into fatigue behaviour of engineering materials, which continues to this day. Understanding fatigue has become essential for ensuring the safety and longevity of structures, particularly as infrastructure ages and environmental conditions evolve.

Concrete, a fundamental material in infrastructure such as dams, bridges, and highways, is particularly vulnerable to fatigue. Despite its high strength in compression, plain concrete is brittle in tension and can fail under cyclic loads below its ultimate strength. Moreover, due to the nature of the applied loads modern infrastructure often faces repeated loading that can lead to fatigue failure. In concrete structures, the initiation and propagation of microcracks under cyclic loading can eventually lead to complete structural failure. These microcracks typically form after a certain

number of load cycles and, with continued loading, grow until the material fractures (Lee & Barr, 2004).

In addition to mechanical loads, environmental factors such as seasonal temperature variations and climate change further impact the fatigue life of concrete structures. For example, dams face fluctuating hydrostatic pressures that can increase due to changing weather patterns, potentially exceeding design loads and increasing the probability of failure. As reported by Ozkan et al. (2023), climate change has brought about increased precipitation, more frequent freeze-thaw cycles, and higher average temperature variations, all of which can increase environmental loads on infrastructure. Temperature fluctuations introduce additional challenges, particularly in cold climates where freeze-thaw cycles induce thermal stresses in concrete, potentially leading to cracking. In mass concrete structures such as dams, varying expansion and contraction rates due to temperature gradients generate tensile stresses that can exceed the material's tensile strength and cause stress reversal fatigue—where concrete experiences both tensile and compressive stresses during the fatigue cycle.

A real-world example of thermal cracking due to stress reversal fatigue is the Wanapum Dam on the Columbia River in Washington. Built in 1963, the dam experienced significant distress in 2014 when a section of the spillway deck was observed to have moved. An investigation revealed that thermal stresses had caused the concrete to crack, a factor that had not been fully considered during the initial design (Thompson et al., 2015). This incident emphasizes the importance of considering thermal forces in the stability analysis of concrete dams.

Given the economic and safety concerns of such infrastructure, particularly with respect to the thermal stress experienced by dams due to temperature variations, understanding the fatigue

behaviour of concrete under low-frequency cyclic loading (below 1 Hz) is crucial. This research aims to explore the stress reversal fatigue of plain concrete under such conditions, to improve life estimation and maintenance strategies for concrete structures, ensuring their longevity and reliability in a changing climate. The typical concrete dam in Manitoba experiences one cycle per year due to thermal variation which is approximately 3.17E-8 Hz.

1.2 Scope and Objectives

The primary goal of this research is to investigate the uniaxial stress reversal fatigue behaviour of plain concrete under low-frequency cyclic loading below 1 Hz. To achieve this objective, an experimental program was developed and conducted at the W.R. McQuade Structures Laboratory at the University of Manitoba, focusing on stress reversal tests at three specific frequencies: 0.2 Hz, 0.5 Hz, and 0.75 Hz. These tests were performed under a constant stress range of 11.4 MPa, with the maximum stress level (S_{max}) set at 90% of the ultimate tensile strength, and the minimum stress level (S_{min}) at 20% of the ultimate compressive strength. The main objective of the research is to find the effect of changing frequency below 1 Hz on fatigue life of plain concrete subjected to uniaxial reverse fatigue. The scope of this research includes the following key activities:

1- Study of fatigue behaviour of plain concrete: The research studies how plain concrete responds to uniaxial stress reversal fatigue, particularly under three specific frequencies of 0.2 Hz, 0.5 Hz, 0.75 Hz.

2- Performance metrics: The study aims to evaluate various performance metrics of concrete under stress reversal conditions, including the number of cycles to failure, strain behaviour, stiffness degradation, and energy dissipation. These metrics are crucial for understanding the long-term performance of concrete structures subjected to repetitive loading.

3- Model validation: The research also aims to validate a uniaxial stress reversal fatigue model by Ferreira et al. (2024). The model's applicability across different frequencies will be tested, providing insights into its accuracy and potential for broader application.

1.3 Thesis organization

This thesis is structured into seven chapters, each focusing on a distinct aspect of the research. The chapters are organized as follows:

1- Introduction: This chapter provides an overview of fatigue loading, with a particular emphasis on the importance of studying stress reversal fatigue in concrete structures, especially in the context of dams. It sets the stage for the research by discussing the background and motivation behind the study.

2- Literature review: A comprehensive review of existing literature related to stress reversal fatigue in concrete structures is presented in this chapter. It covers both experimental and analytical studies that are relevant to the current research, identifying gaps and highlighting the significance of the study.

3- Experimental work: This chapter details the experimental procedures used in the research, including the preparation of concrete specimens, the setup of fatigue tests, and the methodologies employed to gather data. It provides a thorough description of the testing process.

4- Results and analysis: In this chapter, the data obtained from the experimental work are analyzed. The chapter discusses the methods used to analyze the data and presents the results, focusing on the behaviour of concrete under stress reversal fatigue loading.

5- Conclusion and recommendations: This chapter summarizes the key findings of the research, and draws conclusions based on the experimental results and analysis. It also

offers recommendations for future research, suggesting areas where further investigation could build on the current study.

6- References: A comprehensive list of all the sources cited throughout the thesis is provided here, ensuring proper acknowledgment of the work of others.

7- Appendices: This section includes supplementary material that supports the main text, such as detailed data sets, additional charts or graphs, and any other relevant information that aids in the understanding of the research.

Chapter 2 Literature Review

This chapter summarizes past research, identifies gaps, and highlights areas where further research is needed to improve the understanding and propose new approaches for analysis and design. For this research program, various factors influencing the fatigue of plain concrete are examined, including the behavior of concrete under stress reversal fatigue loading and the effect of loading frequency, particularly low frequencies below 1Hz. Under fatigue loading, each parameter affects the fatigue life of concrete differently, making it crucial to understand the influence of these parameters to improve the design and safety of concrete structures. Therefore, the performance of concrete under cyclic loading has been extensively investigated over the years and will be discussed in this chapter.

2.1 Fatigue of concrete

Fatigue is generally defined as the gradual degradation of a material due to repeated, or cyclic loading, which eventually leads to failure before reaching the material's maximum strength. This failure can occur rapidly or slowly, depending on the type of material, and typically causes a reduction in strength, stiffness, and fracture energy. Initially, the concept of material fatigue was not well-known until the incident of the Versailles railway in 1842 (Smith, 1998). The accident occurred due to the breakage of the axles under cyclic stresses, which eventually led to the formation of cracks. Following this incident, the study of material fatigue, particularly in metals, has begun. One of the most prominent contributions was made by Wöhler, who developed the relationship between applied stress and number of cycles to failure, known as the S-N curves to evaluate a metal’s response under cyclic loading (Wöhler,1870).

Similar to metals, various construction materials, including concrete, can exhibit fatigue deterioration when subjected to cyclic loading under certain stress levels. The investigation of concrete fatigue began in the late 19th century and became a significant research topic by the 1970s (Joly. D, 1898). In a pioneering work, to predict fatigue life of concrete Aas-Jakobsen and Lenschow (1973) initially used Wohler's S-N curves originally developed for metals. They discovered that fatigue life depends not only on stress range but also on the applied stress level. Concrete is a heterogeneous, anisotropic material with nonlinear stress-strain behaviour. This characteristic of concrete leads to variations in results from one specimen to another, making the analysis process complex due to data scatter. To counter this issue and to obtain meaningful results, some studies recommended testing a larger number of specimens (Van Ornum, 1907), with some suggesting a requirement of at least five tests to draw a sound conclusion (Peskova & Meyer, 1994). Meanwhile, investigating the significance of the number of data sets for fatigue tests, Ortega et al. (2018) recommended 15-20 specimens to minimize distribution error.

In the context of fatigue loading of concrete, 'fatigue life' refers to the number of cycles (N_f) the concrete can withstand before failure. A cycle consists of the concrete undergoing one complete loading and unloading of stress as shown in Figure 2-1. Fatigue life is categorized into high-cycle and low-cycle fatigue depending on the number of cycles to failure. A fatigue life greater than 10^3 cycles is classified as high cycle fatigue, while a fatigue life lower than 10^3 cycles is classified as low cycle fatigue (Hsu, 1981). To further study the different parameters affecting concrete under fatigue loading, concrete is tested under various types of loading, such as pure tension, pure compression, or stress reversal loading conditions, as shown in Figure 2-1.

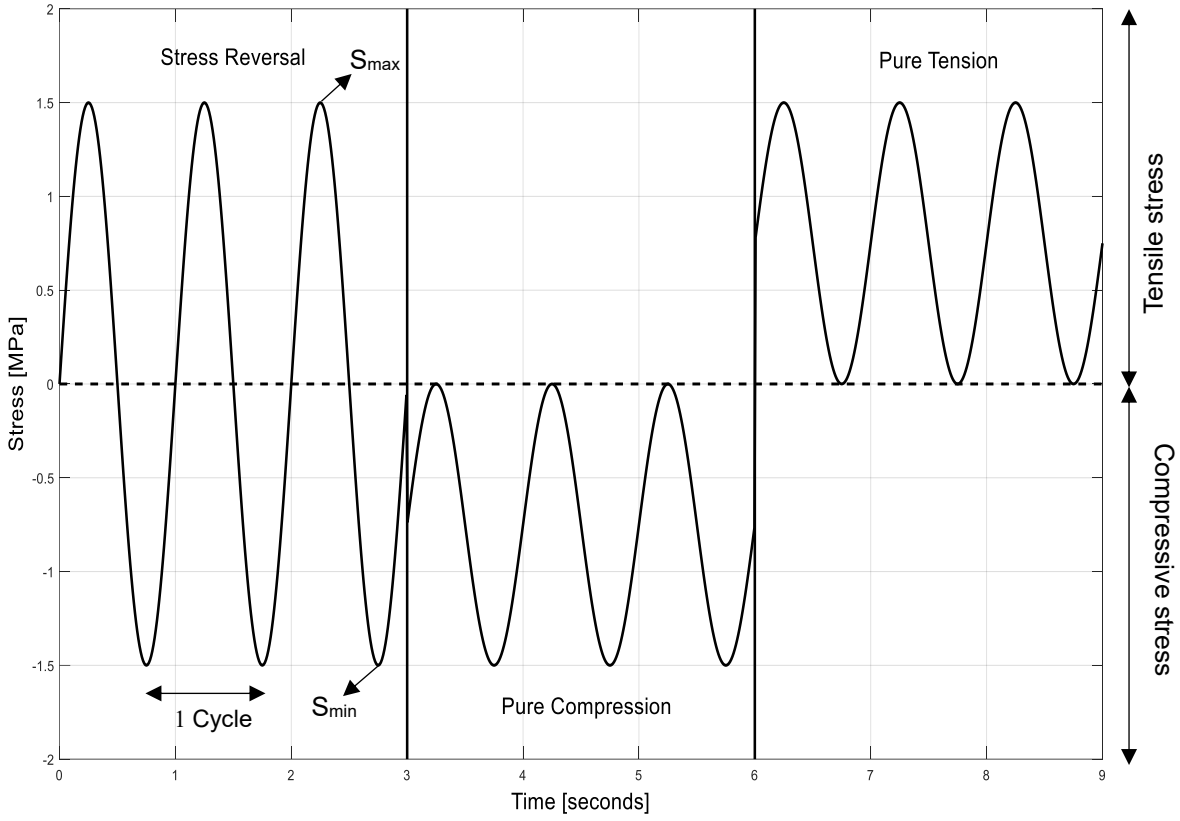

Figure 2-1 Illustration of various types of fatigue loading

2.2 Applied stress

Among the critical factors influencing the fatigue life of concrete, the level of applied stress is one of the most critical ones. Stress level is defined as the ratio of the applied stress to the concrete ultimate strength. During each fatigue cycle, the concrete experiences a maximum stress level (S_{max}), defined as the ratio of highest applied stress to the ultimate strength, and a minimum stress level (S_{min}), which is the ratio of minimum applied stress to the ultimate strength during one cycle. Particularly for uniaxial stress reversal fatigue, S_{max} refers to the maximum stress level in tension, while S_{min} corresponds to the maximum stress level in compression as shown in Figure 2-1.

Fatigue life of concrete is significantly affected by the stress level, particularly by the maximum stress level (S_{max}). There is a linear relationship between S_{max} and the number of cycles to failure (N_f) across all types of fatigue loading. This means that the increase in the maximum stress level, significantly decreases the fatigue life (Murdock & Kesler, 1958; Tepfer & Kutt, 1979; Holmen, 1982; Chen et al., 2017). Clemmer (1922) found that concrete subjected to 51-54% of the ultimate strength in flexural fatigue did not fail under 1 million cycles. Nonetheless, research on concrete beams by Holmen (1982) reported that the threshold for the fatigue strength of concrete ranges between 57-67% of its ultimate strength for 2 million cycles with a zero minimum stress level (S_{max}). Cornelissen (1984) found that the endurance limit depends not only on the maximum stress level but also on the minimum stress level. Moreover, the impact of the stress level is evident in all types of concrete, regardless of their strength and mix composition (Sparks, 1982; Oneschkow, 2016).

Apart from the magnitude of the stress level, the effect of the stress range on the fatigue life of concrete has also been thoroughly studied. The stress range is defined as the difference between the maximum applied load and the minimum applied load in a cycle, with their ratio known as the stress ratio (S_{max}/ S_{min}). The stress ratio is a crucial parameter that differentiates fatigue loading from sustained loading. Although it has a substantially lesser influence on concrete fatigue compared to S_{max}, if S_{max} is kept constant, a decrease in S_{min} leads to a reduction in the fatigue life of the concrete (Hordijk, 1991; Naik, 1993). Therefore, a linear relationship between the stress ratio and fatigue life is observed for both purely tensile and purely compressive loading (Murdock & Kesler, 1958). Meanwhile, the application of both tensile and compressive loading in one cycle introduces stress reversal, which is discussed further below.

2.3 Stress reversal

Among studies on the fatigue of plain concrete, alternating tension and compression load is one of the least explored loading conditions. Tepfers (1982) investigated the degradation of concrete under stress reversal, hypothesizing that concrete cracks propagate in opposite directions under compression and tensile loading. His experiments on 56 concrete cubes of 15 cm and 29 cubes of 20 cm in length showed that the effect of stress reversal is not significant on fatigue life of concrete. Those specimens tested under stress reversal showed a higher degree of scatter in the test results compared to specimens subjected only to pure compression fatigue. However, a definitive conclusion was not provided due to the precision limitations of tensile load application and testing equipment at that time.

Cornelissen (1984) conducted an extensive study to investigate the effects of tensile loading and stress reversal on the fatigue behaviour of plain concrete cylinders with dimensions of 200 mm x 300 mm. The experiments were carried out on two different concrete strengths, under two loading frequencies—6 Hz and 0.06 Hz. The study focused on a range of minimum stress levels (S_{min}) varying from 5% to 40% of compressive strength, and the specimens were tested in both 'drying' and 'wet sealed' conditions. Cornelissen performed a total of 189 tests under pure tension fatigue and 144 tests under stress reversal conditions. His findings demonstrated that stress reversal significantly reduces the fatigue life of concrete compared to pure tension fatigue tests. Furthermore, Cornelissen observed that the environmental conditions—whether drying or wet sealed—affected the fatigue life of concrete under pure tension. However, these environmental conditions appeared to have an insignificant impact on the fatigue life under stress reversal conditions.

Zhang et al. (1996) also studied the effect of stress reversal and frequencies by testing 70 beams under stress reversal at various frequencies ranging between 1Hz, 5Hz and 20Hz. Their experiments were designed at stress ratio ranging between –0.2 to -1, with maximum stress levels varying between 50% - 90% of ultimate tensile strength. They also concluded that the stress reversal causes a decrease in fatigue life. They proposed a model for reverse fatigue loading incorporating negative stress ratios and frequency.

In another experimental series, Lu et al. (2004) explored the effects of stress reversal fatigue on concrete by conducting tests under varying stress levels to develop a predictive theoretical model. The study focused on minimum stress levels of 10% - 20% of compressive strength, with maximum stress levels ranging from 50% to 85% of tensile strength. The experiments were carried out on 32 dog-bone specimens, each with a length of 350 mm and a cross-sectional area of 100x100 mm^2, tested at frequencies between 5 Hz and 15 Hz. The primary objective of the study was to create a theoretical model that could accurately predict the behaviour of concrete under stress reversal fatigue loading. The model was designed to simulate the stress-strain relationship of the concrete during cyclic loading. When comparing the model's predictions with the experimental results, it was found that the theoretical model exhibited good agreement with the observed stress-strain behaviour. However, the model tended to predict a shorter fatigue life than what was determined by experimental linear regression analysis.

In a recent study, Ferreira et al. (2024) conducted an extensive investigation into the effects of uniaxial stress reversal and pure tensile fatigue on concrete under a constant stress range. The study involved testing 53 concrete cylinders, each with dimensions of 101.6 mm in diameter and 202 mm in height. The concrete had a compressive strength of 36 MPa and a tensile strength of 3 MPa. The cylinders were subjected to maximum stress levels of 0.9, 0.85, and 0.8 at a low frequency of

0.1 Hz. The results demonstrated that fatigue life decreases as the maximum stress level increases, confirming the general understanding of fatigue behaviour in concrete. Additionally, it was observed that uniaxial stress reversal leads to a shorter fatigue life compared to pure tensile loading. The study revealed that introducing a small amount of compressive loading (0-10% of the maximum stress level) reduces the fatigue life, while a higher compressive load (10-23.6%) extends it. This increase in fatigue life with introduction of compression was attributed to the crack surface closure mechanism. The compressive loading causes the open cracks to close, leading to an interlocking effect that increases friction and dissipates energy, thereby enhancing fatigue failure resistance. Furthermore, Ferreira performed a macroscopic study of failed surfaces, in which he considered three phases that constitute concrete: cement paste, aggregates that pulled out of the paste, and aggregates that fractured. The study concluded that an increase in percentage of fractured aggregates corresponds to an increase in the fatigue life.

2.4 Frequency and waveform

The effect of loading frequency on the dynamic behavior of concrete has been studied by various researchers (Murdock, 1965; Awad, 1971; Sparks & Menzies, 1973; Raithby and Galloway, 1974; Holmen, 1982; Oneschkow, 2012). Some authors found a notable influence of this parameter on fatigue life (Zhang et al., 1996; Isojeh, 2017) whereas others reported contradictory results (Graf and Brenner, 1931; Murdock, 1965). Although frequency was recognized as an important parameter for concrete fatigue before the 1960s, it was analytically considered in models only in the 1970s (Kachkouch et al., 2022). Graf and Brenner (1934) were the first to investigate the influence of frequency on concrete fatigue life. They concluded that higher frequencies, ranging from 4.5 Hz to 7.5 Hz, do not impact the fatigue life of concrete. Conversely, at lower frequencies (below 0.16 Hz), the fatigue life is reduced.

Some studies found frequency to be an insignificant parameter with only slight effects on fatigue life. Study by Kesler (1953) also reported insignificant effects of frequency on flexural fatigue life. His research involved testing 96 concrete beams, each with a cross-sectional area of 152.4 mm x 152.4 mm and a length of 1524 mm. The experiments were carried out at frequencies ranging from 1.26 Hz to 7.33 Hz, using two different concrete strengths—24.13 MPa (3500 Psi) and 31.03 MPa (4500 Psi). Raithby and Galloway (1974) conducted tests on plain concrete beams at frequencies of 4 Hz and 20 Hz and found no substantial difference in the flexural fatigue life of the beams. Their study involved analyzing the mean fatigue life of 10 specimens at various maximum stress levels at dry and wet conditions, where they also observed that loading frequency had an insignificant effect on the flexural fatigue performance of the concrete.

However, at maximum stress levels (S_{max}) above 75%, a significant increase in the fatigue life of normal concrete was observed with increasing loading frequency (Awad, 1971; Sparks & Menzies, 1973; Holmen, 1982; Zhang et al., 1996; Isojeh, 2017). Similar behaviors were observed by Medeiros et al. (2015) in their study on fibre-reinforced concrete fatigue and by Oneschkow (2012) in her research on high-strength concrete. Oneschkow (2012) investigated the effect of frequency on high-strength concrete under uniaxial compressive fatigue loading, using concrete with a compressive strength of 116 MPa. The experiments were conducted on cylindrical specimens with a diameter of 60 mm and a height of 180 mm. Her findings indicated that increasing the loading frequency from 0.1 to 5 Hz resulted in an increased compressive fatigue life. Additionally, she reported that a triangular waveform led to a higher number of cycles to failure compared to a sinusoidal waveform.

Though frequency has been an important parameter in research discussions, some studies have examined its effects as the loading rate of cyclic loading. The loading rate is defined as the rate at

which stress is applied and removed per cycle, measured in MPa/sec. A wide range of loading rates have been reported, showing that with higher loading rates, the fatigue life of concrete increases (Isojeh, 2017; Sainz-Aja et al, 2019). Similar conclusions were drawn by Sparks (1982), who specifically investigated the effect of compressive loading rates of 0.5 MPa/s and 50 MPa/s on the fatigue life of concrete. This research underlines a critical insight namely that faster fatigue testing, if not carefully accounted for, can lead to an overestimation of concrete's fatigue life. Sparks and Menzies (1973) tested 24 specimens for each of the three different types of concrete, using rectangular prisms measuring 102x102x203 mm^3. The specimens were subjected to loading rates of 0.5 and 50 N/mm^2s under a triangular loading waveform. The study concluded the rate of loading is increased by a hundredfold, and the fatigue life of the material increases by a tenfold factor. Thus, studies have confirmed that at higher stress levels, fatigue life is influenced not only by cyclic loading but also by the duration of loading, primarily due to the significant role of creep (Lloyd et al., 1968; Hordijk, 1993). As a result, the impact of frequency and loading rate becomes more pronounced at higher S_{max}.

Apart from loading frequency, the type of loading waveform also significantly influences the fatigue damage of plain concrete. Tepfers (1973) investigated the effects of three different loading waveforms—rectangular, sinusoidal, and triangular—on concrete fatigue deformation. He reported that, given an equal number of cycles, rectangular loading caused more damage than triangular and sinusoidal waveforms. This is justified because the rectangular waveform subjects concrete to higher stress for a longer period of time compared to the other loading types (Kachkouch et al., 2022). As a result, concrete fails after a smaller number of cycles under rectangular loading, whereas the triangular waveform results in the highest number of cycles to failure among the tested waveforms.

2.5 Concrete strength and composition

The properties and composition of concrete significantly influence its fatigue behavior and its failure mechanisms. Numerous research studies have investigated various parameters of concrete strength and mix proportions (Tepfer and Kutti, 1979; Spark, 1982; Kim and Kim,1996). While many authors believe that fatigue life remains unaffected by the concrete's strength (Murdock, 1965; Do et al, 1993) some studies have reached different conclusions (Kim and Kim,1996; Felix et al. 2022).

In earlier research, Bennet and Muir (1967) investigated the compressive fatigue characteristics of high-strength concrete by examining two different concrete strengths, specifically 41.3 MPa (6000 psi) and 58.6 MPa (8500 psi), along with varying aggregate sizes. They tested 8x3x3 inch prisms under constant S_{min} and varying S_{max}. Their comparative analysis revealed that after a million fatigue cycles at various maximum stress levels (S_{max}), specimens that did not fail were then tested statically to failure. The results showed that the remaining concrete strength varied within the range of 66% to 70% of the concrete's static strength. Additionally, they found that higher-strength concrete with smaller aggregate sizes exhibited slightly lower fatigue life, although the difference was not significant. Kim and Kim (1996) investigated four different concrete strengths ranging from 26 MPa to 103 MPa under fatigue in compression, with maximum stress levels varying from 0.7 to 0.95. Their study involved testing 103 cylinders with dimensions of 100x200 mm at a loading frequency of 1 Hz using a sinusoidal load. They reported that fatigue life decreased as concrete strength increased under the same stress levels. Further studies on high-strength concrete (HSC) were conducted by Do et al. (1993), who examined the strain behaviour of two commercial HSCs with compressive strengths of 70 MPa and 95 MPa under purely compressive fatigue loading. They tested 24 concrete cylinders of each strength, with dimensions of 100x200 mm, at

various maximum stress levels and a frequency of 1 Hz. Their findings showed negligible differences in the longitudinal strain development between the two concrete strengths. Additionally, Lou et al. (2006) investigated crack growth parameters in concrete mortar with varying strengths from 30 MPa to 40 MPa. Their study found that increasing concrete strength did not enhance crack growth resistance. Instead, they observed a higher incidence of stable crack formation in lower-strength concrete.

Another aspect of concrete composition that has gained significant attention in research is the effect of aggregate size and type on concrete fatigue behaviour. Oneschkow and Timmermann (2022) studied the influence of basalt and granite coarse aggregates on the compressive fatigue of high-strength concrete (HSC). With nearly identical compressive strengths, concrete with granite aggregate showed a higher number of cycles to failure at a higher stress level (S_{max}=0.85), while basalt aggregate performed better under a lower stress level (S_{max}=0.75). This behaviour is reversed under different stress levels.

Comparative studies of fatigue life between lightweight concrete (LWC) and normal-weight concrete (NWC) have shown that LWC generally has a lower number of cycles to failure (Spark, 1982; Klaiber & Lee, 1982; Mun et al., 2016). However, Tepfer and Kutti (1979) found no significant difference in fatigue life between NWC and LWC. Similar conclusions were drawn by Seitl et al. (2022), who reported that aggregate size does not affect concrete fatigue life.

Additionally, Saini and Singh (2020) tested 224 beams under flexural fatigue. The beams were made of self-compacting concrete using mixed cement and recycled aggregates. The beams were tested at a frequency of 10 Hz and a stress range of 0.65 to 0.9. The authors observed a reduction in fatigue life in both compression and flexural tests with the addition of recycled aggregates.

In addition to aggregate type, the influence of the water-cement (w/c) ratio and air content in the concrete mix has been extensively investigated. Seitl et al. (2022) reported a 10% increase in fatigue life when the w/c ratio was decreased from 0.5 to 0.3. In contrast, Lee et al. (1978) found no substantial effect of varying the w/c ratio between 0.4 and 0.6. As the effect of air content on fatigue life of concrete, they found that the fatigue life of concrete decreases as the air content increases. Thus, the studies show that decreasing the w/c ratio would result in an increase in concrete endurance limit.

2.6 Analysis of fatigue behaviour

Under cyclic loading, measuring strain development to study fatigue behaviour of concrete specimens has been a focus of various research studies. When the maximum strain is plotted with respect to the number of cycles, an S-shaped curve is typically generated (Paulsen, 2021). Similar curves have been observed in many other studies, proving strain development to be independent of parameters such as frequency and stress level (Saucedo et al., 2013; Poveda, 2017; Isojeh , 2017). The curve is usually divided into three stages, as shown in Figure 2-2.

Stage 1 shows a rapid rise in strain development, typically between 0-20% of the total cycles, due to the formation of microcracks at the aggregate-paste interface. In Stage 2, microcracks continue to form gradually at a nearly constant rate, resulting in a linear path on the strain curve. It ranges from 20-80% of the total number of cycles (Sparks & Menzies, 1973). Stage 3 is characterized by a rapid increase in strain as microcracks convert to macrocracks, leading to quick failure under cyclic loading. It occurs between 80-100% of the total number of cycles (Kachkouch et al., 2022). Research shows that the range of percentage for each stage shows a reduction for high-strength concrete, with Stage 1 and 3 reduced to 5% (Oneschkow, 2012).

In addition to strain development, another widely used method to analyze the degradation of concrete due to fatigue is the stiffness evolution curve under cyclic loading (Holmen, 1979; Banjara and Ramanjaneyulu, 2018). During cyclic loading, concrete undergoes increased deformation, leading to a reduction in stiffness. The remaining strength after this degradation is known as residual strength, and the remaining stiffness is referred to as residual stiffness.

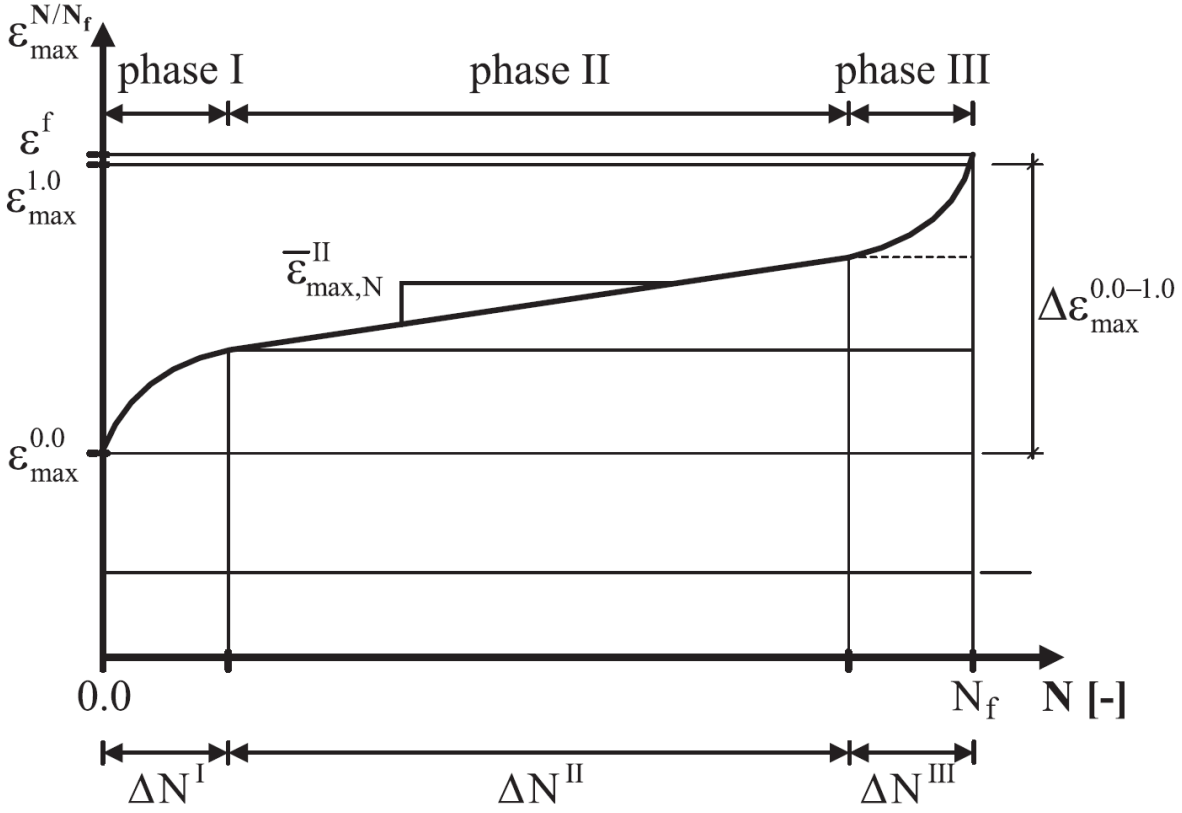

Figure 2-2 Three stages of strain development under cyclic loading (Oneschkow, 2016).

Similar to strain development, the stiffness degradation curve also exhibits a three-stage S-curve, as shown in Figure 2-3. In the first stage, the decrease in stiffness is rapid. During the second stage, where crack formation stabilizes, the curve displays an almost linear degradation of stiffness with a lower slope. In the final stage, there is a significant and rapid decrease in stiffness, indicating the

detrimental effect of the formation of macro cracks on stiffness of concrete that leads to failure of the concrete.

Furthermore, when concrete is subjected to stresses that exceed the proportional limit for the material, plastic deformations occur. With each cycle of loading and unloading, hysteresis loops can be observed. The area within each loop correlates with the energy per volume of each cycle under fatigue loading. This energy can be calculated per cycle, and when plotted with respect to the cycle numbers, is known as the dissipated energy curve. This energy dissipation reflects the inelastic processes leading to irreversible strains (Afaghi et al., 2023). Chen et al. (2017) tested concrete cylinders under uniaxial tensile fatigue and discovered that the stiffness degradation of concrete diminishes as the frequency increases. They noted that energy dissipation in concrete under fatigue loading is initially high and rapid. This dissipation rate slows and stabilizes midway through the test, before increasing again at failure due to accelerated crack development. A similar observation was made by Lei et al. (2017), who conducted tests on concrete prisms under compressive fatigue loading, incrementally increasing the maximum stress level every 1,000 cycles until the failure of the concrete. They proposed a model to calculate fatigue life based on energy dissipation.

In a recent study, Ferreira et al. (2024) conducted a detailed analysis of the stiffness of concrete cylinders under stress reversal fatigue loading, considering compressive and tensile stiffness separately. They found that within a constant stress range, reducing the maximum stress level causes the concrete to lose more tensile stiffness by the end of its fatigue life. By comparing pure tensile fatigue with uniaxial stress reversal fatigue, they also concluded that reversal loading conditions result in a higher loss of tensile stiffness. Moreover, their energy curves indicate that the energy dissipation for specimens tested under stress reversal with constant stress is higher than

for those tested purely in tension. Comparing tests with a constant range of stress reversal, they concluded that reducing the maximum stress level leads to decreased energy dissipation. Additionally, they identified compression loading as the primary source of energy dissipation in stress reversal fatigue, noting that increased compression loading results in greater energy dissipation.

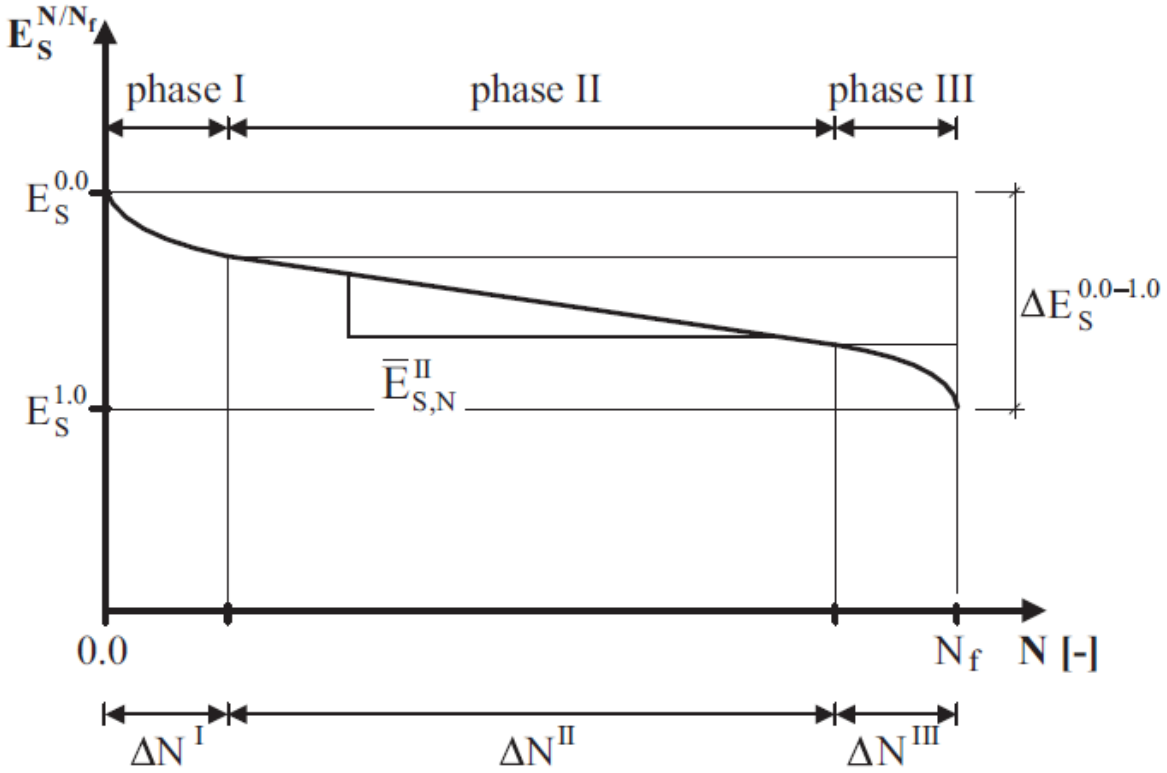

Figure 2-3 General trend of stiffness degradation curve under fatigue loading (Oneschkow, 2016).

2.7 Weibull distribution

Concrete is known for its inherent variability in both fatigue and static strength, even when specimens are drawn from the same batch of concrete and are subjected to identical testing protocols. Due to this inherent variability, designing an experimental campaign that includes a

sufficient number of data sets is crucial for accurately determining the statistical distribution of concrete properties. However, machine availability, cost and time constraints often limit the number of tests to 10-15, which is generally recommended for obtaining more reliable results (Ortega et al., 2018; Ferreira et al., 2023).

Various statistical probability models are employed to analyze the distribution of fatigue data and to predict fatigue life of plain concrete (Cornelissen, 1984; Zhang et al, 1996; Lu et al. 2004; Isojeh et al. 2017; D'Amore et al., 2021). Among these, the two-parameter Weibull distribution function is the most common model (Cornelissen, 1984; D'Amore et al., 2021). It is the most common because of its physically valid assumptions, ease of use, and extensive experimental verification by researchers (Castillo & Fernández-Canteli, 2009). In a recent study, Ortega et al. (2018) conducted statistical analyses on 100 specimens tested under compressive fatigue to determine the optimal number of tests required to minimize error in fatigue life predictions. They suggest appropriate sample size between 15 and 20 to obtain the best fit for fatigue life prediction. Additionally, they proposed an adjustment to the 2-parameter Weibull fit to determine the optimal sample size for fatigue testing, considering an admissible error. Building on this approach, Ferreira et al. (2023) applied the same methodology to analyze data from stress reversal fatigue tests. They extended this concept further to include static strength tests and to establish testing stress levels based on a chosen safety margin. They recommended using the adjusted Weibull distribution fit for both determining static strength and fatigue life when the sample size is below 15. The use of the Weibull distribution in these studies demonstrates its effectiveness in capturing the variability inherent in concrete testing.

2.8 Fracture mechanisms.

The mechanism of fatigue in concrete develops gradually as a result of continuous changes in the material's internal structure. These changes are characterized by formation of microcracks due to the application of loading. These microcracks extend with each additional loading cycle, which eventually leads to the development of macrocracks and ultimately result in failure of the concrete (Kachkoch et al., 2022). As shown in Figure 2-4a**,** these microcracks propagate the fracture process zone (FPZ), merging with other microcracks due to accumulating stress until they form larger macrocracks. Unlike metals and alloys, predicting crack formation under fatigue loading in concrete is challenging due to its heterogeneous nature. As shown in Figure 2-4b, concrete exhibits a nonlinear fracture process zone, also known as the plastic zone, where numerous microcracks form at the crack tip (Mihashi, 1987). Moreover, in tensile loading, the opening of cracks decreases along the length of crack and closes until the end due to cohesive stresses, which affects the deformation behavior. This phenomenon is illustrated in Figure 2-4b, where the cohesive stress helps close the crack openings and reduce displacement until the end of end of the crack, resulting zero displacement at the end of crack (Shah & Ouyang, 1994).

Heilmann et al. (1969) conducted experiments on concrete specimens measuring 600 mm in length with a cross-sectional area of 80 mm x 150 mm. The specimens were tested in direct tension. Strain gauges were placed at different locations along the length of the specimen to investigate the effects of concrete fracture on localized strain under tensile loading. The result under eccentric loading showed two distinct behaviors in the strain measurement. One group of strains showed an increasing trend with the application of the load. These were the strain gauges that were placed at the locations that experienced crack initiation. The other group of strain gauges outside the fracture zone showed decreasing strain trend. This shows that when concrete is tested under uniaxial tensile

loading, the specimen experiences both compressive and tensile strains, depending on the location of the strain gauges relative to the point of damage initiation.

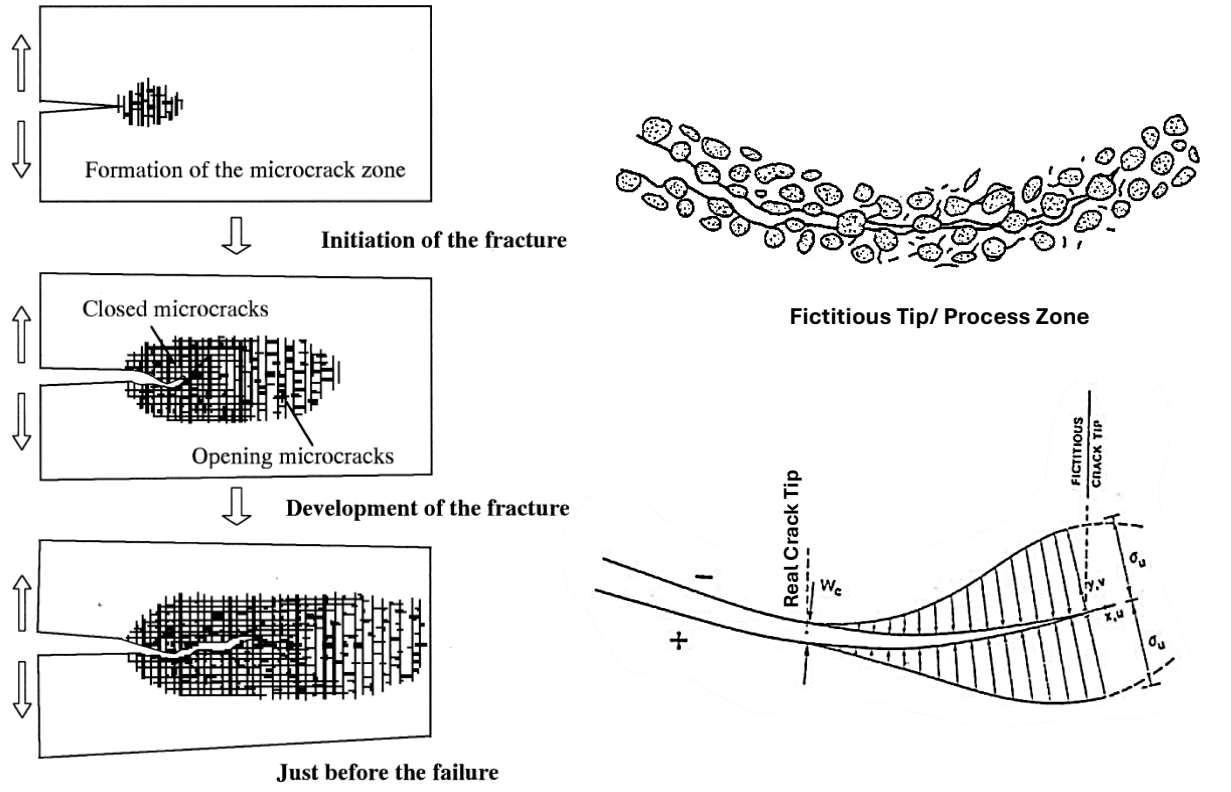

Figure 2-4 (a) Stages of fracture development in concrete under fatigue loading (Mihashi, 1987) (b) The process zone and closing cohesive stress in concrete (Carpinteri, 2021)

2.9 Fatigue life prediction models

Fatigue life prediction models are crucial for the design and monitoring of engineering structures. Various fatigue models have been developed, typically categorized into deterministic and probabilistic models.

2.9.1 Deterministic models

The earliest deterministic model, proposed by Aas-Jakobsen in 1970, was based on the Wohler curve, known as the S-N equation, where 'S' represents the applied stress and 'N' is the number of cycles. This model was designed for specimens under compressive loading, relating fatigue life with material parameters and the stress ratio.

Hsu (1981) extended Jacobsen's model by incorporating the effect of loading rate for different numbers of fatigue loading cycles. Hsu introduced two distinct models for high-cycle (10^3 to 10^7 cycles) and low-cycle (1 to 10^3 cycles) compressive fatigue loading scenarios that are presented in equations 2-1 and 2-2, respectively.

$$S_{max} = 1 - 0.0662(1 - 0.556R)logN_f - 0.294logt \quad 2\text{-}1$$

$$S_{max} = 1.2 - 0.2R - 0.133(1 - 0.779R)logN_f - 0.053(1 - 0.445R)logt \quad 2\text{-}2$$

Where ‘t’ is the time period for one cycle, and ‘R’ is the stress ratio.

Zhang et al. (1996) modified Jacobsen's model for flexural fatigue loading by introducing parameters for stress reversal and the effect of frequency which is represented by equation 2-3 Isojeh et al. (2017) proposed a damage evolution model based on the Aas-Jakobsen model, integrating elements from Hsu (1981) and Zhang et al. (1996). This model considered the effects of frequency, fatigue loading waveform, and stress ratio. Additionally, it predicts the residual strength of concrete, and the fatigue secant modulus based on the damage concept, with critical damage thresholds set at $D_{cr} = 0.4$ for the secant modulus and $D_{cr} = 0.35$ for the residual strength. The damage evaluation model is given in equations 2-4 to 2-6.

$$\frac{S_{max}}{f_c} = \left(ab^{-\log f} + c\right)[1 - (1 - R)\beta \log [N] \quad 2\text{-}3$$

Where 'a', 'b', 'c' and 'β' are material parameters that must be determined experimentally.

$$D = D_{cr} \exp [s(S_{max} - u)]N^{v} \quad 2\text{-}4$$

$$u = C_f((1 - \gamma_2 \log(\zeta N_f t)) \quad 2\text{-}5$$

$$v = 0.434C_f(\beta_2(1 - R)) \quad 2\text{-}6$$

Where 's' and 'u' are the damage parameter; 't' is time period; γ_2=2.47x10^{-2}; 'ζ'is a transformation coefficient, and 'C_f' and 'β_2' are the material parameter.

Deterministic models typically require testing data at various maximum stress levels to determine parameters for complex equations. This leads to relatively limited applicability of such equations for situations where experimental data was not available.

2.9.2 Probabilistic models

Due to the significant variability in experimental fatigue life data for concrete, deterministic approaches often exhibit larger deviations between the predicted fatigue life and the actual experimental test results (Wang, 2023). Consequently, several probabilistic models based on Weibull distribution have been developed (Oh, 1986; Saucedo et al., 2013; Ortega et al., 2013).

Oh (1986) demonstrated that the Weibull distribution appropriately fits his experimental data for flexural fatigue at specific stress levels. He used various approaches (graphical method, method of moments, and maximum likelihood method) to calculate the Weibull distribution parameters. His work found minimal differences among the various approaches. He also proposed a method to derive the distribution parameters from the S-N curve for flexural fatigue of plain concrete.

Saucedo et al. (2013) developed a probabilistic model for predicting compressive fatigue life in plain and fibre-reinforced concrete, utilizing a 3-parameter Weibull distribution. This model accounted for factors such as frequency, maximum stress level, and stress ratio for probability of failure, as given in equation 2-7. The model was validated using a total of 153 fatigue tests conducted on two high-strength plain concrete mixes and two fiber-reinforced concretes (steel and polypropylene fibers), tested at two distinct stress ratios and four different loading frequencies. However, it is important to note that no fatigue tests were carried out on normal strength concrete.

$$PF(N;\sigma_{max},f,R) = 1 - exp\left\{-\left[\frac{\sigma_{max}\left(\frac{\sigma_0}{2f\Delta\sigma}\right)^{\alpha}-\sigma_{min_0}}{\lambda N^{-[b+cln(1+f)](1-R)}}\right]^{k}\right\} \quad 2\text{-}7$$

Where, σ_0 is loading rate of the compressive characterization test, $\Delta\sigma$ is stress range; $\sigma_{min_0}$is minimum stress below which no failure will occur; λ is scale parameter, k is shape parameter; α=0.014, b and c are coefficients related to loading frequency.

Ortega et al. (2018) proposed a model based on a 2-parameter Weibull distribution for self-compacting steel fibre-reinforced concrete under compressive fatigue loading with a stress ratio of 0.44. They also adjusted the design model to calculate the ideal sample size for fatigue testing based on admissible error. The method is thoroughly described in section 4.1.3.

Ferreira et al. (2024) constructed a database consisting of 201 uniaxial stress reversal fatigue life data points, derived from both his experimental results and existing literature. Using this dataset, he proposed a model to calculate the fatigue life of concrete under uniaxial stress reversal fatigue loading. The model proposed two equations to estimate the scale and shape parameters, given as equations 2-8 and 2-9, respectively. This model is valid for maximum tensile stress levels ranging from 60% to 90% and minimum compressive stress levels ranging from 5% to 30%. The model

does not account for frequency or stress range, as it considers only maximum stress level as its only input. Ferreira also suggested adjusting the model using the statistical approaches proposed by Ferreira et al. (2023) and Ortega et al. (2018) to obtain more conservative results when number of available tests results are limited. The adjusted Weibull distribution showed 100% conservatism for sample sizes greater than eight, whereas for smaller sample sizes 79% of the predictions were conservative with respect to available data.

$$Scale = -7.24 \times S_{max} + 9.23 \quad \text{2-8}$$

$$Shape = -17.63 \times S_{max} + 19.10 \quad \text{2-9}$$

While probabilistic models have been shown to provide more comprehensive insights and are better suited to account for the inherent uncertainties in concrete's fatigue behavior, the fatigue prediction model proposed by Ferreira et al. (2024) will be used in this program due to its simplicity.

Chapter 3 Experimental program

This chapter provides a comprehensive discussion of the experimental program designed to study the effect of low frequency stress reversal fatigue loading on plain concrete. All stress reversal fatigue tests conducted in this research maintained a constant stress range of 11.4 MPa. This stress range was determined through Finite Element Analysis performed on a spillway of an existing gravity dam located in northern Manitoba. All experiments were carried out at the McQuade Structures Laboratory, University of Manitoba. The subsequent sections will discuss the preparation and material properties of the research specimens, the various testing setups, and the methodologies utilized throughout these tests.

3.1 Overview

The experimental work was carried out using two different batches of concrete, each possessing distinct static strengths. Although these batches differed in their strength characteristics, the preparation methods and experimental procedures applied to both were identical. In total, 125 concrete specimens were tested throughout the experimental program, as summarized in Table 3-1. The experimental program began with a series of tests aimed at determining the mechanical properties of the concretes, through various static loading tests.

Following the static tests, the concrete specimens were tested under stress reversal fatigue to investigate concrete's performance under stress reversal cyclic loading. The maximum stress level (S_{max}) was set to 90% of the ultimate tensile strength for each concrete batch, while the minimum stress level (S_{min}) was set to 20% of the ultimate compressive strength. The fatigue tests were conducted at three different loading frequencies: 0.2 Hz, 0.5 Hz, and 0.75 Hz.

Table 3-1 Summary of experimental work

	Material properties		Number of specimens
Tested mechanical properties	Compressive strength		41
	Direct tensile strength		9
	Split tensile strength		12
	Modulus of elasticity and Poisson's ratio		5
Fatigue testing	**Frequency**	0.2 Hz	20
		0.5 Hz	19
		0.75 Hz	19

3.2 Specimen preparation

A normal weight concrete with a design strength of 36 MPa was targeted in this research. This strength was specified based on the average concrete strength of various batches used in an existing gravity dam located in Northern Manitoba. To meet these specifications, concrete was supplied by a local batch plant according to the design requirements. However, the mix design details were not disclosed by the plant due to confidentiality reasons. The maximum aggregate size of 20 mm was used in the mix. This decision was made to accommodate the size restrictions of the cylinders and ensuring uniform compaction across all specimens.

For casting of the cylinders, molds with a diameter of 101 mm ± 1 mm and a height of 202 mm ± 2 mm were used. To ensure uniformity in the dimensions, particularly the diameter at both the top

and bottom of the cylinders, two different types of plastic molds with varying wall thicknesses were used, as shown in Figure 3-1.

(a) (b)

Figure 3-1 Plastic cylinder molds (a) Molds with 3 mm thick walls, equipped with lids; (b) Molds with 6.2 mm thick walls, used without lids

The dimensions of these cylinders were chosen based on standard test requirements (ASTM C470–15). Before casting, the molds were thoroughly cleaned to remove any debris or residue, and lightly coated with release agent for ease of demolding. This step facilitates easy demolding after the concrete sets, ensuring that the cylinders could be removed without damage.

Two different batches of concrete were used which were supplied by the same local plant for the casting of cylinders. Only one batch was cast as part of this program, the second batch was cast by Ferreira et al. (2023). The cylinders were distributed across different workstations to complete the casting before the concrete's setting time. Each station was staffed by lab technologist and trained graduate students. Upon the arrival of the concrete truck, air content and slump tests were conducted. Using the pressure method specified by ASTM C231-22 (2022), an air content of 3%

was obtained, and a slump of 125 mm was measured using the ASTM C143-03 (2003) test procedure.

The concrete was placed into the molds in three distinct layers to ensure even distribution and compaction throughout the cylinder. To achieve uniformity across these layers, each layer was compacted using 25 strokes of a tamping rod, followed by 10 to 15 strikes with a mallet. After pouring, the cylinders were immediately capped with lids, while those with thicker walls were covered with plastic sheets as shown in Figure 3-2 to prevent premature dehydration,

Figure 3-2 Placement of specimens after casting

After 24 hours, all concrete cylinders were demolded and labeled with ID numbers. They were subsequently moved to a curing room where they remained for 7 days, as shown in Figure 3-3. After this period, the cylinders were transferred to an enclosed space in the laboratory. This space

maintained a controlled climate with a temperature of 22 ± 2° where they were stored until further testing.

Figure 3-3 Curing of concrete cylinders with labeled ID numbers

3.2.1 Set up for direct tensile and fatigue testing

To accurately evaluate the mechanical properties of concrete under direct tension or stress reversal fatigue conditions, it is essential to develop a reliable setup that ensures the precise transfer of load from the testing machine to the specimen. To ensure the proper distribution of the load and prevent misalignment during testing, it is recommended to flatten the end surfaces of both ends of the concrete cylinders (ASTM C617-23, 2023; ASTM C39-23, 2023). Accordingly, the end surfaces of the concrete cylinders were ground by approximately 3.5 mm on each side using a concrete cylinder end grinder. This machine has the capacity to handle three specimens simultaneously, as

shown in Figure 3-4. Notably, after grinding, the average height of the concrete cylinders was reduced to 195 mm.

(a) (b)

Figure 3-4 Concrete surface preparation. (a) Concrete grinding process in progress using the grinding machine; (b) Surface of concrete cylinders after grinding

A set of steel discs was glued to the ends of the cylinders to connect the specimens to the testing machine. These discs, fabricated from mild steel, had a thickness of 31.75 mm (1.25 inches) and a diameter of 101.6 mm (4 inches). To minimize the eccentricity of the load,19.05 mm (¾ inch) Unified National Fine (UNF) threads were drilled into the center of each disc to a depth of 19.05 mm (¾ inch) as shown in the Figure 3-5. The choice of UNF threads was due to their fine pitch, which provides a higher density of threads, better joint integrity, and reduced vibration under fatigue loading conditions. In addition, the surface of the discs was sand blasted to form a uniform rough surface profile, which significantly improved the adhesion of epoxy when bonding the discs to the concrete cylinders.

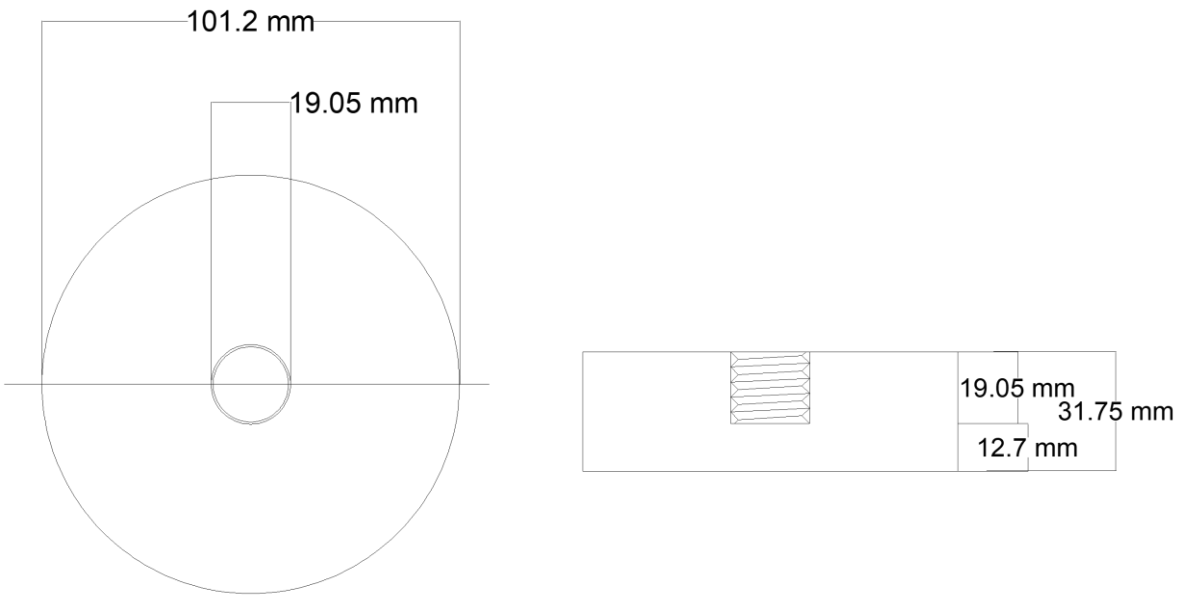

Figure 3-5 Specifications of steel discs. (a) Top view showing the disc's diameter and central thread; (b) Side view illustrating the disc's thickness and the depth of the threaded hole.

A special frame was designed for the epoxy application process, as shown in Figure 3-6. This frame consisted of two C200x28 steel channels positioned above and below the specimens. To stabilize the channels and prevent vertical movement, 8 long steel rods were spaced at a desired distance to maintain a uniform height. This setup not only mimicked the placement of cylinders in the testing machine but also allowed for adjustments in case of misalignment. The frame was designed to accommodate up to five specimens simultaneously; however, for this series of experiments, generally three specimens were prepared at a time. Each slot in the frame had top and bottom adjustable rods, which facilitated the placement and removal of specimens and applied pressure to maintain the alignment of the discs with the concrete cylinders. The entire frame was positioned on a level surface to ensure it remained horizontal.

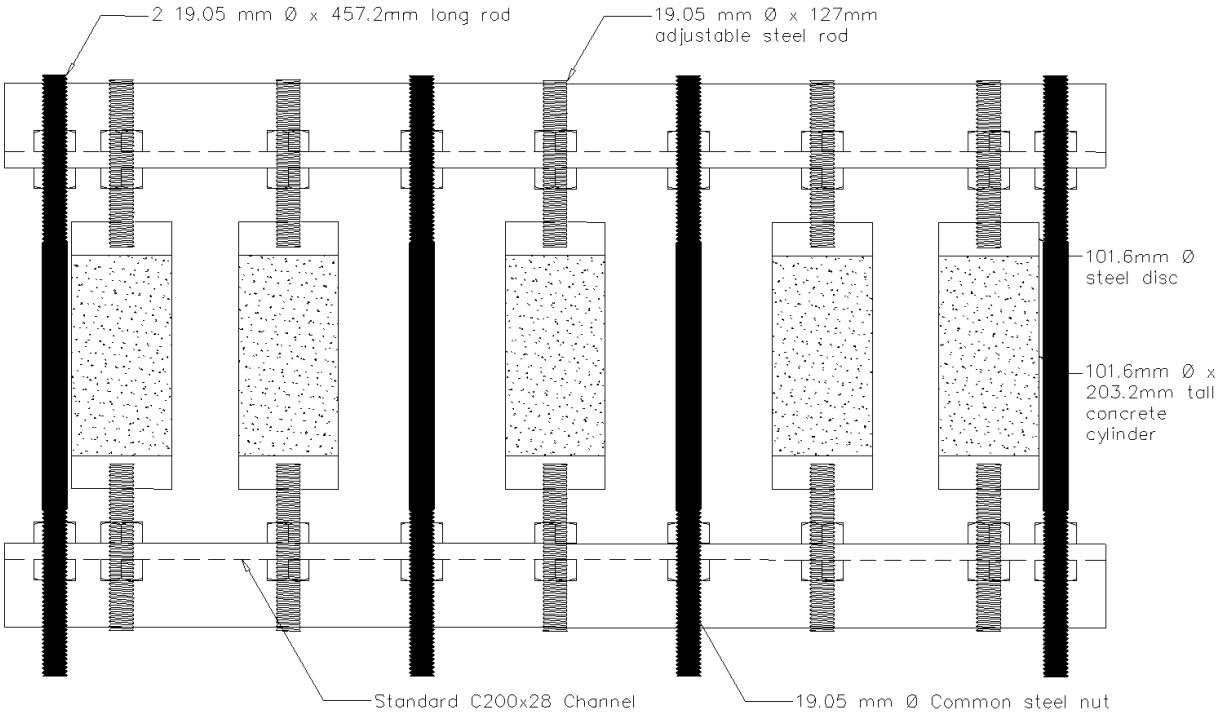

Figure 3-6 Schematic of custom frame for epoxy application on concrete cylinders.

The application of tensile load, especially in the case of stress reversal fatigue or direct tensile testing, is complex due to potential bond failure between the disc and the concrete. During initial evaluations it was observed that the discs could detach from the concrete before failure, leading to delays and wasted specimens. To mitigate these issues, Dural Fast Set Gel, a rapid-setting, non-sag epoxy with a high modulus of elasticity, was used. This gel is compatible with both steel and concrete and provides a bond strength exceeding 17 MPa after two days of curing.

Prior to bonding, the surfaces of both the concrete and the discs were cleaned with a damp cloth and pressurized air was applied to remove any residual sand from the surface pores. Afterwards, the epoxy was thoroughly mixed on a clean, non-sticky plastic surface. Following application instructions provided by the manufacturer, the epoxy was applied in thin layers, each at least 1 mm thick, to both the concrete surface and the disc.

After applying the epoxy layer, the concrete cylinder was carefully positioned in the frame. During this process, vertical pressure was applied to ensure that the epoxy filled all surface pores. The specimens were left in the frame for at least one day before removal and were not tested until at least two days after epoxying to allow adequate time for the epoxy to fully cure. Figure 3-7 shows the final set up used for preparing the specimens.

Figure 3-7 Set up for applying epoxy to the steel discs and specimens.

3.3 Testing methods

A variety of tests were performed throughout the experiment to establish the values of material properties of concrete, which were later used to determine the stress levels for the fatigue testing program. The following section details the various testing methods used.

3.3.1 Compressive strength

Compressive strength is a fundamental mechanical property of concrete. Compressive strength tests were conducted at three different ages of 7, 14 and 28 days to monitor the progression of strength in the concrete. The 28-day strength is considered as the benchmark compressive strength value, with results to be discussed in a subsequent chapter.

It is important to determine the mechanical properties of concrete prior to conducting fatigue testing. A total of 18 cylinders were tested to determine compressive strength of concrete cast in this testing program according to the procedures specified by ASTM C39-23. The second batch of concrete that was cast by Ferreira et al. (2024) as part of his research program tested 24 cylinders. These tests were conducted using a Test Mark Industries compression machine with a capacity of 1334 kN and a manual controller. Before load application, each specimen was precisely centered between the lower and upper bearing blocks of the machine, shown in Figure 3-8. A monotonic load was applied at a rate of 241.3 kPa ± 48.2 kPa (35 psi/s ± 7 psi/s) until failure.

The compressive strength of the concrete was calculated using equation 3-1 as specified by ASTM C39-23 to convert the load obtained from the machine:

$$f_c' = \frac{4P_{max}}{\pi d^2} \qquad 3\text{-}1$$

Where, 'f_c' is the concrete compressive strength, 'P_{max}' is the maximum load obtained from the testing machine, and 'd' is the average value of the top and bottom diameters of cylinder.

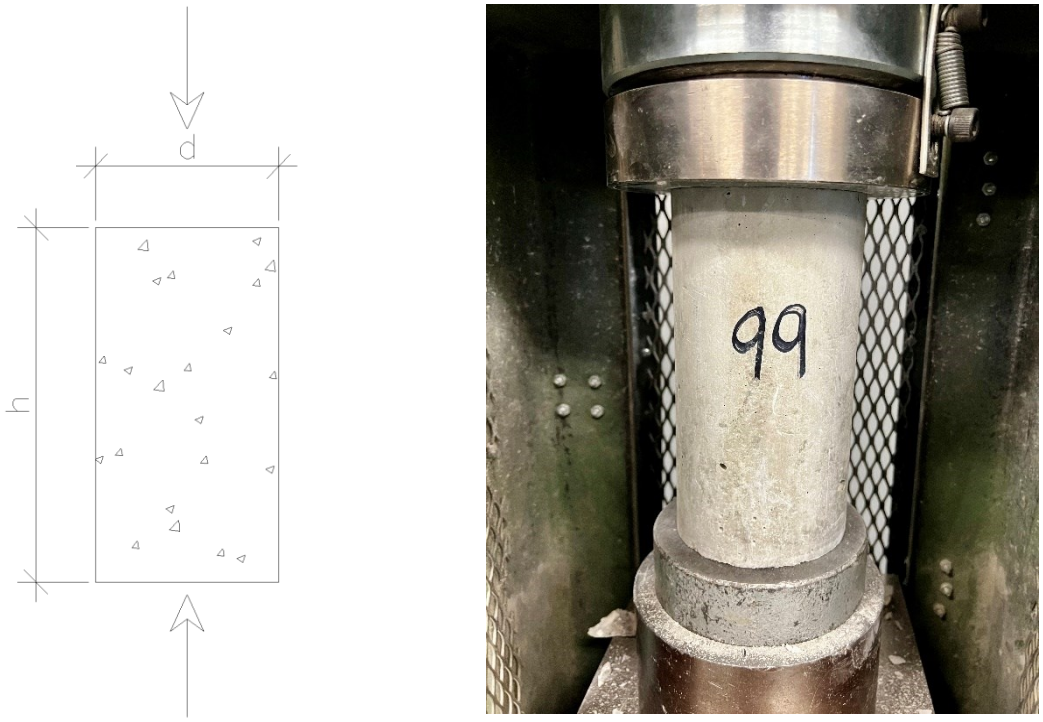

(a) (b)

Figure 3-8 Compressive strength testing setup. (a) Schematic of the loading configuration; (b) Actual compressive testing in progress.

3.3.2 Tensile strength

There are numerous ways to study the tensile behavior of concrete. For this research program, concrete specimens were tested using direct tensile testing. Direct tensile testing is considered a complex but highly accurate method to determine the tensile strength of concrete, as it subjects the material to pure tension. CSA A23.2-6B (2019c) standard was adopted to measure the direct tensile strength of concrete. For this direct tensile testing, steel discs were attached to the cylinders as described previously. Two rods with UNF threads were securely fastened to these discs and then placed in a 1000kN MTS testing machine equipped with a hydraulic actuator. The rods were gripped by the top and bottom pistons of the MTS machine, as shown in Figure 3-9. The direct

tensile tests were conducted by applying a monotonically increasing load at a constant rate of 0.12 kN/s until failure.

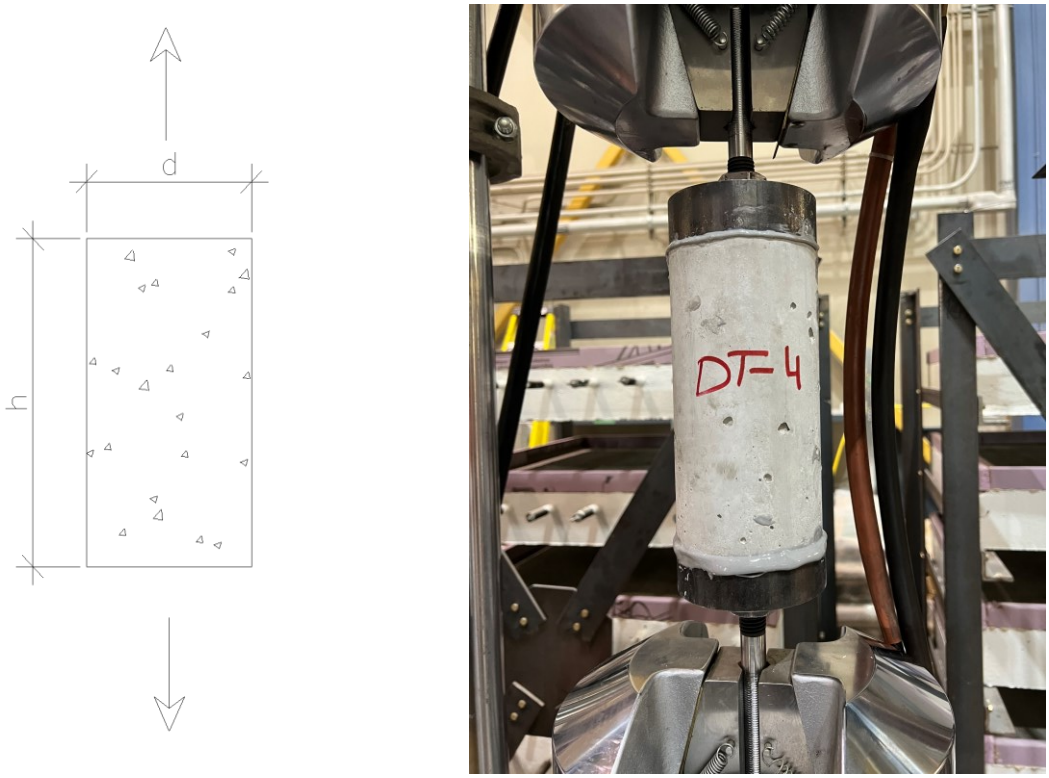

Figure 3-9 Direct tensile testing setup. (a) Schematic of the loading configuration; (b) Actual compressive testing in progress.

The tensile strength was calculated using equation 3-2 below:

$$f_t = \frac{P}{A} \qquad 3\text{-}2$$

Where 'f_t' is the tensile strength of the concrete, 'P' is the load obtained from the MTS, and 'A' is the average cross-sectional area of the specimen. Throughout the experimental program, 9 specimens were tested for direct tensile strength at different ages of the concrete.

3.4 Modulus of elasticity and Poisson's ratio

The tests to evaluate modulus of elasticity and Poisson's ratio were performed using ASTM C469-14 standard. The 28 days average compressive strength was used as the ultimate compressive strength of the concrete. Before placing the cylinder under the testing machine, a compressometer equipped with two Linear Variable Differential Transformers (LVDTs) was fitted around the concrete cylinder to measure displacement in both longitudinal and lateral directions.

An MTS machine was used for applying the load, with both load and deformation recorded by a computer acquisition system. The load was applied at a constant rate of 241.3 ± 34.5 kPa (35±5 psi/s). After placing the cylinders in the machine, the specimens were loaded until 40% of the ultimate load for three successive times. The test setup is shown in the Figure 3-10. The data from the first loading stage was not considered in the analysis, as this was a trial to ensure the instrumentation was functioning correctly. The average of the remaining two loading stages was used to evaluate the modulus of elasticity and Poisson's ratio of the specimens. In total, five specimens were tested to measure these properties.

The modulus of elasticity was calculated using equation 3-3:

$$E = \frac{S_2 - S_1}{\varepsilon_2 - 0.000050} \qquad 3\text{-}3$$

Where, 'S_2' is the stress at 40% of ultimate compressive strength, 'S_1' is the stress at longitudinal strain of 0.000050, and 'ε_2' is the strain at 40% of ultimate compressive strength.

Poisson's ratio was calculated using equation 3-4:

$$\nu = \frac{\varepsilon_{t2} - \varepsilon_{t1}}{\varepsilon_2 - 0.000050} \qquad 3\text{-}4$$

where, 'ε_{t2}' is the mid-height transverse strain at 40% of ultimate strength, 'ε_{t1}' is the mid-height transverse strain at longitudinal strain of 0.000050 and 'ε_2' is the strain at 40% of ultimate strength.

Figure 3-10 Test setup for modulus of elasticity and Poisson's ratio measurement.

3.5 Stress reversal fatigue testing

For fatigue testing, the concrete cylinders were first removed from the steel jigs. The epoxy between the steel disc and the cylinder which had been squeezed out due to the applied load, was cleaned using a wire brush grinder to ensure a flat surface on the cylinder, as shown in Figure 3-11a. The removal of excessive epoxy allows for the placement of a steel ring assembly around the cylinder, as shown in Figure 3-11b. The assembly was designed to hold LVDTs at five different positions along the perimeter of the cylinder. It consists of two rings, one at the top and one at the bottom of the cylinder. The rings have five brackets that are used to clamp vertical rods to connect

the top and bottom rings. The diameter of the ring is approximately 103 mm, and the distance from the top ring to the bottom ring is 175 mm, which was later used as the gauge length to calculate strains.

(a) (b)

Figure 3-11 Preparation for fatigue testing. (a) Removing excess epoxy with a wire brush grinder; (b) Steel ring assembly for LVDT attachment.

Once the ring was positioned and tightened with bolts ensuring that the top and bottom hinges were perfectly aligned, the rods were removed. Subsequently, a threaded rod was tightened onto the steel disc, and the specimen was then positioned in the MTS machine. The bottom grip of the machine was secured first, followed by the placement of the LVDTs on the rings. For calculating the displacement in the concrete cylinder under cyclic load, up to five vertical LVDTs were placed on the cylinder. Two of them had a range of 2 mm, while the other three had a range of 10 mm. The readings from the LVDTs were transferred to a Data Acquisition (DAQ) system connected to the MTS machine.

After these preparations, the top grip was tightened. Each LVDT was specifically located and marked on the specimen. Before commencing the test, the LVDTs were calibrated and zeroed to ensure accuracy of the readings. Once calibration was complete, the stress reversal fatigue tests were initiated according to the specified parameters, including frequency, maximum stress level, and minimum stress level. Figure 3-12a shows a schematic of loading application under reversal fatigue and Figure 3-12b shows the testing setup, highlighting the arrangement of the specimen, grips, and LVDTs within the testing apparatus.

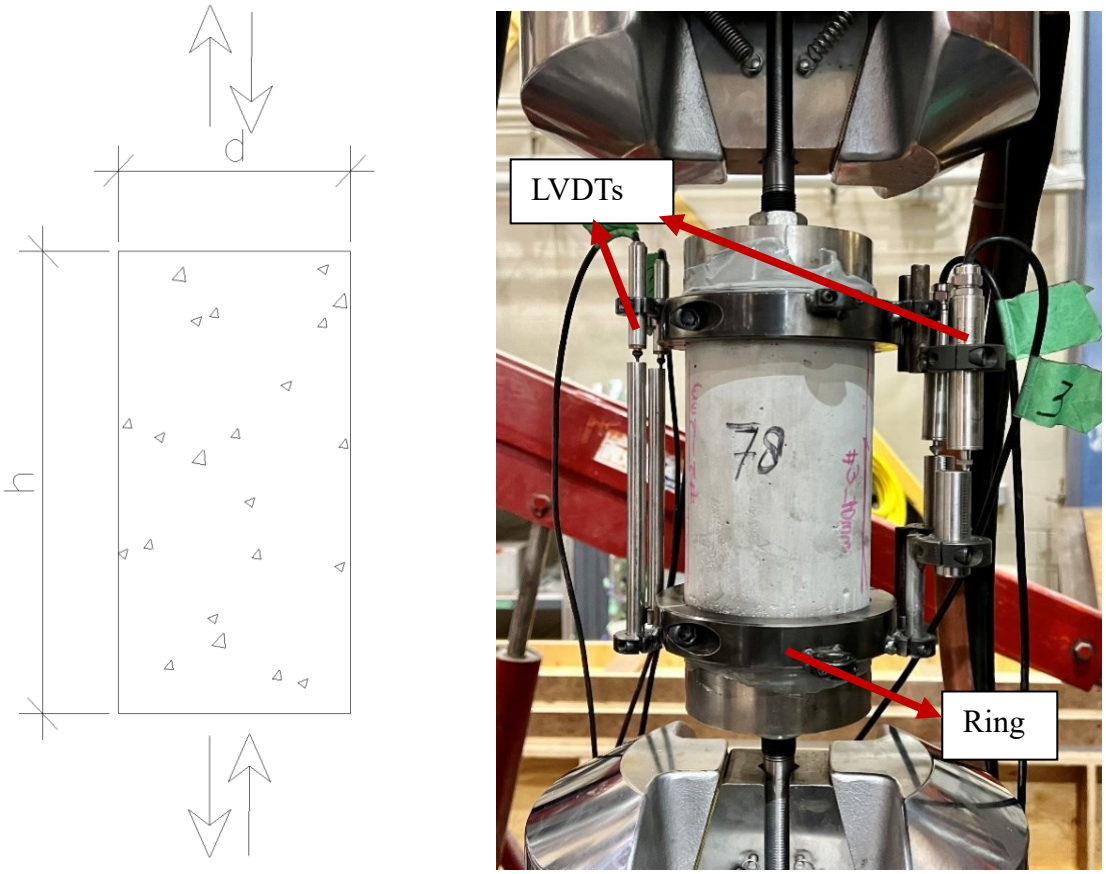

Figure 3-12 Setup for stress reversal fatigue testing. (a) Schematic illustration of the loading application under stress reversal fatigue; (b) Actual testing setup

Chapter 4 Results and Analysis

The following section discusses the results obtained from the experimental program. These results are further analyzed to examine various aspects of plain concrete behavior under uniaxial stress reversal fatigue. This chapter begins with a discussion of the material properties of the concrete, followed by the fatigue testing results and their analysis.

In the fatigue tests analysis, several key aspects are thoroughly examined, including:

- The fatigue life of concrete using the Weibull distribution
- The relationship between the maximum strain per cycle and fatigue life
- Stiffness degradation due to the application of fatigue load
- Energy dissipation under stress reversal fatigue for frequencies of 0.2Hz, 0.5Hz, and 0.75Hz

Additionally, the fatigue life prediction model proposed by Ferreira et al. (2024) is used to assess its applicability for predicting fatigue life of specimens subjected to low frequencies below 1 Hz.

4.1 Material properties

After casting the concrete, several tests were conducted to determine its mechanical properties. These tests included compressive strength, tensile strength, and modulus of elasticity tests. Conducting these tests is crucial for selecting the appropriate testing and loading parameters for the fatigue experiments. The results of the material properties tests are discussed in the following sections.

4.1.1 Compressive strength

Two types of concrete with different mechanical strengths were used in this study and will be referred to as Concrete 1 and Concrete 2. Concrete 1 was cast and tested as part of this research program. Concrete 2 was prepared and tested by Ferreira et al. (2023) as part of his Ph.D. thesis. To assess the development of compressive strength over time, tests were conducted at three different intervals: at 7, 14, and 28 days after casting. The ultimate compressive strengths for both types of concrete are presented in Table 4-1. The average ultimate compressive strength for Concrete-1, based on 12 specimens, was 44 MPa, while for Concrete-2, based on 23 specimens, was 36 MPa. From the coefficient of variation (COV), which was around 5% for Concrete-1 and 11% for Concrete-2, indicating that the values were not widely scattered. For further analysis of concrete under stress reversal fatigue, the average compressive strength is considered as the ultimate compressive strength of both concrete. Meanwhile, detailed results for each specimen tested for both types of concrete can be found in Section A of the Appendix in Table A.1.

Table 4-1. Average compressive strength of concrete-1 and concrete-2.

Material	**Number of Specimen**	**Average compressive strength (MPa)**	**COV (%)**
Concrete-1	12	44	5.17
Concrete-2	23	36	11.18

4.1.2 Tensile strength

The tensile strength of the two concrete mixes are provided in Table 4-2.

Table 4-2 Tensile strength test result for specimens of Concrete 1 and Concrete 2.

Material	Stress (MPa)	Average (MPa)	COV (%)
Concrete-1	2.89	3.13	9.05
	3.2		
	2.99		
	2.75		
	3.13		
	2.93		
	3.70		
	3.30		
	3.28		
Concrete-2	3.49	3.04	11.4
	2.92		
	3.40		
	3.50		
	3.06		
	2.85		
	2.46		
	3.49		
	2.71		
	3.02		
	2.78		
	2.86		

As determining the maximum stress level (S_{max}) in uniaxial stress reversal fatigue testing is directly related to tensile strength of concrete, accurate estimation of such parameter is very important. Given the inherent heterogeneity of concrete and the complexity of the direct tensile test, there was significant variability in the tensile testing data. Specifically, Concrete 1 exhibited differences

of up to 25% between the lowest and highest experimental tensile strength values, while Concrete 2 showed a variance of 30%, as detailed in Table 4-2.

To account for this variability, a precise statistical distribution model based on admissible error and safety level was used. This model, proposed by Ortega et al. (2018) and later used by Ferreira et al. (2023), was used to generate a new design curve at a safety level of 99% to calculate the median tensile strength values. The method and details of the statistical model is explained in detail below.

4.1.3 Statistical analysis of material properties

As discussed in Chapter 2, the fatigue life of concrete is significantly influenced by the maximum stress level (S_{max}), which, in this research corresponds to 90% of the tensile strength of concrete. To select a conservative value of this test parameter, a statistical model is utilized to calculate the median tensile strength of the concrete. This model incorporates admissible error and the number of specimens to generate a probabilistic design curve based on a specified safety level.

The statistical analysis was performed using MATLAB R2022b. This analysis employs a two-parameter Weibull distribution to fit the experimental data obtained from direct tensile tests performed on the concrete specimens. The Weibull fit is achieved using MATLAB's built-in 'wblfit' function. The Weibull distribution is expressed by equation 4-1,

$$F(x) = 1 - exp^{\left(-\left(\frac{x}{n}\right)^{\beta}\right)} \qquad 4\text{-}1$$

Where, 'x' is the tensile strength of concrete, 'n' is the scale parameter, and 'β' is the shape parameter. For the given data, the Weibull distribution parameters obtained for the two types of concrete are presented in Table 4-3.

Table 4-3 Scale and shape parameters of the Weibull distribution obtained from the experimental data.

Material	Scale parameter	Shape parameter
Concrete 1	3.25	11.34
Concrete 2	3.19	10.18

After defining the Weibull distribution parameters, 25,000 samples were randomly generated from the real distribution curve based on the calculated parameters. It is crucial that the newly generated random data points mirror the number of data points in the actual experimental dataset. For instance, if there are nine experimental data points, the new set should also contain nine randomly distributed values. This alignment is achieved by using the cumulative distribution function $P(x \leq x_i = \frac{i}{n})$, where 'n' is the total number of experimental data points. Subsequently, a two-parameter Weibull curve is plotted for each randomly generated dataset using the 'wblinv' function in MATLAB. This results in 25,000 Weibull fits, forming a region that encompasses every randomly generated data point around the real distribution curve as shown in Figure 4-1.

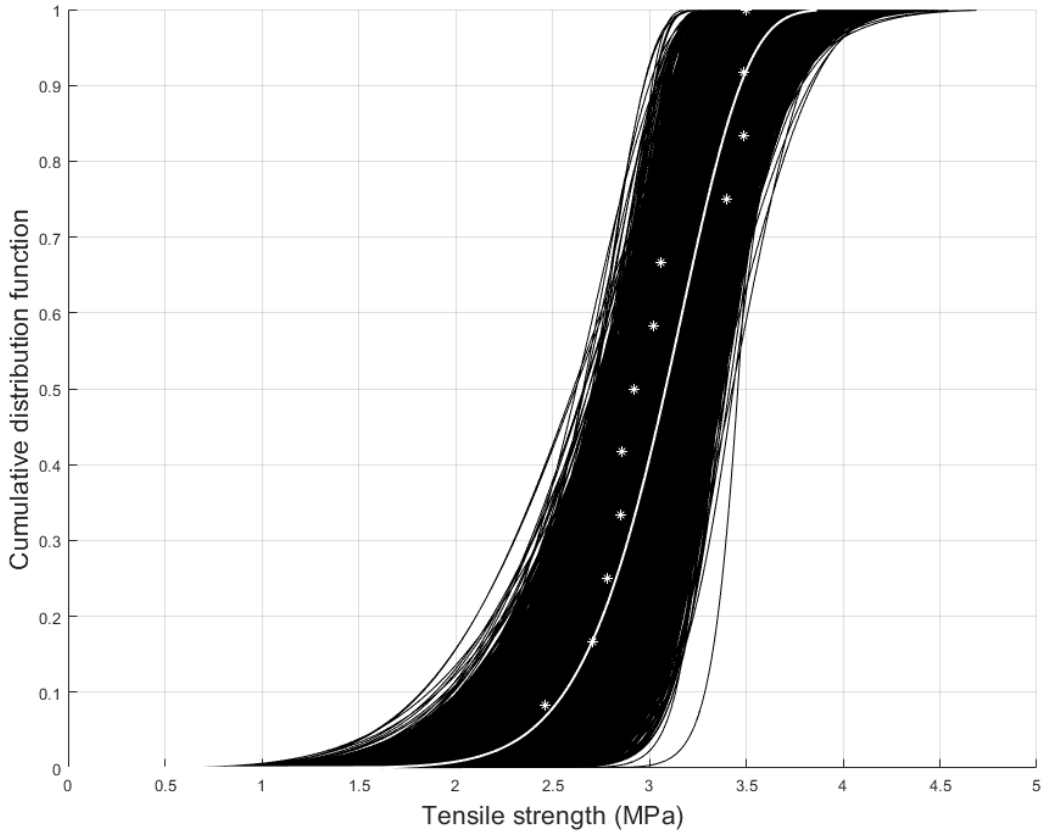

Figure 4-1 Region formed by 25,000 Weibull fits of randomly generated data around the real distribution curve for Concrete 1.

Once the random realizations were generated, an error was observed for each randomly generated fit compared to the real distribution. The observed error is defined as the difference between the real distribution and each randomly generated curve at each interval of 0.001 across 1000 cumulative probability levels. The observed error ensures how the randomly generated fit deviates from the real distribution and it is measured for each randomly generated fit using equation 4-2.

$$e_o(p) = \frac{x(P)_{random\ sample} - x(p)_{real}}{x(p)_{real}} \qquad 4\text{-}2$$

Where: $e_o(p)$ is the observed error at each probability level,$x(P)_{random\ sample}$ is the tensile strength value from the random sample at each probability, and $x(p)_{real}$ is the tensile strength value from the real distribution at each probability.

The observed errors at different cumulative probabilities were considered to follow a normal distribution. The mean and standard deviation of these errors were calculated using the entire set of randomly generated datasets. In the context of the observed error distribution, the safety level (SL) represents the probability that an error at each probability level will not be exceeded, effectively defining the maximum allowable error. The maximum error at each probability level (e_p) is calculated as the inverse of the cumulative normal distribution function of the observed errors.

A design curve is then formed by adjusting the real distribution curve to account for these maximum errors at a safety level of 99%. Specifically, the design curve is created by deducting the corresponding maximum error (e_p) from the real distribution curve at each probability interval. The adjusted design curve can be obtained by multiplying the real value at each probability with a correction factor, as expressed in equation 4-3

$$[N]_{design\ curve} = [N]_{real\ curve} \times [\frac{1}{1+e_p}] \quad 4\text{-}3$$

Where $[N]_{design\ curve}$represents the tensile strength of the concrete obtained from the design curve, and $[N]_{real\ curve}$ represents the tensile strength of the concrete obtained from the real distribution curve. This equation ensures that the design curve reflects a conservative estimate of tensile strength.

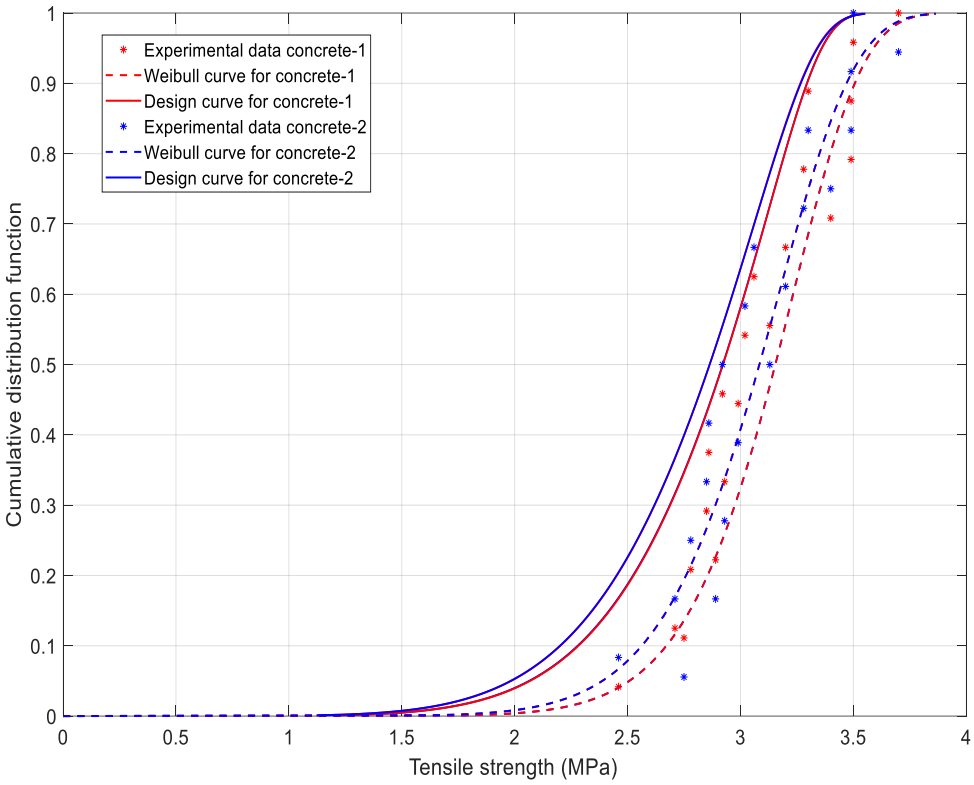

Figure 4-2. Cumulative distribution function for direct tensile strength of concrete specimens.

The plots obtained from the application of the statistical model to the tensile tests data of both concretes are shown in Figure 4-2. The solid lines represent the design curves derived from the statistical model at a 99% safety level. The red and blue markers indicate experimental data points for Concrete 1 and Concrete 2, respectively. The dotted line for Weibull fit depicts some data points to the left of the curve, indicating specimens that failed earlier than predicted by the distribution. Consequently, design curves with solid lines were derived from the statistical model to provide a conservative representation of the experimental data. Accounting for the variability of strength data in plain concrete, design curves ensure a higher level of safety by producing a more conservative result. Using the design curve, the median tensile strengths of Concrete 1 and Concrete 2 were calculated as 2.9 MPa and 2.8 MPa, respectively. These values are considered as

the ultimate tensile strengths of the concrete mixes used in the analysis. The use of this statistical approach on tensile strength data ensures that the fatigue loading for maximum stress levels are set conservatively.

4.2 Modulus of Elasticity and Poisson's Ratio

The modulus of elasticity (E) and Poisson's ratio (ν) are important mechanical properties that characterize the static stiffness and deformation behavior of materials. These properties are significant for understanding how plain concrete responds to cyclic loading, particularly with respect to strain degradation over its fatigue life. In this study, these tests were performed on five specimens of Concrete 1, and the results are presented in Table 4-4.

Table 4-4 Modulus of elasticity and Poisson's ratio for Concrete 1

Specimen	E (GPa)	ν
1	32.59	0.29
2	31.46	0.28
3	34.28	0.28
4	36.81	0.27
5	34.2	0.26
Average	**33.87**	**0.27**
Standard deviation	**2.02**	**0.01**
COV (%)	**5.97**	**4.13**

The average modulus of elasticity (E) for the tested concrete specimens was found to be 33.87 GPa, with a standard deviation of 2.02 GPa and a variation of 5.97%. This level of variation is

expected, given the heterogeneous nature of concrete, and indicates relatively consistent stiffness among the specimens. Similarly, the average Poisson's ratio was recorded as 0.276, with a standard deviation of 0.011 and a coefficient of variation of 4.13%. These values fall within the typical range for plain concrete, which generally ranges between 0.2 and 0.3. Overall, the results indicate that the concrete specimens possess consistent properties, with relatively low variation in both modulus of elasticity and Poisson's ratio.

4.3 Uniaxial stress reversal fatigue test

The stress reversal fatigue tests were conducted at three distinct frequencies: 0.75 Hz, 0.5 Hz, and 0.2 Hz. In total 58 specimens were tested: 19 specimens each were tested at 0.75 Hz, and at 0.5 Hz, and 20 specimens were tested at 0.2 Hz. All specimens were tested under uniaxial stress reversal fatigue with a maximum stress level (S_{max}) of 0.9 in tension and a minimum stress level (S_{min}) of 0.2 in compression, maintaining a constant stress range of 11.4 MPa. All tests were performed using a sinusoidal loading waveform recording 200 data points/sec as shown in Figure 4-3. The waveform depicts the cyclic nature of the applied load, alternating between tensile and compressive forces. The tensile region is marked above the dashed line, while the compressive region is below the dashed line. The results of the fatigue testing for each frequency with number of cycles to failure of the cylinder are detailed in Tables 4-5.

Table 4-5 Fatigue test results—number of cycles to failure for each loading frequency

Specimen	Frequency		
	0.2 Hz	**0.5 Hz**	**0.75 Hz**
	C1-02	**C1-05**	**C1-075**
1	1009	19693	1478
2	1002	1470	1315
3	769	520	1254
4	369	495	643
5	81	127	367
6	69	79	307
7	63	79	286
8	33	66	55
9	29	66	31
10	19	16	19
11	15	15	16
12	11	7	3
13	8		
	C2-02	**C2-05**	**C2-075**
1	2604	564	659
2	160	513	455
3	150	272	234
4	147	169	219
5	98	64	60
6	33	4	15
7	5	4	8
Average	**334**	**1275**	**391**
5^{th} Percentile	**5.15**	**4**	**3**

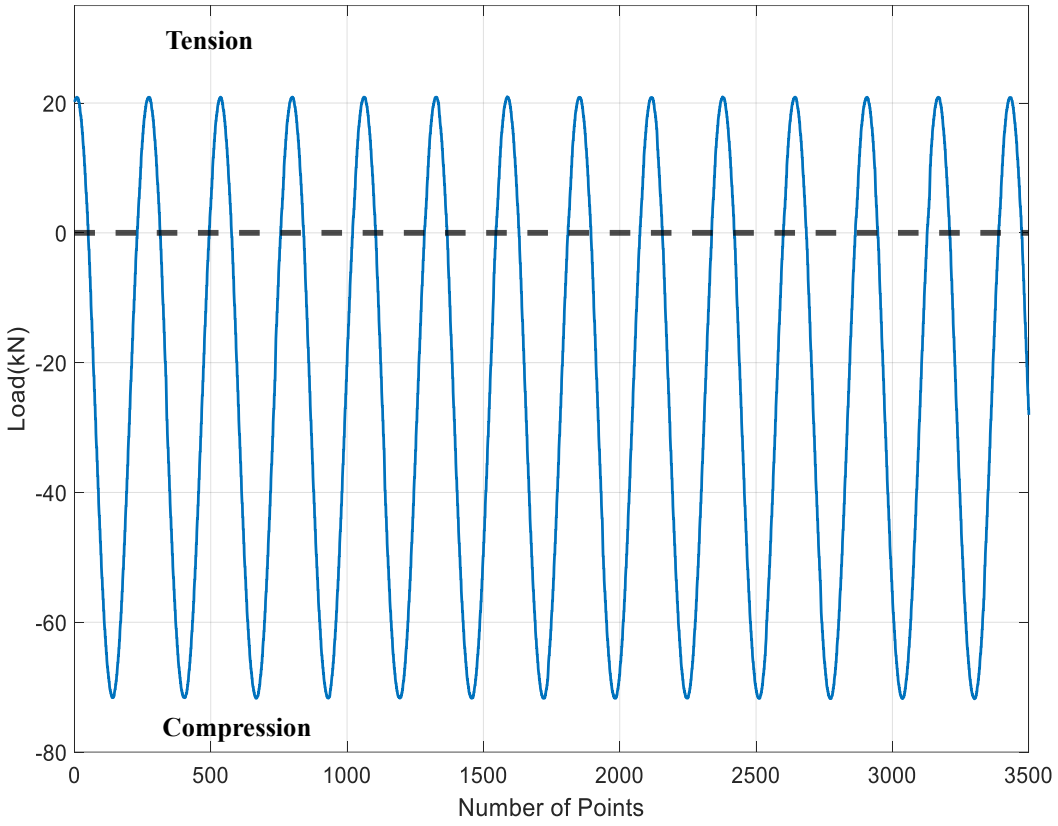

Figure 4-3 Sinusoidal loading waveform applied during stress reversal fatigue testing.

For clarity and consistency, each specimen was labeled according to a specific coding system. Specimens were marked with "C1" or "C2" indicating a concrete compressive strength of 36 MPa or 44 MPa, respectively. The frequencies of testing were indicated with labels "02," "05," and "075," representing 0.2 Hz, 0.5 Hz, and 0.75 Hz, respectively, followed by the specimen number. For instance, the test code "C1-02-01" corresponds to the first specimen of the fatigue test conducted on concrete with a compressive strength of 36 MPa at a frequency of 0.2 Hz.

The average fatigue life of the concrete specimens at different frequencies shows clear variation. At 0.2 Hz, the concrete exhibited an average fatigue life of 334 cycles, while at the higher frequency of 0.75 Hz, the average increased slightly to 391 cycles. In contrast, the 0.5 Hz

frequency shows a dramatic increase, largely influenced by one of the specimens failed at an extremely high number of cycles, 19693. Furthermore, looking at the 5th percentile values which provide a conservative estimate of the lowest fatigue life observed. For 0.2 Hz, the 5th percentile was 5.15 cycles, while for 0.5 Hz and 0.75 Hz, the values were 4 cycles and 3 cycles, respectively. Given the variability in the data, it would not be appropriate to draw conclusions about the relationship between fatigue life and frequency based solely on the average or 5th percentile values. Therefore, analyses were conducted in this research to study the relationship between fatigue life and frequency in more detail.

Notably, the difference in compressive strength between the two concrete types was approximately 8 MPa. A similar difference in concrete strength was also considered by Cornelissen (1984), who demonstrated that the stress reversal fatigue behavior of plain concrete is independent of its compressive strength for normal weight concrete having a slight difference. Therefore, the fatigue data from these two concrete batches will be considered as a single group.

Before combining the results from both types of concrete however, it is important to emphasize that all data analyses were initially conducted separately for each concrete type. These independent analyses revealed that the differences in fatigue performance between the two concrete types were statistically insignificant. Consequently, to provide a more comprehensive understanding, the results from both concrete types were combined for the subsequent analysis presented in this thesis. To investigate the effect of low frequency on fatigue life under uniaxial stress reversal, a box plot is presented in Figure 4-4, corresponding to the experimental data shown in Table 4-4. In this plot, the y-axis represents the frequencies considered in this study: 0.2 Hz, 0.5 Hz, and 0.75 Hz, while the x-axis depicts the logarithm of the number of cycles to failure.

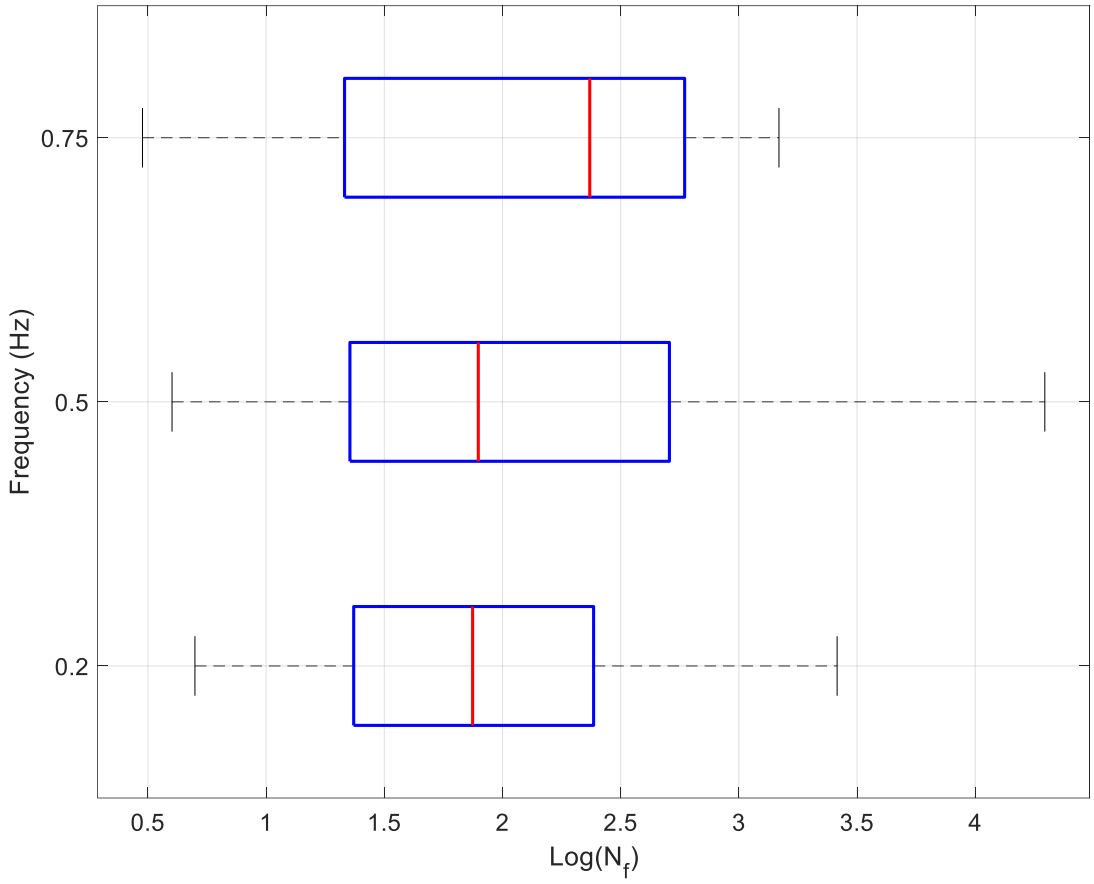

Figure 4-4 Box plot showing the relationship between loading frequency and the fatigue life.

From the plot, it is evident that as the frequency increases, either the mean fatigue life or data variability increase. This is indicated by the red line (mean) within each box, which shifts to the right as the frequency rises to 0.75 Hz, suggesting that concrete specimens tend to withstand a greater number of cycles before failure at this frequency. Additionally, the width of the boxes, representing the interquartile range (IQR) of the data, becomes wider at higher frequencies, reflecting greater variability in the fatigue life. This implies that the behavior of concrete under fatigue loading becomes more erratic as the frequency increases. The whiskers, which extend to the furthest data points not considering any outlier data point, do not show a trend of increasing spread with frequency. The longer whiskers at higher frequencies (particularly at 0.5 Hz) indicate

that while most data points fall within the IQR, there are some extreme values—higher cycle counts for 0.5 Hz—that still fall within this acceptable range.

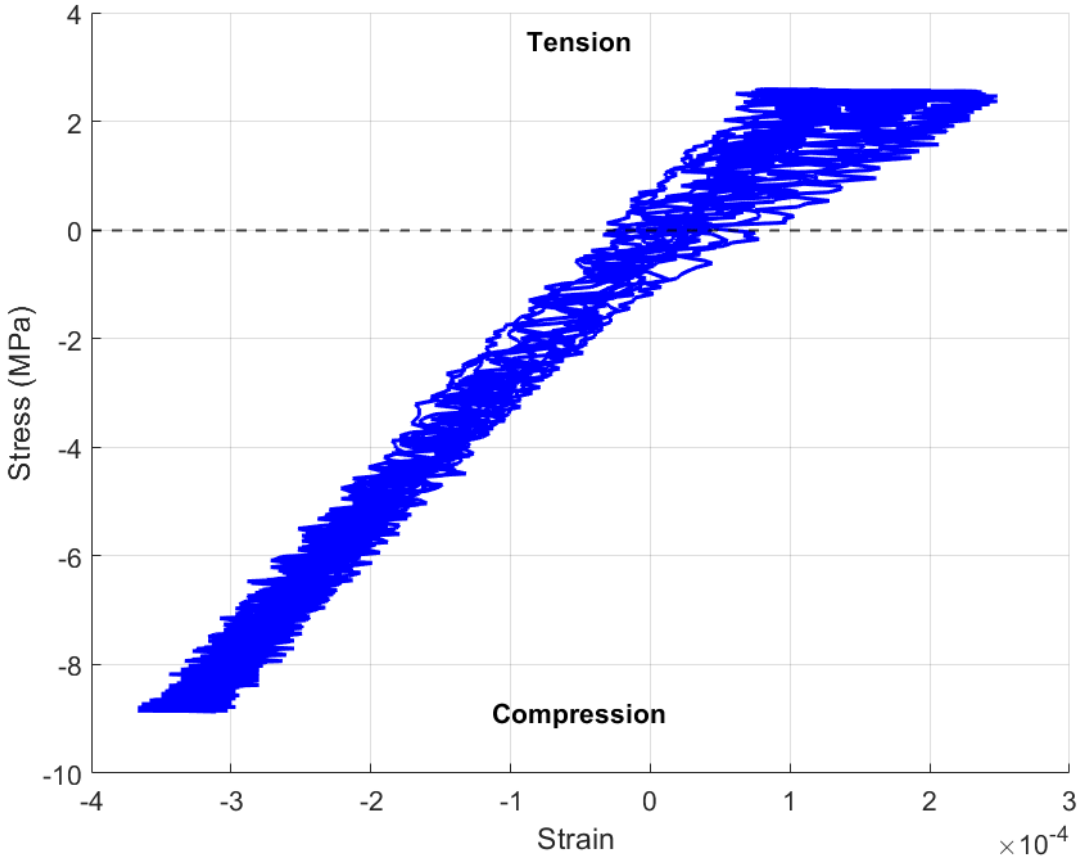

Figure 4-5 Hysteresis loop of stress-strain relationship for specimen ‘C1-02-07’.

Moreover, five Linear Variable Differential Transformers (LVDTs) were utilized to measure the displacement of the specimens during fatigue loading. These LVDTs provided precise and continuous displacement measurements. Figure 4-5 depicts the stress-strain relationship obtained from the data acquisition system (DAQ) for specimen ‘C1-02-07’, with stress (MPa) on the vertical axis and strain on the horizontal axis. The specimen failed after 63 cycles, and the development of the maximum tensile strain throughout the fatigue testing can be observed in Figure 4-5. Even though not clear from the figure, the plot contains 63 stress-strain hysteresis loops. The stress-

strain hysteresis loops provide information about the specimen behaviour when subjected to cyclic load. For example, decreasing stiffness can be observed in tensile region when specimen is reaching its failure. The data presented in Figure 4-5 is the basis of the analysis that was completed as part of this thesis.

To further investigate the behavior of concrete under uniaxial stress reversal cyclic loading, Figure 4-6 presents the stress-strain hysteresis loops for the first and final cycles of the same specimen. The plot in Figure 4-6 demonstrates two distinct patterns of strain degradation in the compressive and tensile loading regions. In the tensile loading region, there is a noticeable increase in deformation by the end of the test. This increased strain in the tensile region indicates that significant degradation occurs during tensile loading. In contrast, the compressive loading region shows almost negligible change in strain, suggesting that the concrete specimen experiences less damage under compressive loads. The noticeable strain degradation in the tensile region supports the conclusion that the failure of the concrete specimen is primarily due to tensile loading during the uniaxial tensile-compression fatigue cycles. This observation aligns with the applied loading conditions used in the fatigue tests, where the maximum stress level was set at 90% of the median tensile strength. In comparison, the compression stress levels were considerably lower being set to 20% of the average compressive strength.

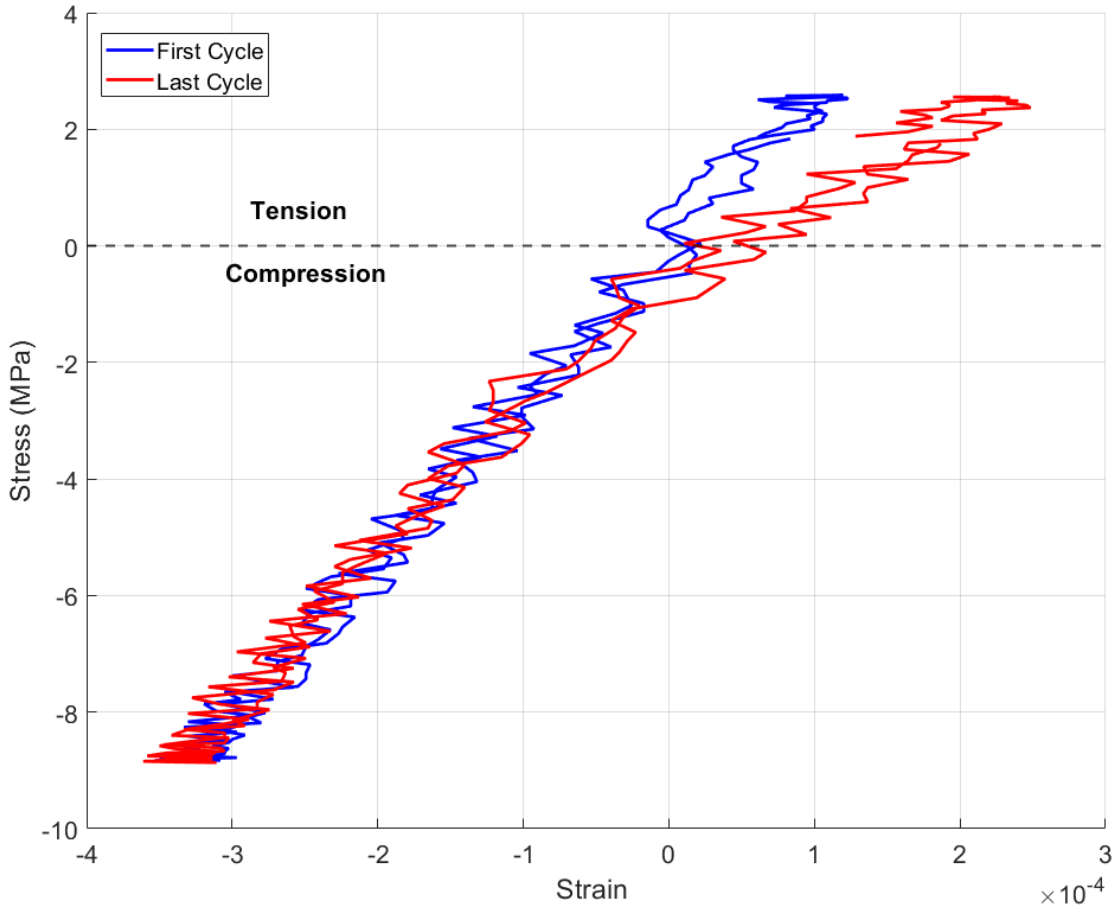

Figure 4-6 Stress-strain hysteresis loops for the first and last cycles for the specimen ‘C1-02-07’.

4.3.1 Weibull distribution of experimental data

Using the Weibull distribution is a widely accepted analytical approach for modeling the fatigue life of materials that experience brittle failure, including plain concrete. In this study, the Weibull distribution was applied to the experimental fatigue data for plain concrete tested under varying loading frequencies. Weibull distribution fits for each frequency with respect to the number of cycles to failure can be found in Figure 4-7. The red dots represent the experimental data points while vertical axis in the graph represents the Cumulative Distribution Function (CDF), which shows the probability that a given specimen will fail by a certain number of cycles. The horizontal

axis displays the logarithm of the number of cycles to failure (N_f). In all cases, the data points closely follow the Weibull distribution curve, indicating a good fit.

Figure 4-8 presents the direct comparison of the Weibull distributions for all three frequencies considered in this study: 0.2 Hz, 0.5 Hz, and 0.75 Hz. The figure shows fatigue life of concrete varies with the loading frequency. The three distributions have a similar shape and spread, indicating that there is no significant difference in the fatigue life of concrete tested under the three frequencies. The following observations were made while examining the distributions in Figure 4-8. The 0.2 Hz curve is positioned towards the left side of the graph, indicating a lower fatigue life, meaning that concrete specimens subjected to this frequency tend to fail after fewer cycles compared to those tested at the two other higher frequencies studied in this thesis. Subsequently, the 0.75 Hz curve is positioned towards the right, indicating a higher fatigue life, with specimens enduring more cycles before failure. Whereas the behavior under 0.5 Hz loading frequency is more complex: up to approximately the 30th percentile, the fatigue life is the shortest among the three frequencies, indicating early failures. However, beyond this point, the fatigue life significantly improves, and by the 75th percentile, the concrete exhibits a higher fatigue life compared to the 0.2 Hz and 0.75 Hz frequencies.

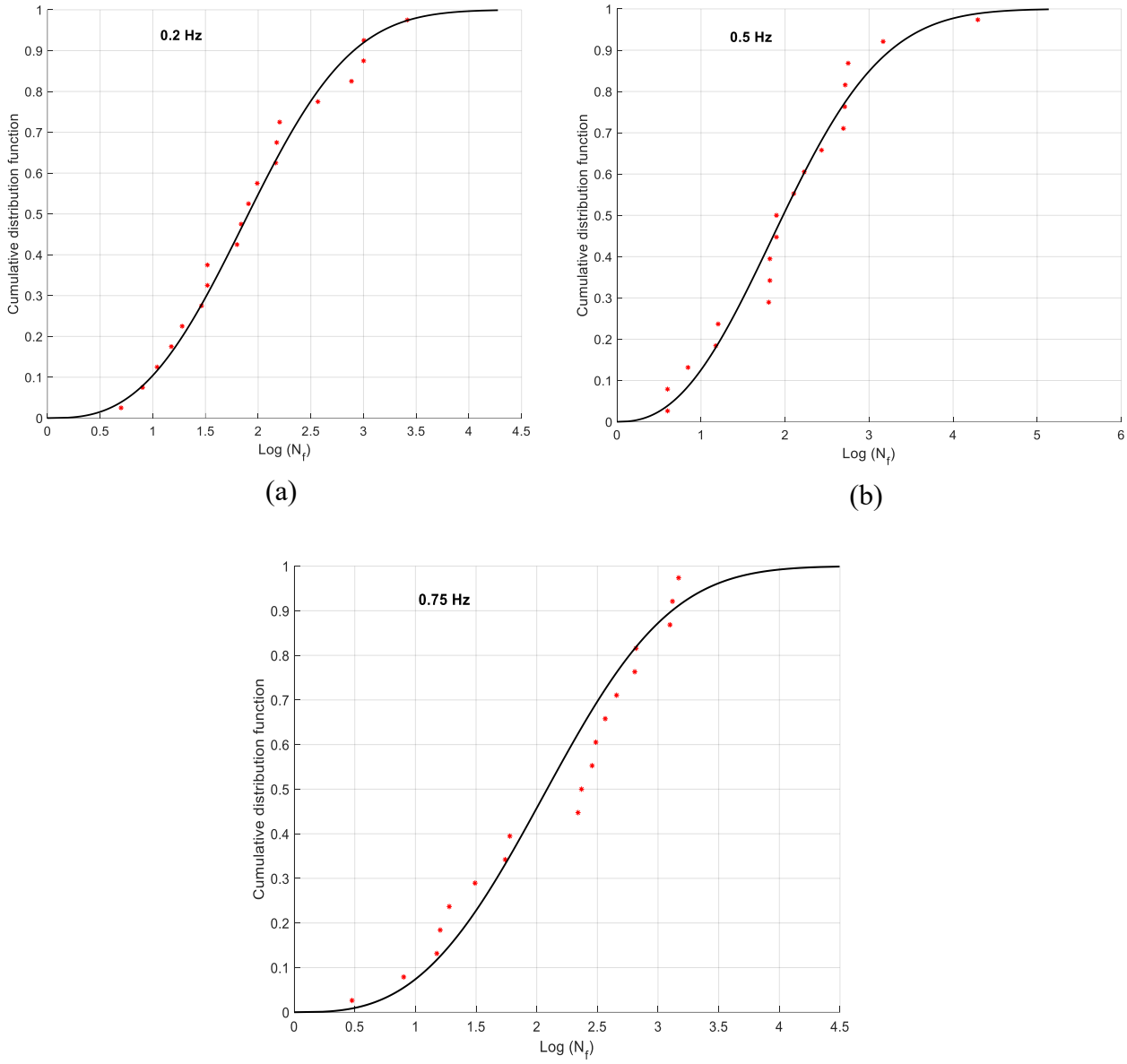

Figure 4-7 Weibull distribution fits for stress reversal fatigue experimental data at different loading frequencies: (a) 0.2 Hz, (b) 0.5 Hz, and (c) 0.75 Hz.

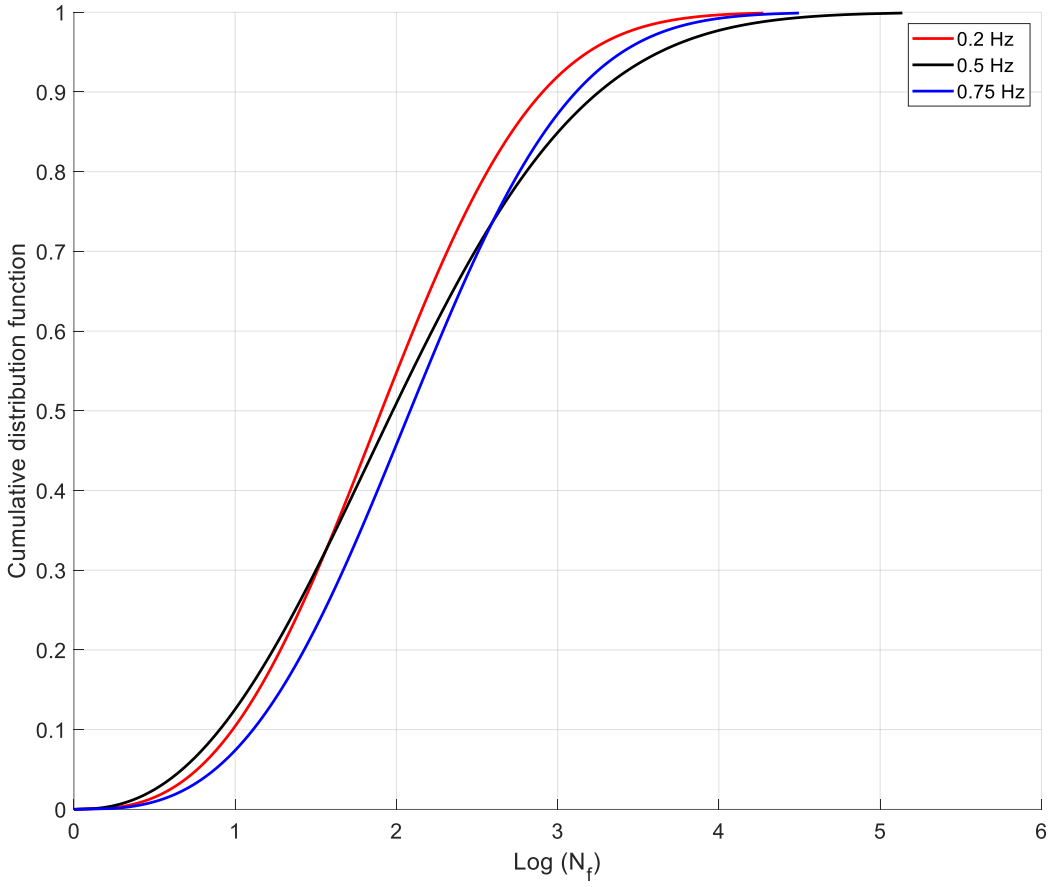

Figure 4-8 Weibull distribution fits for fatigue life of concrete subjected to 0.2 Hz, 0.5 Hz, and 0.75 Hz loading frequencies.

These variations can be attributed to how the rate of stress application affects the internal damage mechanisms within the concrete. Lower frequencies might allow more time for micro-cracks to propagate, leading to earlier failure. In contrast, higher frequencies might induce different stress responses, enhancing overall fatigue life (Bagde & Petros, 2009). However, this is not a conclusive remark as results for all frequencies studied in this thesis are in close proximity to each other.

4.3.2 Data analysis using MATLAB R2022b

In this section, the process of analyzing the raw data collected from the tests is described. The data was analysed using MATLAB R2022b. MATLAB is a high-performance programming language that includes a wide array of built-in functions and toolboxes, making it an ideal platform for processing experimental data and performing complex analyses. The analysis in this research focuses on three key areas: Maximum Strain Calculation, Energy Dissipation Analysis, and Stiffness Degradation Analysis. Each of these analyses provides critical insights into how plain concrete behaves under uniaxial stress reversal cyclic loading. A detailed explanation of the methodology used for each analysis is presented below.

4.3.2.1 Maximum strain calculation

The maximum strain values for each cycle were determined using data recorded by five LVDTs during the fatigue test. The steps involved processing the raw data, identifying load cycles, and extracting the maximum strain values for each cycle. The following steps were undertaken:

Step 1: Importing data

The first step involved importing the data from the DAQ system. The file path for the data was specified, and a built-in function was used to read the data into MATLAB. The data contained the recorded load and displacement values from the LVDTs.

Step 2: Defining key parameters and calculating stress and strain

After importing the data, key parameters such as the specimen diameter (101.6 mm) and gauge length (170 mm) were defined. These parameters were used to calculate the stress and strain in the concrete specimen during each cycle. Stress was calculated by dividing the recorded load by the

cross-sectional area of the specimen. Strain was determined by dividing the displacement values from the LVDTs by the gauge length.

Step 3: Identifying load cycles

To analyze the data for individual load cycles, a load threshold of 15 kN, which is less than the applied load of 20 kN, was set. This threshold was used to detect where the load crossed a specific value, marking the beginning and end of each cycle. The information on number of cycles was added to the main data matrix in MATLAB.

Step 4: Calculating and plotting maximum strain per cycle

For each identified cycle, the maximum strain value was selected by iterating through the data points corresponding to each cycle. The maximum strain was taken as the peak strain in the tensile region, which is further discussed in this chapter. This process was performed for all LVDTs, and the maximum strain values were plotted against the normalized cycle numbers to visualize how strain evolved during the fatigue test.

4.3.2.2 Energy dissipation calculation

Energy dissipation is measured by calculating the area enclosed by the stress-strain hysteresis loop for each fatigue cycle. Figure 4-9 illustrates the hysteresis loop for a single cycle, where the curve CBA represents the loading path, and the curve ADC shows the unloading path. Notably, the unloading curve lies below the loading curve. The area under the loading curve CBA represents the total energy absorbed per unit volume per fatigue cycle. Meanwhile, the area under the unloading curve ADC corresponds to the elastic energy per unit volume per fatigue cycle. The difference between these areas, enclosed by the curve ABCD, represents the energy dissipated per

unit volume per fatigue cycle, which can be determined as the area of the stress 'σ' and strain 'ε' hysteresis loop by using equation 4-4.

$$Dissipated\ energy = \oint \sigma d\varepsilon \qquad 4\text{-}4$$

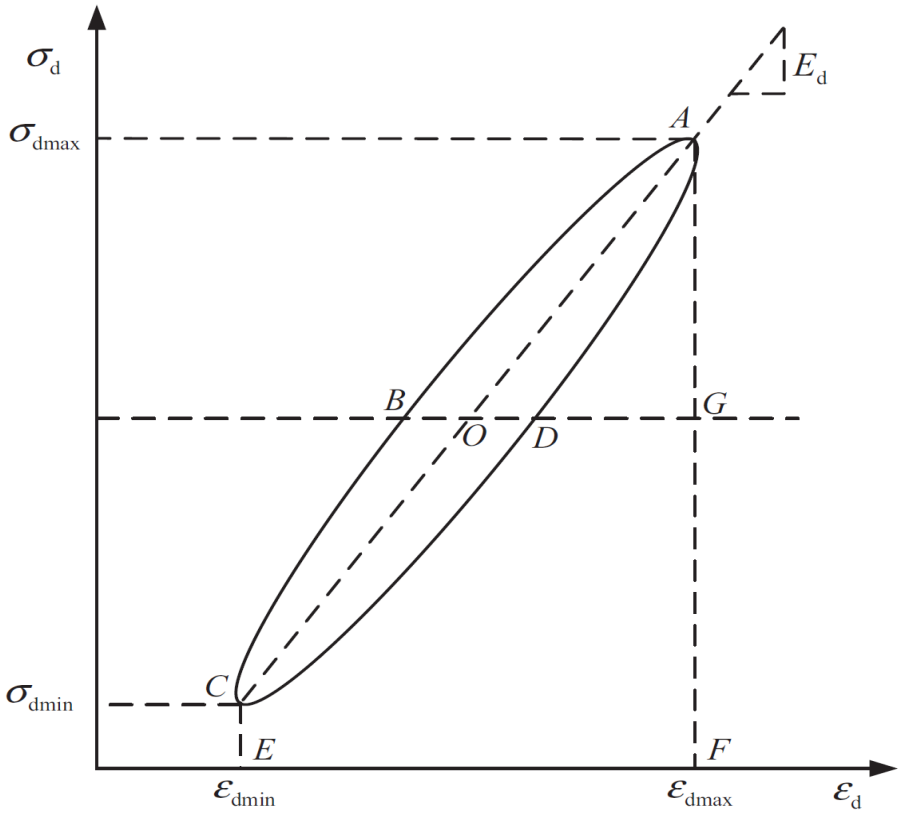

Figure 4-9 Illustration of the stress-strain hysteresis loop for a single cycle (Chen et al., 2017).

In the following analysis, the code developed for calculating the energy dissipated for each cycle follows a similar process to the maximum strain calculation. The main challenge was to ascertain that the code was capable to identify each loop clearly, so its area can be found. Additional steps were implemented to compute the area under the stress-strain loop for each cycle. The steps for importing data**,** defining key parameters and calculating stress and strain**,** and identifying the load cycles are the same as steps 1, 2, and 3 from the maximum strain curve calculation. The additional steps are discussed below:

Step 1: Energy dissipation per cycle

For each identified cycle, the energy dissipation value was calculated by iterating through the data points corresponding to that cycle. The stress and strain values were used to compute the area under the stress-strain hysteresis loop, which corresponds to the energy dissipated during that cycle. The value of energy was then stored in a pair with its corresponding cycle number to be used in further analysis.

Step 2: Energy band and mean curve

Once the energy dissipation values for all specimens were obtained, the next step involved interpolating the energy dissipation values using linear interpolation across a uniform set of normalized cycle numbers. This ensures that the energy dissipation patterns from different specimens can be compared and averaged. The midline represents the mean energy dissipation behavior across the cycles. Both the midline and the energy bandwidth were plotted to visualize how energy dissipation evolves over the fatigue cycles.

4.3.2.3 Stiffness degradation calculation

Stiffness is defined as the ratio of the change in stress to the change in strain, and it is analyzed in both the tensile and compressive regions of the stress-strain curve. The steps for importing data, defining key parameters, calculating stress and strain, and identifying load cycles are the same as in steps 1, 2, and 3 of the maximum strain curve calculation.

Step 1: Stiffness in tensile and compressive regions

The stiffness analysis begins by dividing each loading cycle into tensile and compressive regions. For each cycle, the points where the stress changes from tension to compression (and vice versa)

are identified. The stiffness is then calculated as the slope of the maximum strain values for both the tensile and compressive regions during loading and unloading phases of each cycle.

Step 2: Averaging stiffness and plotting results

For each cycle, the stiffness values for both the loading and unloading phases are averaged separately for the tensile and compressive regions. These average values represent the stiffness per cycle. The stiffness values are then plotted across the fatigue life to visualize how stiffness degrades over time as the specimen undergoes cyclic loading.

4.3.3 Maximum strain curves

In this study, the maximum strain is defined as the largest tensile strain recorded in each cycle under tensile stress conditions and the normalized fatigue life is calculated as the ratio of the current cycle to the total fatigue life of the specimen. The value of maximum strain was plotted for each cycle with respect to the given cycle when that strain occurred. As discussed in Section 2.6, a typical S-shaped curve is observed in the evolution of strain and can be divided into three distinct stages. The first stage is characterized by a rapid increase in strain, the second stage shows a more gradual and linear progression, and in the third stage the concrete experiences a rapid increase in strain leading up to failure. The strain for each specimen in this research were measured using five LVDTs placed around the specimen.

The maximum strain obtained from the LVDTs for specimen ‘C1-075-07’ is plotted against the normalized fatigue life in Figure 4-10**.** The plot depicts varying strain behaviors for LVDTs. LVDT-1 and LVDT-3 show an upward trend in strain, consistent with the typical strain evolution patterns reported in the literature (Tarliercio and Gobbit, 1996; Song et al., 2005; Ferreira et al., 2023). This behavior aligns with the expected strain increase due to crack propagation and uniaxial tensile

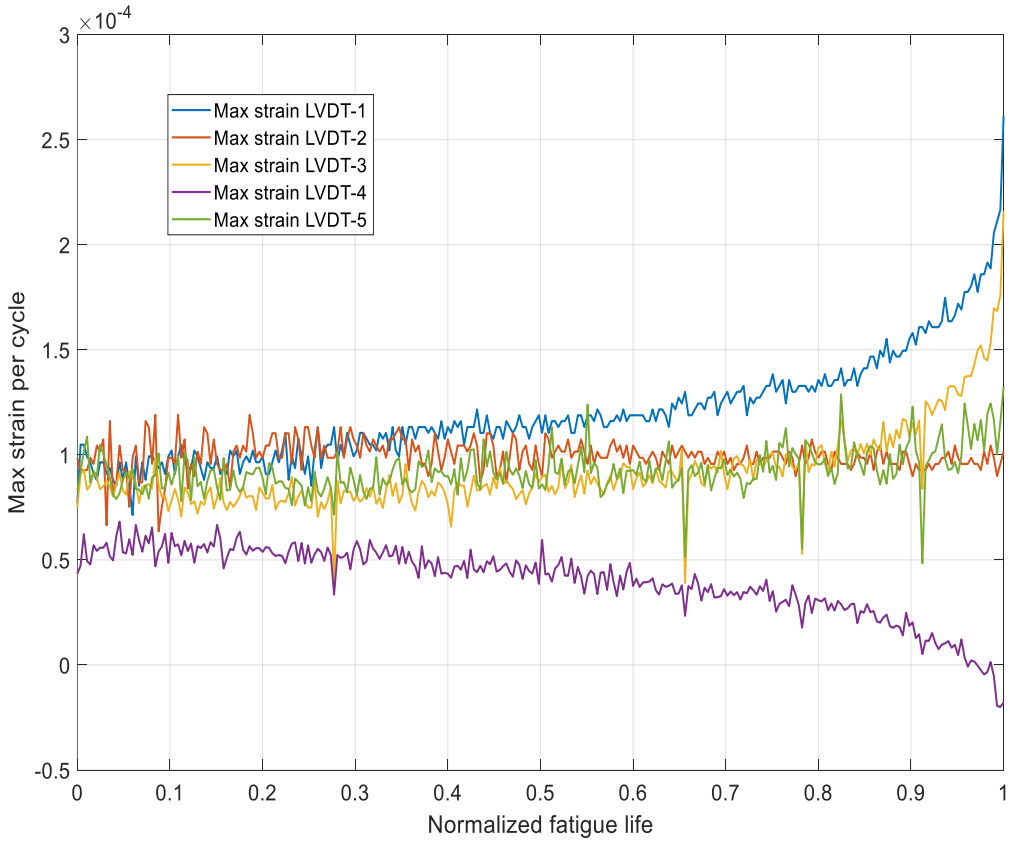

Figure 4-10 Maximum strain per cycle versus normalized fatigue life for specimen ‘C1-075-07’.

fatigue loading. LVDT-2 and LVDT-5 show a relatively constant trend with no significant strain change. This behavior indicates that these LVDTs are likely positioned in regions where the crack activity is minimal. However, LVDT-4 exhibits a downward trend, indicating a reduction in strain over the test duration. Similar trends were observed for maximum strain for all the specimen irrespective of the frequencies. The reducing trend could be attributed to the LVDT’s placement on the opposite side of the crack initiation zone or due to the influence of cohesive stresses within the fracture process zone as discussed in Section 2.8. Similar behavior of reduced strain was reported by Chen et al. (2023) while testing beams under flexural fatigue loading, where strain measurements decreased when cracks formed outside the LVDT's effective range.

For the purposes of this study, only LVDTs with increasing tensile strain trends, indicating significant strain development and crack propagation, were considered for detailed analysis. This approach ensures a focus on the most relevant data for understanding fatigue behavior. The maximum strain plots for all LVDTs of specimens tested at different frequencies are provided in Section B of the Appendix as Figure B.1 to Figure B.3 for further reference and validation.

To analyze the effect of low frequency on strain behavior, the bandwidth of maximum strain curves for each frequency was plotted alongside their mean values, as shown in Figure 4-11. Data from a total of 13, 14, and 19 LVDT readings were considered to construct the bandwidths for frequencies of 0.2 Hz, 0.5 Hz, and 0.75 Hz, respectively. Detailed plots of the maximum strain of LVDTs versus fatigue life for specimen tested at each frequency can be found in Appendix B, as Figures B4.

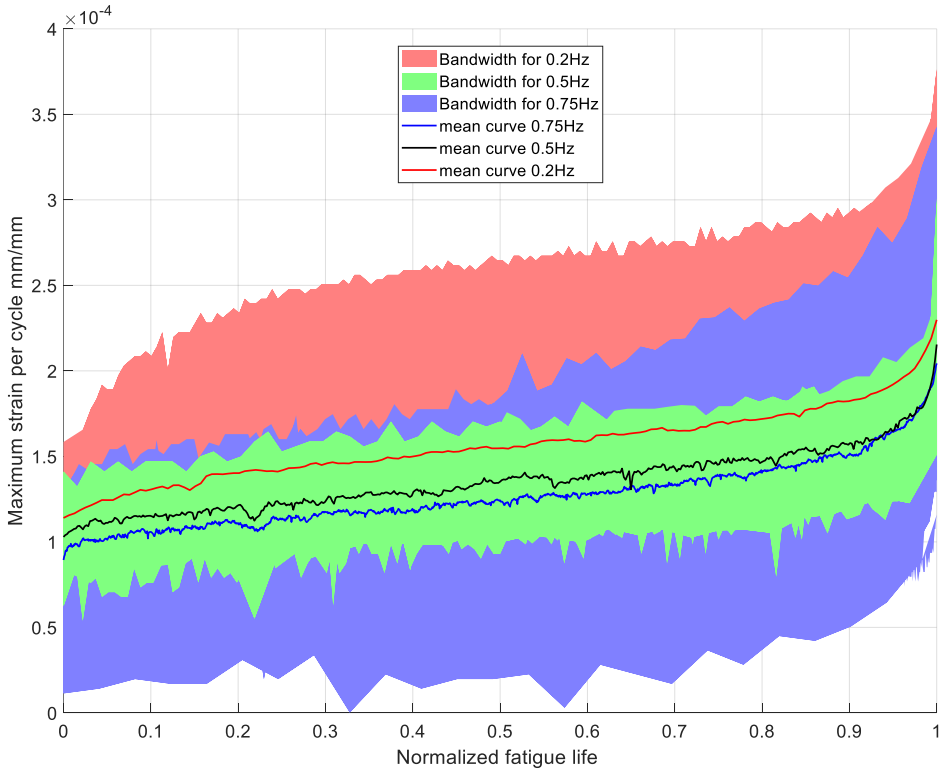

Figure 4-11 Maximum strain bandwidth and mean curves across normalized fatigue life.

Looking at Figure 4-11, although the maximum strain bandwidths show some overlap from one frequency to another, the mean curves indicate that specimens tested at lower frequencies tend to show higher maximum strain deformations. This trend suggests that lower frequencies lead to increased strain in the tensile region, possibly due to the longer time available for crack formation and stress accumulation. Moreover, the mean curves for each frequency display a characteristic S-shaped pattern as the fatigue life progresses. This pattern can be divided into three distinct stages: stage 1, encompassing the initial 10% of fatigue life, stage 2, covering the middle 80% of fatigue life, and stage 3, representing the final 10% of fatigue life. In stage1, there is a sharp increase in strain during the first 10% of fatigue life, followed by a plateau throughout stage 2. The plateau indicates that the microcracking pattern has stabilized. The curve then culminates in a steep rise during the final 10% of fatigue life in stage 3, ultimately leading to failure. This S-shaped curve is consistent across all frequencies and aligns with findings from previous studies (Saucedo et al., 2012; Poveda, 2017; Isojeh et al., 2017), which suggest that the shape of the curve is primarily influenced by material properties rather than frequency or stress level. This study shows that the shape indeed is similar throughout the various frequencies, however the values of the strain are higher for the lowest frequency tested.

Another parameter that describes the concrete behavior throughout its fatigue life is the rate of strain change at different stages of its life. Table 4-6 summarises the slopes of the mean strain curves for all three stages of the fatigue life. Although the initial slope at 0.2 Hz is slightly lower, this difference is insignificant, and the slope remains nearly consistent across all stages for each frequency. It shows that the overall pattern and progression of strain across the fatigue life are consistent and appear to be material dependent.

Table 4-6 Slope of mean strain curves at different stages of fatigue life for various frequencies

Frequency (Hz)	Slope of mean strain curves		
	Stage-1	Stage-2	Stage-3
0.2	0.074	0.057	0.426
0.5	0.101	0.050	0.411
0.75	0.107	0.052	0.429

4.3.4 Energy dissipation curves

When concrete proportional limit is exceeded due to fatigue loading, the axial deformation of concrete does not return to its initial state, resulting in irreversible deformation. During fatigue loading, as the material experiences repeated loading and unloading cycles, the stress-strain hysteresis loops for each loading cycle are observed to shift parallel to one another which indicates the accumulation of deformation with each cycle.

To measure the energy dissipation in this study, one representative LVDT data was chosen from each specimen. The data were collected from 5 specimens tested at 0.2 Hz, 5 specimens at 0.5 Hz, and 7 specimens at 0.75 Hz. These data were then used to plot the energy dissipation bandwidths and the corresponding mean lines, which summarize the energy dissipation behavior across the different frequencies.

Figure 4-12 displays the bandwidth for energy dissipation for each frequency, along with the mean lines that summarize the data. The energy dissipation values for all frequencies fall below 0.2 kJ/m^3. To visualise the behaviour at three studied frequencies, the energy dissipation values were divided into three segments: first 10% of fatigue life, middle 80% of fatigue life, and last 10% of

fatigue life. The lines were obtained by connecting the first and last point of each segment as can be seen in Figure 4-13.

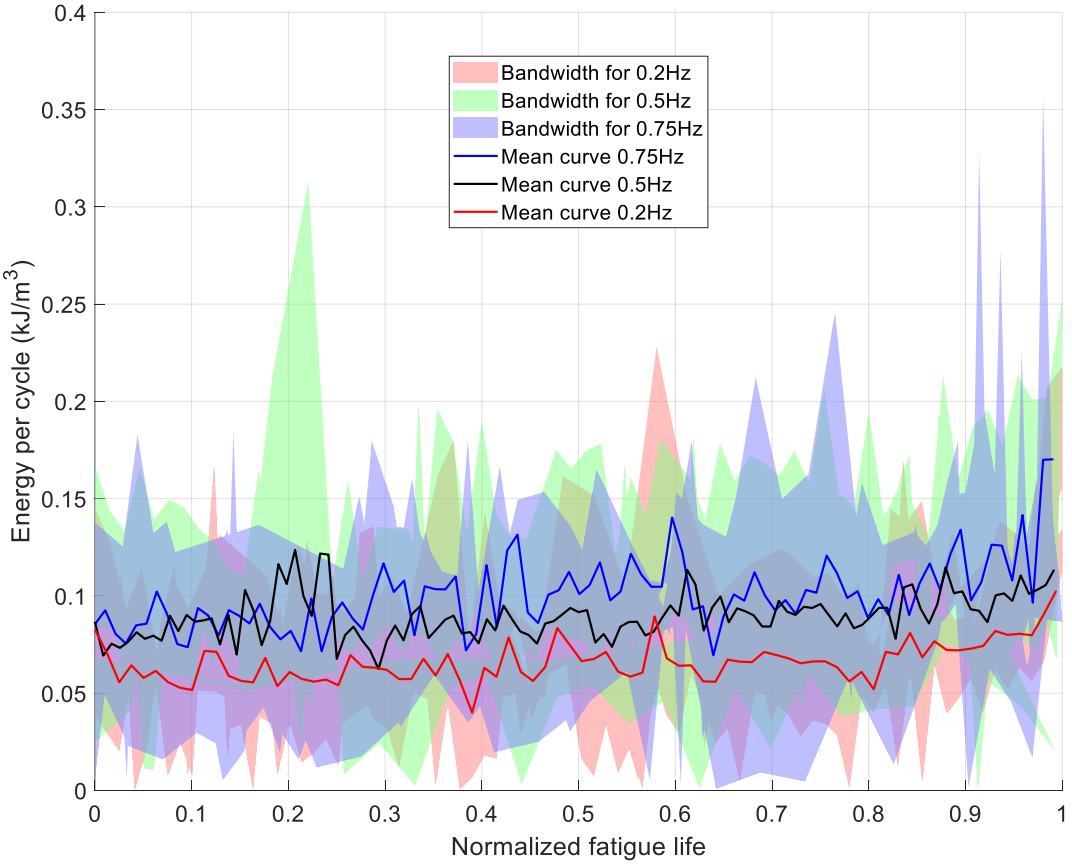

Figure 4-12 Bandwidth and mean for energy dissipation curves across normalized fatigue life.

The curves exhibit a U-shaped trend, with energy dissipation decreasing during the first stage, gradually increasing through the second stage, and rising rapidly in the final stage. The rapid increase in energy dissipation indicates the accumulation of damage and onset of failure. A similar pattern was observed by Song et al. (2018) during compressive fatigue testing of concrete. The slope and average energy dissipation per cycle values during each stage are presented in Table 4-4. These indices help define how energy dissipation evolves over the fatigue life of the concrete specimens.

The mean lines in Figure 4-13 indicate that specimens tested at 0.2 Hz dissipated less energy per cycle on average compared to those tested at 0.5 Hz and 0.75 Hz. This suggests that higher frequencies result in increased energy dissipation during each fatigue cycle. From the smoothed curves represented in Figure 4-13, it is evident that during stage-1, energy dissipation decreases, with a more pronounced drop observed at 0.2 Hz compared to the higher frequencies. The rate of energy dissipation per cycle decreased by 28.5% in this stage. However, the average energy dissipation per cycle was the lowest for 0.2 Hz and increased by 34% as frequency rose to 0.75 Hz. In stage-2, energy dissipation gradually increased across all frequencies, exhibiting plateau behavior in the rate of energy dissipation, but the average energy dissipation per cycle rose by 53%, reflecting a steady accumulation of fatigue damage. Stage-3 showed a rapid increase in energy dissipation, with the rate increasing by 106% from 0.2 Hz to 0.75 Hz, and the average energy per cycle increased by 51%. The slope for 0.75 Hz in this stage was nearly double that of the other frequencies, suggesting that higher frequencies lead to a more rapid exhaustion of energy per cycle toward the end of the specimen's fatigue life. Overall, the energy dissipation curves followed a U-shaped pattern, with a significant rise towards the end, corresponding to the rapid increase of damage. These deductions are also reflected in the values reported in Table 4-7 for different stages of fatigue life. In general, it is evident from the results that increasing frequency directly impacts the amount and the rate of energy that is exhausted during a specimen's fatigue life.

These observations in energy curve trend are consistent with previous studies, such as those by Ferreira et al. (2023) and Chen et al. (2017), which report similar behavior in energy curve trend for concrete under stress reversal and pure tensile cyclic loading conditions.

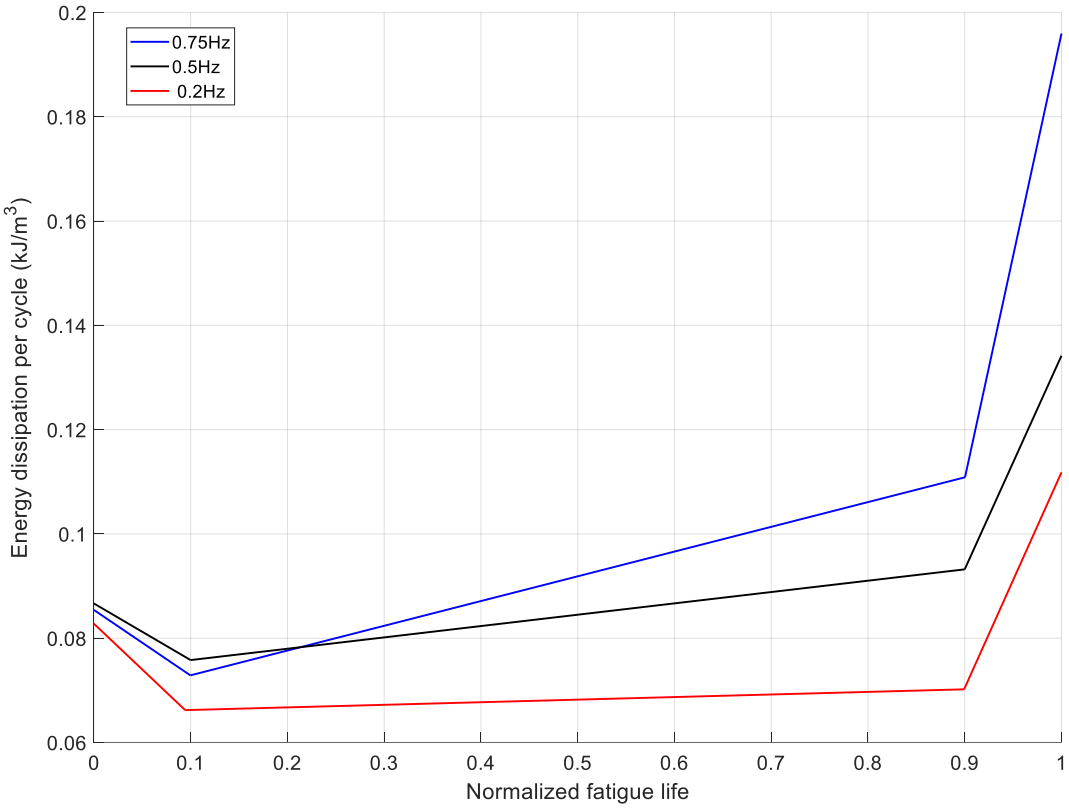

Figure 4-13 Slope of energy dissipation curves for different phases of fatigue life.

Table 4-7 The average energy per cycle and slope of energy dissipation curves across different phases of fatigue life.

Frequency (Hz)	**Slope for energy curve**			**Average energy dissipation per cycle (kJ/m^3)**		
	Stage-1	Stage-2	Stage-3	Stage-1	Stage-2	Stage-3
0.2	-0.175	0.005	0.413	0.061	0.064	0.084
0.5	-0.108	0.021	0.409	0.079	0.089	0.105
0.75	-0.125	0.047	0.853	0.082	0.098	0.127

4.3.5 Stiffness degradation

In the context of fatigue loading, stiffness refers to the average slope of the stress-strain relationship throughout the loading and unloading cycles. When considering stress reversal, the stiffness can be differentiated between the tensile and compressive regions based on loading application. The values of the stiffness for each cycle can be plotted with respect to the cycle number. Such stiffness curves under fatigue loading also exhibit three stages: an initial rapid decrease, a stable phase, and a final rapid decrease leading to failure. However, under stress-reversal conditions with maximum stress in the tensile region, the rate of stiffness degradation differs between the tensile and compressive regions. This was expected, as the same behaviour was seen earlier when strains were investigated. For clarity, the stiffness degradation in tensile and compressive loading are plotted with normalized fatigue life for the specimen 'C1-075-02' in Figure 4-14. the y-axis represents the average stiffness (GPa), while the x-axis represents the normalized fatigue life.

Figure 4-14a shows a pronounced decrease in stiffness over the fatigue life, with a significant decline during the initial phase. This degradation continues steadily until the final stage, where stiffness diminishes rapidly leading up to failure. The higher stiffness degradation observed in the tensile stress is likely due to the increased strain and crack propagation under tensile loading conditions, and due to the fact that the specimens were subjected to 90% of their tensile strength each cycle. In contrast, Figure 4-14b shows that stiffness degradation in compressive loading is less severe compared to the tensile loading. While there is some initial degradation, the overall rate of stiffness loss remains relatively stable throughout the fatigue life, with no significant decline in the final phase. This behavior of concrete exhibiting higher strain degradation and stiffness loss in the tensile region compared to compressive region can be attributed to the application of higher

stress level in tension compared to the compression. Additionally, scatter in the stiffness data across the fatigue life is also evident. The rate at which internal cracks form and expand vary between cycles, leading to fluctuations in the stiffness measurements. For both 0.2 Hz and 0.5 Hz, Figure 4-15 shows the stiffness degradation over the fatigue life, similar to the trends seen at 0.75 Hz. The figure shows identical patterns of stiffness degradation are observed across different frequencies, indicating that frequency variation does not significantly alter the fundamental degradation pattern. Similar conclusions were made by Chen et al, 2017 while testing concrete under compressive fatigue loading at various frequencies. The stiffness degradation plots for specimens tested at different frequency can be found in Appendix Section B, Figures B5 to Figure B7.

Based on the work of Ferreira et al. (2024) to better understand the stiffness degradation in concrete specimens under stress reversal fatigue, a deterioration index (D) is introduced to quantify the overall loss of structural integrity from the beginning to the end of the fatigue life. The stiffness degradation percentage (D) from the initial 10% to the final 10% of fatigue life can be calculated using equation 4-5.

$$D = \left(1 - \frac{K_f^{10}}{K_i^{10}}\right) \times 100 \qquad 4\text{-}5$$

Where D is the stiffness deterioration index $'K_i^{10'}$ and $'K_f^{10'}$represent the average stiffness within the first and last 10% of the specimen's fatigue life, respectively. To evaluate the stiffness degradation, the indices '$D_{\,T}$' and '$D_{\,C}$' were calculated for each specimen and LVDTs at three different frequencies. Subscripts 'C' and 'T' refer to compressive and tensile regions, respectively. The detailed results for each specimen are provided in Appendix Section B, Tables B1-3. The average deterioration indices for all specimens across frequencies are summarized in Table 4-8.

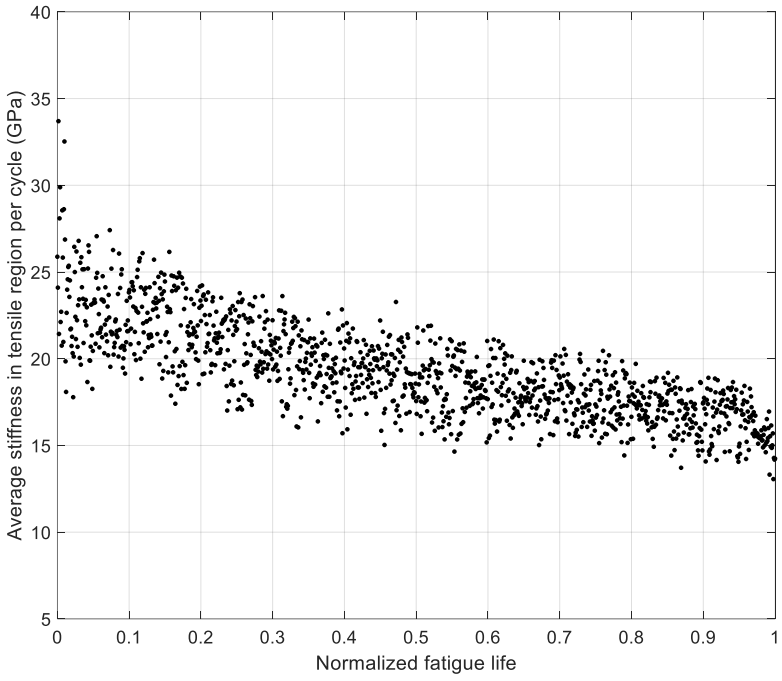

(a)

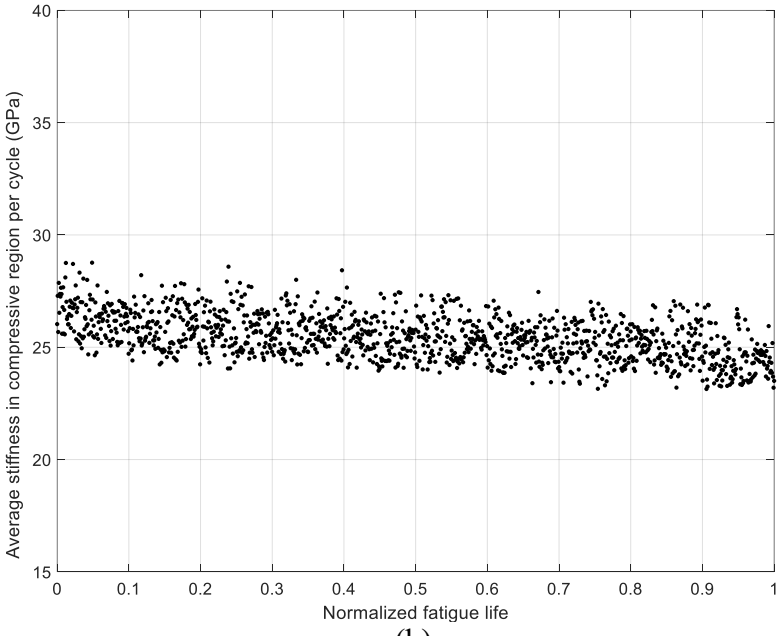

(b)

Figure 4-14 Stiffness degradation versus normalized fatigue life for specimen ‘C1-075-02’ ; (a) Tensile region; (b) Compressive region.

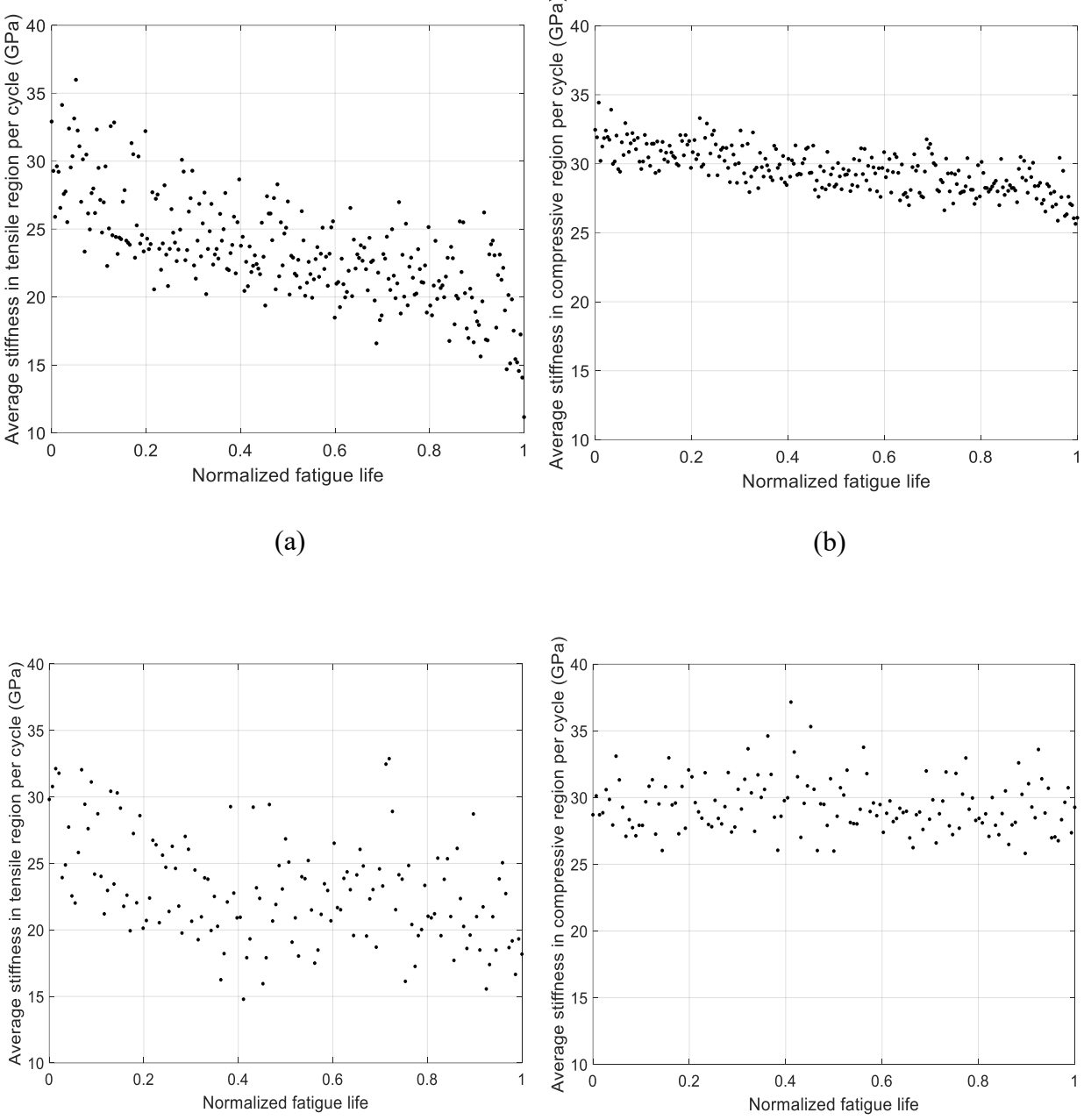

Figure 4-15 Stiffness degradation versus normalized fatigue life; (a) tensile region for ‘C2-05-03’, (b) compressive region for ‘C2-05-03’, (c) tensile region for ‘C2-02-04’, and (d) compressive region for ‘C2-02-04’.

Table 4-8 Average stiffness deterioration indices for tensile and compressive regions across frequencies

Frequency (Hz)	K_{Ti}^{10}(GPa)	K_{Ci}^{10}(GPa)	K_{Tf}^{10}(GPa)	K_{Cf}^{10}(GPa)	D_T (%)	D_C (%)
0.2	25.04	28.77	18.08	26.64	27.81	7.75
0.5	23.67	28.44	17.61	26.09	25.61	8.26
0.75	24.06	27.54	17.72	25.28	26.37	8.20

From Table 4-8, it is evident that the stiffness deterioration in tension is significantly higher than compression for all frequencies. This highlights the substantial impact of maximum tensile stress on structural degradation, leading to pronounced stiffness loss. The tensile stiffness degradation for 'C-02' is 8% higher than 'C-05' and 5% higher than 'C-075' Conversely, the stiffness deterioration in the compressive region has an average value of around 7.5%, indicating that the stress level that was applied in compression was low. The data shows negligible differences in deterioration indices between 0.5 Hz and 0.75 Hz frequencies, both for tensile and compressive regions. This suggests that the effect of frequency on stiffness behavior may be more pronounced, as the frequencies get smaller. The stiffness degradation is primarily governed by the stress levels applied to the tensile and compressive regions rather than frequency variations. It should also be reiterated that this holds true for the range of frequencies considered in this study.

4.3.6 Fatigue life prediction

In this section, a fatigue prediction model proposed by Ferreira et al. (2024) is used to estimate the fatigue life of the specimens tested in this experimental program. As discussed in Section 2.9, various fatigue models have been developed by researchers to predict the behavior of concrete

under cyclic loading. Ferreira's model is designed for uniaxial stress reversal fatigue and is based on an extensive experimental database from their experimental work and from existing available literature. The model is notable for its simplicity, and for utilizing only one parameter, namely the maximum stress level (S_{max}). They calculated the scale and shape parameters by plotting the Weibull distribution fit for a dataset of 201 specimens, with maximum stress levels ranging from 0.60 to 0.90. Using linear regression on these scale and shape parameters at various maximum stress levels, they derived equations to predict the shape and scale parameters for the Weibull distribution specific to stress reversal fatigue life. The model proposes Equations 4-6 and 4-7 to calculate these parameters for a two-parameter Weibull distribution under stress reversal fatigue conditions, based solely on the maximum stress level.

$$Scale = -7.24 \times S_{max} + 9.23 \quad \text{4-6}$$

$$Shape = -17.63 \times S_{max} + 19.10 \quad \text{4-7}$$

The slope and intercept of these equations are produced using the existing experiments in literature in stress reversal. These equations were employed to determine the Weibull distribution parameters for the experimental data in this study. As a recommendation, it is proposed that for more conservative estimations of fatigue life, an adjustment be applied to the base model if the number of tested specimens in the desired category is less than 12.

Although the test results of the current study are already more than the recommended threshold for application of adjustment, the Adjusted Weibull Distribution (AWD) curves for each group were still produced. AWD curves are essentially the application of the statistical methodology proposed by Ferreira et al. (2023) and Ortega et al. (2018) to the base model. The AWDs were plotted for all experimental data with a 95% safety level. To achieve this, 25,000 random

realizations were generated. The number of data points for each random set matched the number of specimens tested at each frequency, with 19 specimens for 0.75 Hz, 19 specimens for 0.5 Hz, and 20 specimens for 0.2 Hz. The base model and the AWDs for each frequency are presented in Figure 4-16 to Figure 4-18. In these figures, the superscript on the AWD denotes the safety level, while the subscript indicates the number of specimens tested at that frequency. For instance, $AWD_{19}^{95\%}$ represents the adjusted Weibull distribution curve for 19 specimens at a 95% safety level.

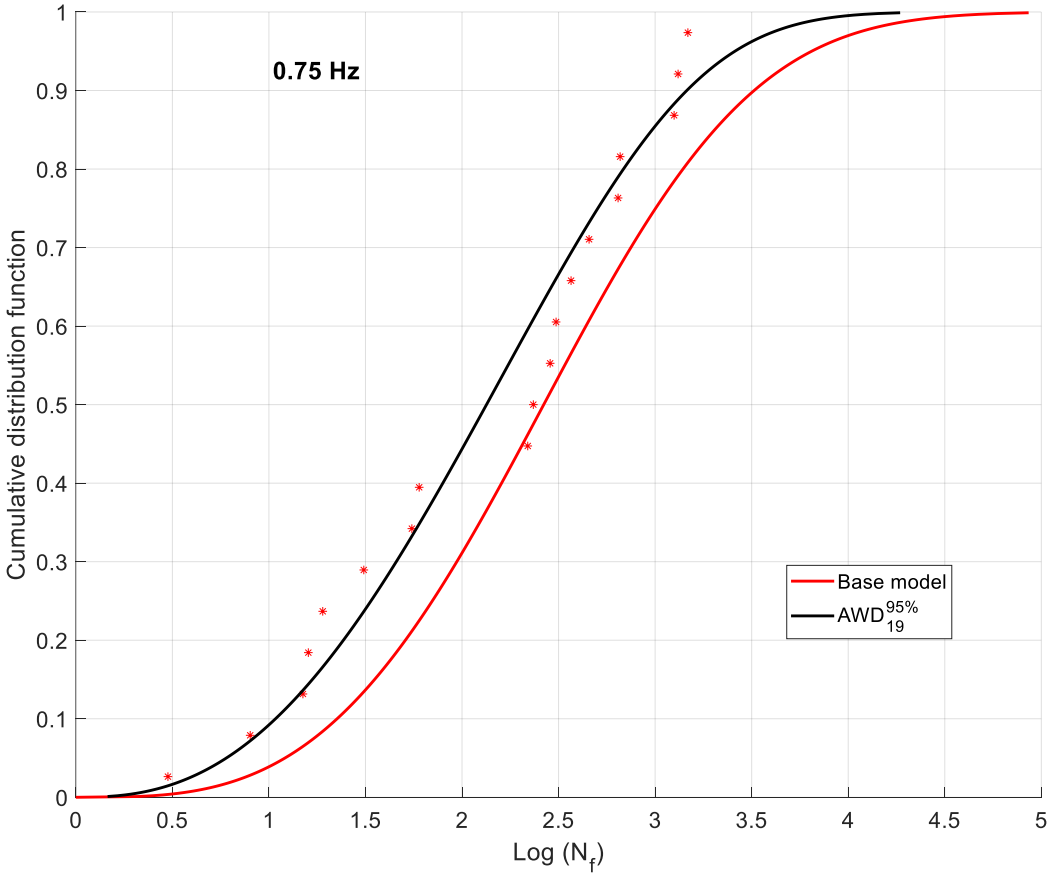

Figure 4-16 Base model and Adjusted Weibull Distribution (AWD) for specimens at 0.75 Hz.

It can be seen in Figure 4-16 that at 0.75 Hz almost all the experimental data points lie to the left of the base model's distribution curve. This indicates that the concrete specimens tend to fail earlier

than predicted by the base model. Although the base model predictions are nonconservative for the most part when compared with experimental data, the AWD adjustment provides a more conservative prediction that shows a very good agreement with the experimental data. The adjustment has been successful in capturing a better estimation of the case at hand.

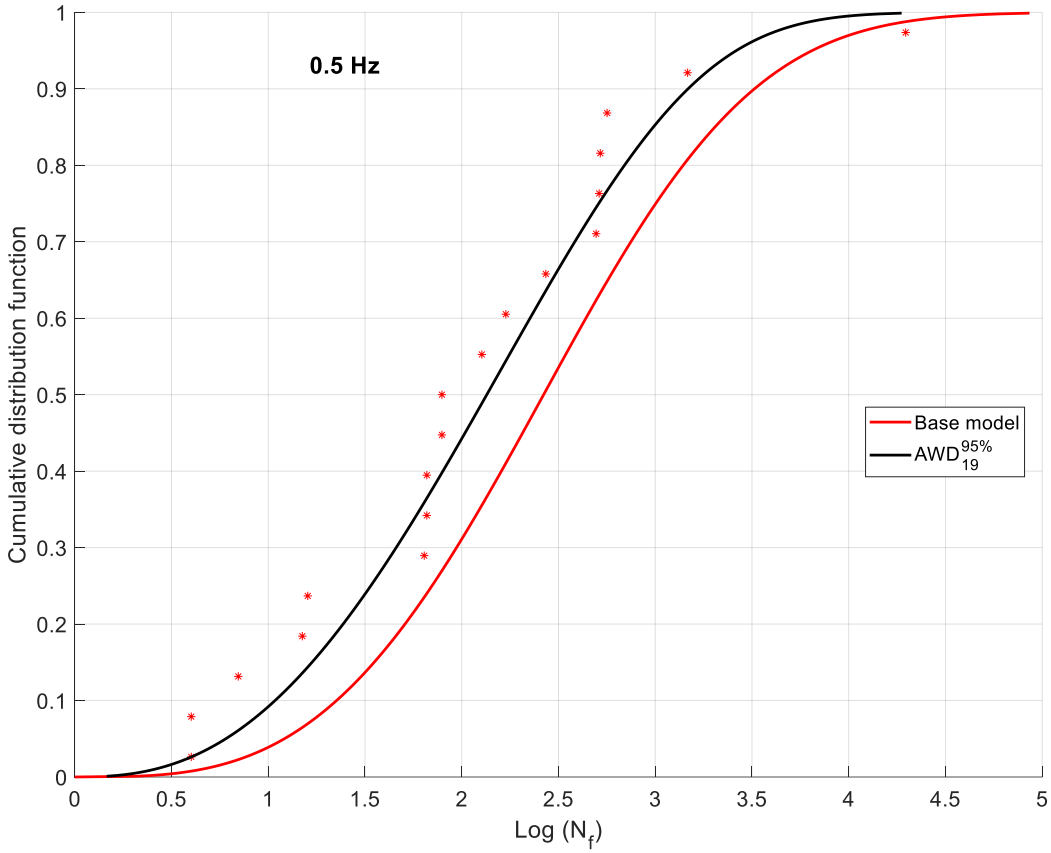

Figure 4-17 Base model and Adjusted Weibull Distribution (AWD) fits for specimens at 0.5 Hz

Similar to the 0.75 Hz case, the experimental data for 0.5 Hz in Figure 4-17 also falls entirely to the left of the base model curve, indicating a tendency for earlier failure. The adjusted Weibull curve produces a better approximation of fatigue life and although it is not fully conservative, the results are in good agreement with the experiment.

For 0.2 Hz, the discrepancy between the model predictions and the experimental data is even more pronounced as shown in Figure 4-18. All experimental data points fail significantly earlier than predicted by both the base model and the AWD.

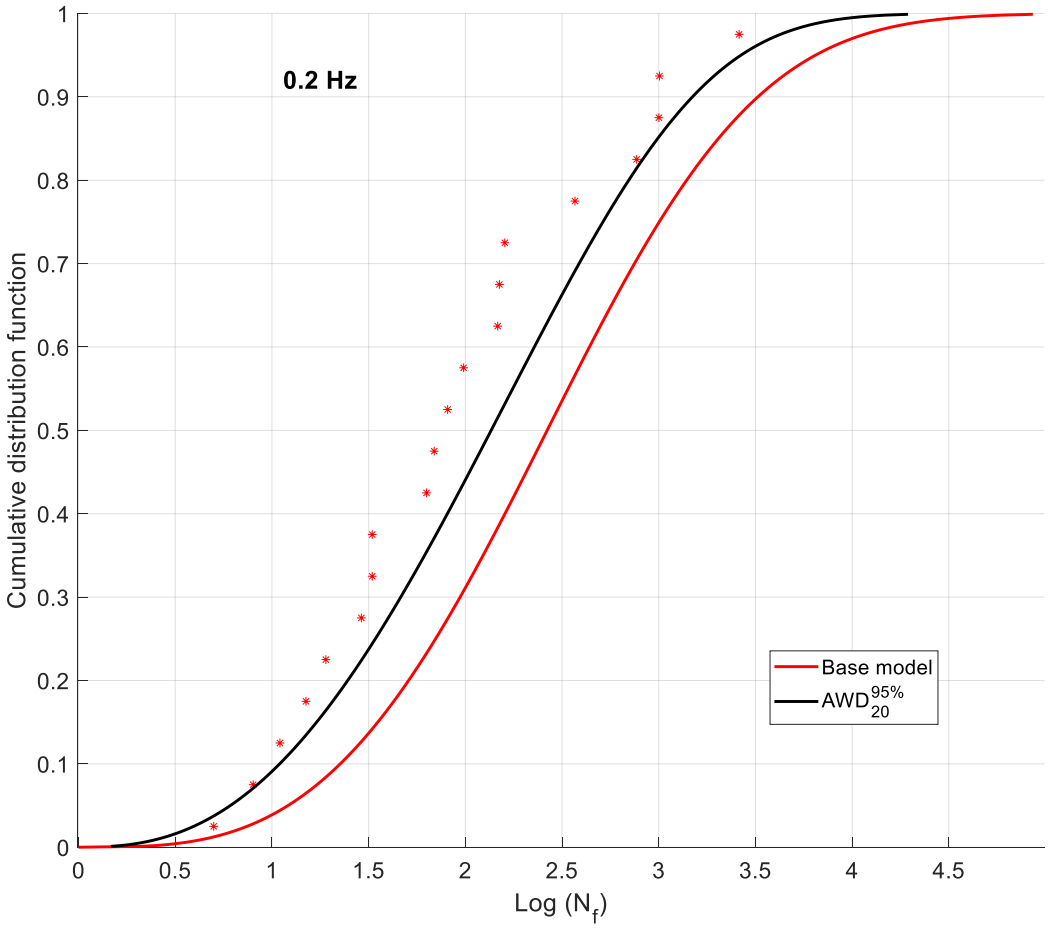

Figure 4-18 Base model and Adjusted Weibull Distribution (AWD) for specimens at 0.2 Hz

Overall, the application of model adjustment for all the frequencies improved the predictions substantially and provided a better fit. However, in terms of conservatism, neither the base model nor the adjusted model is completely successful in producing conservative results. This could be because the model itself doesn't recognize frequency as a parameter in the estimation of fatigue life which could in fact be an important parameter for a more precise estimation of fatigue life.

Overall, the base model consistently underestimates the likelihood of early failures across all tested frequencies, particularly at lower frequencies where the discrepancy is most significant. While the AWD provides a more conservative estimate, it still falls short of accurately predicting fatigue life. These results underscore the need for a more robust model that incorporates the influence of lower frequencies on fatigue life. Integrating frequency as a parameter could provide a more comprehensive understanding of fatigue behaviour and lead to more reliable predictions of concrete performance under stress reversal fatigue loading.

Chapter 5 Conclusions and Recommendations

This thesis aimed to investigate the uniaxial stress reversal fatigue behavior of plain concrete under low-frequency cyclic loading, focusing specifically on frequencies below 1 Hz. The research was driven by the need to enhance the understanding of concrete's fatigue life, particularly in critical infrastructure subjected to repeated loading. The specimens in this study were tested under uniaxial stress reversal fatigue at three specific frequencies: 0.2 Hz, 0.5 Hz, and 0.75 Hz, with a constant stress range of 11.4 MPa. The testing regime set the maximum stress level at 90% of the tensile strength and the minimum stress level at 20% of the compressive strength. The results were analyzed in terms of number of cycles to failure, stiffness degradation, maximum strain, and energy dissipation.

5.1 Conclusions

The following conclusions can be drawn from this thesis:

1. The experimental results demonstrated that the fatigue life of plain concrete specimens tested at 0.75 Hz was higher than those tested at 0.2 Hz. However, no clear trend was observed among the three frequencies (0.2 Hz, 0.5 Hz, and 0.75 Hz). A further investigation is needed to establish a definitive pattern.
2. The variations in the duration of fatigue life suggest that frequency influences the internal damage mechanisms in concrete, with lower frequencies potentially allowing more time for micro-crack propagation, leading to earlier failure. Despite these observations, the differences in fatigue life across frequencies were generally minor. This could potentially be attributed to the relatively small differences in frequency chosen for the research. The frequencies (0.2 Hz, 0.5 Hz, and 0.75 Hz) are all within a low-frequency range.

3. The maximum strain analysis revealed that tensile loading was the primary cause of failure in the concrete specimens. The highest maximum strain per cycle was observed at 0.2 Hz, followed by 0.5 Hz and 0.75 Hz, indicating that lower frequencies resulted in larger maximum strain per cycle. This strain behaviour suggests that higher frequencies are associated with lower maximum strain, correlating with the increased fatigue life observed at higher frequencies.
4. The analysis of maximum strain and stiffness degradation data revealed a characteristic S-shaped curve across all tested frequencies. This behavior is consistent with results reported in previous studies, which suggest that the progression of strain is primarily governed by the inherent material properties of the concrete, rather than the frequency of loading.
5. The stiffness degradation is on average 27% in tension and 8% in compression for all frequencies. Notably, the frequency of loading did not significantly affect the overall pattern of stiffness degradation, with negligible differences in deterioration indices between 0.5 Hz and 0.75 Hz.
6. The energy dissipation curves followed a U-shaped pattern with three defined stages. Stage-1 represents the first 10% of the fatigue life, stage-2 represents the mid 80% of fatigue life, and stage-3 that represents the last 10% of fatigue life. There was a significant increase in energy dissipation per cycle towards the end of the fatigue life, corresponding to the rapid accumulation of damage. From 0.2 Hz to 0.75 Hz, the average energy dissipation per cycle increased by 34% in stage-1, 53% in stage-2, and 51% in stage-3, indicating that higher frequencies resulted in greater energy dissipation as the fatigue progressed.

7. The rate of energy dissipation per cycle exhibited different behaviors across the three stages which were defined in conclusion 6. From 0.2 Hz to 0.75 Hz, there was a 28.5% decrease in stage-1, plateau behavior in stage-2 across all frequencies, and a 106% increase in stage-3, reflecting the significant increase in energy dissipation rate as the fatigue life approached failure.
8. The stress reversal fatigue model proposed by Ferreira et al. (2024) was validated against the experimental data. The model demonstrated reasonable accuracy in predicting the fatigue life of plain concrete across different frequencies. The adjusted model provides a better approximation of the fatigue life, though it is still not fully conservative. However, the model performed better with increasing frequency. These results highlight the potential applicability of the model for predicting uniaxial stress reversal fatigue behavior in concrete, but also suggest that further refinement may be needed to include the effect of frequency.

5.2 Recommendations

The following recommendations are suggested for future research based on identified areas of improvement:

1. Future studies should consider the use of advanced instrumentation, such as acoustic emission sensors, and infrared camera during fatigue testing. These tools could significantly enhance the accuracy of predicting concrete failure under stress reversal conditions, thereby improving the reliability of fatigue life assessments.
2. It is recommended to conduct a detailed microstructural analysis of concrete specimens both before and after fatigue testing. This approach would provide valuable insights into

crack mechanisms and propagation under stress reversal loading, helping to better understand the degradation processes that affect the fatigue life of concrete.

3. Future research should focus on developing predictive models that incorporate stiffness degradation and energy dissipation, with a particular emphasis on the effects of stress reversal and low-frequency loading. Such models would contribute to a more accurate prediction of the fatigue behavior of concrete.
4. Future studies should include tests using various loading waveforms, such as triangular or square waves. These waveforms may influence the fatigue performance of concrete differently compared to the sinusoidal waveform used in this study, especially under stress reversal conditions.

References

Aas-Jakobsen, K. (1970). Fatigue of concrete beams and columns. Division of Concrete Structures, Norwegian Inst. of Technology, University of Trondheim.

Aas-Jakobsen, K., & Lenschow, R. (1973, March). Behavior of reinforced columns subjected to fatigue loading. In Journal Proceedings (Vol. 70, No. 3, pp. 199-206).

Afaghi, M., Anja, B. K., & Øverli, J. A. (2023). A Review on Fatigue Performance of Concrete Structures Part I: Loading Parameters, Current Prediction Models and Design Approaches. Nordic Concrete Research, 68(1), 105-126.

ARAFAH, D. Z. R. (2014). Fracture assessment of cracked components under biaxial loading.

ASTM International. (2003). *ASTM C143/C143M-03: Standard test method for slump of hydraulic-cement concrete*. ASTM International. https://doi.org/10.1520/C0143_C0143M-03

ASTM International. (2014). *ASTM C469/C469M-14: Standard test method for static modulus of elasticity and Poisson's ratio of concrete in compression*. ASTM International. https://doi.org/10.1520/C0469_C0469M-14

ASTM International. (2015). *ASTM C470/C470M-15: Standard specification for molds for forming concrete test cylinders vertically*. ASTM International. https://doi.org/10.1520/C0470_C0470M-15

ASTM International. (2017). *ASTM C496/C496M-17: Standard test method for splitting tensile strength of cylindrical concrete specimens*. ASTM International. https://doi.org/10.1520/C0496_C0496M-17

ASTM International. (2017). *ASTM C497-17: Standard test methods for concrete pipe, manhole sections, or tile*. ASTM International. https://doi.org/10.1520/C0497-17

ASTM International. (2022). *ASTM C231-22: Standard test method for air content of freshly mixed concrete by the pressure method*. ASTM International. https://doi.org/10.1520/C0231_C0231M-22

ASTM International. (2023). *ASTM C39/C39M-23: Standard test method for compressive strength of cylindrical concrete specimens*. ASTM International. https://doi.org/10.1520/C0039_C0039M-23

ASTM International. (2023). *ASTM C617/C617M-23: Standard practice for capping cylindrical concrete specimens*. ASTM International. https://doi.org/10.1520/C0617_C0617M-23

Awad, M. E.-M. (1971). Strength and Deformation Characteristics of Plain Concrete Subjected to High Repeated and Sustained Loads [Ph.D. Thesis]. University of Illinois at Urbana.

Bagde, M. N., & Petroš, V. (2009). Fatigue and dynamic energy behaviour of rock subjected to cyclical loading. *International Journal of Rock Mechanics and Mining Sciences*, *46*(1), 200-209.

Banjara, N. K., & Ramanjaneyulu, K. (2018). Experimental investigations and numerical simulations on the flexural fatigue behavior of plain and fiber-reinforced concrete. Journal of Materials in Civil Engineering, 30(8), 04018151.

Bathias, C., & Pineau, A. (Eds.). (2013). *Fatigue of materials and structures: application to design and damage*. John Wiley & Sons.

Bennett, E. W., & Muir, S. E. S. J. (1967). Some fatigue tests of high-strength concrete in axial compression. Magazine of Concrete Research, 19(59), 113–117. https://doi.org/10.1680/macr.1967.19.59.113

Canadian Standards Association. (2019). *CSA A23.2-6B: Standard method of test for density and compressive strength of concrete cylinders*. CSA Group.

Carpinteri, A. (2021). Fracture and Complexity: One Century since Griffith's Milestone (Vol. 237). Springer Nature.

Castillo, E., & Fernández-Canteli, A. (2009). *A unified statistical methodology for modeling fatigue damage*. Springer Science & Business Media.

Chen, H., Sun, Z., Zhang, X., & Fan, J. (2023). Tensile Fatigue Properties of Ordinary Plain Concrete and Reinforced Concrete under Flexural Loading. *Materials*, *16*(19), 6447.

Chen, X., Bu, J., Fan, X., Lu, J., & Xu, L. (2017). Effect of loading frequency and stress level on low cycle fatigue behavior of plain concrete in direct tension. Construction and Building Materials, 133, 367–375. https://doi.org/10.1016/j.conbuildmat.2016.12.085

Clemmer, H. F. (1922). Fatigue of Concrete. ASTM Proceedings of the Twenty-Fifth Annual Meeting, 408–419. Cornelissen, H. A. W. (1984). Fatigue Failure of Concrete in Tension. HERON, 29(4). http://resolver.tudelft.nl/uuid:bece66f3-8b5d-4448-8318-48c00583a0f6

D'Amore, A., Califano, A., & Grassia, L. (2021). Modelling the loading rate effects on the fatigue response of composite materials under constant and variable frequency loadings. *International Journal of Fatigue*, *150*, 106338.

Do, M.-T., Chaallal, O., & Aïtcin, P.-C. (1993). Fatigue Behavior of High-Performance Concrete. Journal of Materials in Civil Engineering, 5(1), 96–111. https://doi.org/10.1061/(ASCE)0899-1561(1993)5:1(96)

Félix, E. F., Carrazedo, R., & Possan, E. (2022). Fatigue life of concrete: Experimental study on the influence of loading conditions and material strength. Revista ALCONPAT, 12(1), 1-15.

Ferreira, E. C., Sotoudeh, P., Fiorillo, G., & Svecova, D. (2023). The probabilistic fatigue life of plain concrete under low-frequency stress reversal loading. In *Life-Cycle of Structures and Infrastructure Systems* (pp. 3492-3499). CRC Press.

Ferreira, E., Sotoudeh, P., & Svecova, D. (2024). Fatigue life of plain concrete subjected to low frequency uniaxial stress reversal loading. Construction and Building Materials, 411, 134247.

Ferreira, E., Sotoudeh, P., Fiorillo, G., & Svecova, D. (2024, June 19). Fatigue life estimation model for plain concrete under uniaxial stress reversal loading condition. Department of Civil Engineering, University of Manitoba.**(Under review for international journal publication)**

Graf, O., & Brenner, E. (1934). Experiments for investigating the resistance of concrete under often repeated compression loads. Bulletin, 1, 17-25.

Hannant, D. J., Buckley, K. J., & Croft, J. (1973). The effect of aggregate size on the use of the cylinder splitting test as a measure of tensile strength. Matériaux et Construction, 6, 15-21.

Heilmann HG, Hilsdorf HH, Finsterwalder K (1969) Festigkeit und Verformung von Betonunter Zugspannungen. Deutscher Ausschuss für Stahl-beton, 203

Holmen, J. O. (1982). Fatigue of concrete by constant and variable amplitude loading. ACI Special Publication, 75, 71–110. https://www.concrete.org/publications/internationalconcreteabstractsportal/m/details/id/6402

Hordijk, D. A. (1993). Local approach to fatigue of concrete.

Hsu, T. T. (1981, July). Fatigue of plain concrete. In *Journal Proceedings* (Vol. 78, No. 4, pp. 292-305).

Hsu, T. T. (1984). Fatigue and microcracking of concrete. *Materiaux et construction*, *17*, 51-54.

Indriyantho, B. R. (2014). Finite element modeling of concrete fracture in tension with the Brazilian splitting test on the case of plane-stress and plane-strain. Procedia Engineering, 95, 252-259.

Isojeh, B. (2017). Fatigue damage analysis of reinforced concrete structural elements. University of Toronto (Canada).

Joly D (1898) La resistance et l, ‘‘elasticite des’’ ciments Portland. Ann Pons Chaussees 16(7):198–244

Kachkouch, F. Z., Noberto, C. C., de Albuquerque Lima Babadopulos, L. F., Melo, A. R. S., Machado, A. M. L., Sebaibi, N., Boukhelf, F., & el Mendili, Y. (2022). Fatigue behavior of concrete: A literature review on the main relevant parameters. Construction and Building Materials, 338(March), 127510. https://doi.org/10.1016/j.conbuildmat.2022.127510

Kesler, C. E. (1953, January). Effect of speed of testing on flexural fatigue strength of plain concrete. In Proceedings, Highway Research Board (Vol. 32, pp. 251-258).

Kim, J.-K., & Kim, Y.-Y. (1996). Experimental study of the fatigue behavior of high strength concrete. Cement and Concrete Research, 26(10), 1513–1523. https://doi.org/10.1016/0008-8846(96)00151-2

Klaiber, F. W., & Lee, D. Y. (1982). The effects of air content, water-cement ratio, and aggregate type on the flexural fatigue strength of plain concrete. ACI Special Publication, 75, 111–131. https://www.concrete.org/publications/internationalconcreteabstractsportal/m/details/id/6403

Lee, D. Y., Klaiber, F. W., & Coleman, J. W. (1978). Fatigue behavior of air-entrained concrete. Transportation Research Record, (671).

Lee, M. K., & Barr, B. I. G. (2004). An overview of the fatigue behaviour of plain and fibre reinforced concrete. *Cement and Concrete Composites*, *26*(4), 299-305.

Lloyd, J. P., Lott, J. L., & Kesler, C. E. (1968). Fatigue of concrete. University of Illinois. Engineering Experiment Station. Bulletin; no. 499.

Lou, J., Bhalerao, K., Soboyejo, A. B. O., & Soboyejo, W. O. (2006). An investigation of the effects of mix strength on the fracture and fatigue behavior of concrete mortar. Journal of Materials Science, 41(21), 6973–6977. https://doi.org/10.1007/s10853-006-0219-0

Lü, P., Li, Q., & Song, Y. (2004). Damage constitutive of concrete under uniaxial alternate tension-compression fatigue loading based on double bounding surfaces. International journal of solids and structures, 41(11-12), 3151-3166.

Medeiros, A., Zhang, X., Ruiz, G., Rena, C. Y., & Velasco, M. D. S. L. (2015). Effect of the loading frequency on the compressive fatigue behavior of plain and fiber reinforced concrete. International Journal of Fatigue, 70, 342-350.

Mihashi, H. (1987). States of the art and a view of the fracture mechanics of concrete. *Journal of JCI*, *25*(2), 14-25.

Mun, J.-S., Yang, K.-H., & Kim, S.-J. (2016). Tests on the Compressive Fatigue Performance of Various Concretes. Journal of Materials in Civil Engineering, 28(10), 04016099. https://doi.org/10.1061/(ASCE)MT.1943-5533.0001612

Murdock, J. W. (1965). A critical review of research on fatigue of plain concrete. University of Illinois. Engineering Experiment Station. Bulletin; no. 475.

Murdock, J. W., & Kesler, C. E. (1958). Effect of Range of Stress on Fatigue Strength of Plain Concrete Beams. ACI Journal Proceedings, 55(8). https://doi.org/10.14359/11350

Naik, T. R., Singh, S. S., & Ye, C. (1993). Fatigue behavior of plain concrete made with or without fly ash.

Oh, B. H. (1986). Fatigue analysis of plain concrete in flexure. *Journal of Structural Engineering*, *112*(2), 273-288.

Oneschkow, N. (2012, July). Influence of loading frequency on the fatigue behaviour of highstrength concrete. In Proceedings of the 9th FIB International PhD Symposium in Civil Engineering. July 22nd to 25th (pp. 235-240).

Oneschkow, N. (2016). Fatigue behaviour of high-strength concrete with respect to strain and stiffness. International Journal of Fatigue, 87, 38–49. https://doi.org/10.1016/j.ijfatigue.2016.01.008

Oneschkow, N., & Timmermann, T. (2022). Influence of the composition of high-strength concrete and mortar on the compressive fatigue behaviour. Materials and structures, 55(2), 83.

Ortega, J. J., Ruiz, G., Rena, C. Y., Afanador-García, N., Tarifa, M., Poveda, E., ... & Evangelista Jr, F. (2018). Number of tests and corresponding error in concrete fatigue. International journal of fatigue, 116, 210-219.

Ozkan, I. F. (2023). Adaptation of dams to climate change: gap analysis/authors: Istemi F. Ozkan, Bessam Kadhom, Ehsan Roshani, Hamidreza Shirkhani, Juan Hiedra-Cobo, Daniel Cusson, Pierre Claver Nkinamubanzi. CNRC: National Research Council Canada.

Paskova, T., & Meyer, C. (1994). Optimum Number of Specimens for Low-Cycle Fatigue nTests of Concrete. Journal of Structural Engineering, 120(7), 2242–2247. https://doi.org/10.1061/(ASCE)0733-9445(1994)120:7(2242)

Paulsen, T. H. (2021). Fatigue of Concrete (Master's thesis, NTNU).

Poveda, E., Ruiz, G., Cifuentes, H., Rena, C. Y., & Zhang, X. (2017). Influence of the fiber content on the compressive low-cycle fatigue behavior of self-compacting SFRC. International Journal of Fatigue, 101, 9-17.

Raithby, K. D., & Galloway, J. W. (1974). Effects of moisture condition, age, and rate of loading on fatigue of plain concrete. ACI Special Publication, 41, 15–34. https://www.concrete.org/publications/internationalconcreteabstractsportal/m/details/id/17675

Saini, B. S., & Singh, S. P. (2020). Flexural fatigue strength prediction of self compacting concrete made with recycled concrete aggregates and blended cements. Construction and Building Materials, 264, 120233.

Sainz-Aja, J., Thomas, C., Polanco, J. A., & Carrascal, I. (2019). High-frequency fatigue testing of recycled aggregate concrete. Applied Sciences, 10(1), 10.

Saucedo, L., Rena, C. Y., Medeiros, A., Zhang, X., & Ruiz, G. (2013). A probabilistic fatigue model based on the initial distribution to consider frequency effect in plain and fiber reinforced concrete. International journal of fatigue, 48, 308-318.

Seitl, S., Benešová, A., Pascual, Á. P., Malíková, L., Bujdoš, D., & Bílek, V. (2022). Fatigue and fracture properties of concrete mixtures with various water to cement ratio and maximum size of aggregates. Procedia Structural Integrity, 42, 1512-1519.

Shah, S. P., & Ouyang, C. (1994). Fracture mechanics for failure of concrete. *Annual review of materials science*, *24*(1), 293-320.

Smith, R. A. (1998). FATIGUE IN TRANSPORT: Problems, Solutions and Future Threats². Trans IChemE, 76(Part B).

Sparks, P. R. (1982). The influence of rate of loading and material variability on the fatigue characteristics of concrete. ACI Special Publication, 75, 331–341.

Sparks, P. R., & Menzies, J. B. (1973). The effect of rate of loading upon the static and fatigue strengths of plain concrete in compression. Magazine of Concrete Research, 25(83), 73–80. https://doi.org/10.1680/macr.1973.25.83.73

Tepfers, R. (1982). Fatigue of plain concrete subjected to stress reversals. ACI Special Publication, 75, 195–215. https://www.concrete.org/publications/internationalconcreteabstractsportal/m/details/id/6407

Tepfers, R., & Kutti, T. (1979). Fatigue Strength of Plain, Ordinary, and Lightweight Concrete. ACI Journal Proceedings, 76(5), 635–652. https://doi.org/10.14359/6962

Thompson, D., Marshall, K., Rollins, G., & Barrie, R. (2015). Wanapum Dam: Spillway Damage Repair and Preventative Measures. *Proceedings of HydroVision International 2015*.

Van Ornum, J. L. (1907). The Fatigue of Concrete. In Transactions of the American Society of Civil Engineers (LVIII, pp. 294–320). American Society of Civil Engineers.

Wang, X. (2023). LITERATURE REVIEW ON FATIGUE BEHAVIOR OF REINFORCED CONCRETE BRIDGE DECKS.

Wöhler, A. (1870). Über die festigkeitsversuche mit eisen und stahl. Ernst & Korn.

Zhang, B., Phillips, D. V., & Wu, K. (1996). Effects of loading frequency and stress reversal on fatigue life of plain concrete. Magazine of concrete research, 48(177), 361-375.

Appendix

A. Material Properties.

Table A 1 Compressive strength test result for specimens of concrete-1 and concrete-2

Material	Age	Stress (MPa)	Average (MPa)
Concrete-1	Day-7	28.4	27.5
		27.9	
		26.4	
	Day-14	38.2	38.9
		39.2	
		39.4	
	Day-28	45.8	43.9
		44.8	
		45.3	
		38.0	
		44.7	
		41.7	
		45.4	
		46.3	
		42.7	
		44.0	
		44.0	
		43.5	

		43.7	
		42.8	
		32.9	
		36.2	
		35.7	
		35.9	
		34.5	
		36.8	
		34.9	
		36.1	
		33.1	
Concrete-2	**Day-28**	25.2	36.0
		36.1	
		36.8	
		26.9	
		37.5	
		38.9	
		37.2	
		37.5	
		36.1	
		39.6	
		37.1	
		36.9	

B. Stress reversal fatigue test

Table B. 1 Stiffness deterioration indices for tensile and compressive regions for specimen tested at 0.2 Hz

Specimen ID	LVDTs	K_{Ti}^{10}(GPa	K_{Ci}^{10}(GPa)	K_{Tf}^{10}(GPa)	K_{Cf}^{10}(GPa	D_T (%)	D_C (%)
C1-02-06	1	26.60	31.17	17.25	27.87	35.15	10.56
	2	22.89	26.78	15.60	24.99	31.86	6.69
C1-02-07	1	21.85	24.23	15.06	23.07	31.05	4.78
	2	21.31	25.04	16.54	23.46	22.35	6.27
	3	25.82	28.50	20.81	27.21	19.38	4.54
C1-02-09	1	18.12	23.68	13.69	21.93	24.45	7.38
	2	16.32	20.05	14.74	19.44	9.70	3.03
C2-02-02	1	28.81	33.27	25.34	32.00	12.04	3.80
	2	22.89	27.46	17.74	23.25	22.49	15.34
C2-02-04	1	27.72	29.11	20.37	29.08	26.50	0.11
	2	23.99	30.24	15.54	26.27	35.22	13.12
C2-02-06	1	27.98	27.49	21.30	25.86	23.87	5.92
	2	32.90	37.90	18.30	34.12	44.37	9.98
	3	33.35	37.85	20.78	34.41	37.69	9.07
Average		**25.04**	**28.77**	**18.08**	**26.64**	**26.87**	**7.18**

Table B. 2 Stiffness deterioration indices for tensile and compressive regions for specimen tested at 0.5 Hz

Specimen ID	LVDTs	K_{Ti}^{10}(GPa	K_{Ci}^{10}(GPa)	K_{Tf}^{10}(GPa)	K_{Cf}^{10}(GPa)	D_T (%)	D_C (%)
C1-05-01	1	27.38	31.25	24.04	29.66	12.19	5.08
C1-05-04	1	24.56	30.11	18.23	26.65	25.77	11.49
	2	26.25	34.78	21.31	32.01	20.17	8.24
C1-05-07	1	23.08	26.35	17.38	24.52	24.70	6.93
C1-05-08	1	18.84	22.75	15.93	21.08	15.46	7.33
	2	19.04	23.30	13.67	21.70	28.19	6.88
C1-05-09	1	19.04	21.87	12.14	21.50	36.26	1.69
	2	18.61	22.16	13.08	20.38	29.73	8.02
C2-05-04	1	29.13	31.46	18.76	27.66	35.59	12.06
	2	21.74	24.84	18.35	24.01	15.61	3.35
	3	22.24	25.89	14.79	23.39	33.49	9.65
C2-05-05	1	33.16	42.81	25.08	38.40	24.37	10.30
	2	24.67	32.15	16.18	28.24	34.40	12.14
Average		**23.67**	**28.44**	**17.61**	**26.09**	**25.84**	**7.94**

Table B. 3 Stiffness deterioration indices for tensile and compressive regions for specimen tested at 0.75 Hz

Specimen ID	LVDTs	K_{Ti}^{10}(GPa	K_{Ci}^{10}(GPa)	K_{Tf}^{10}(GPa)	K_{Cf}^{10}(GPa	D_T (%)	D_C (%)
C1-075-02	1	22.27	25.88	19.93	24.33	10.50	5.95
	2	22.89	26.37	16.32	24.45	28.69	7.25
	3	26.99	32.33	21.63	31.54	19.86	2.41
C1-075-05	1	23.47	27.50	19.32	25.22	17.66	8.29
	2	22.45	25.90	16.43	23.93	26.80	7.56
	3	24.54	27.24	22.06	26.70	10.09	1.97
C1-075-07	1	25.05	28.15	15.68	25.14	37.37	10.68
	2	24.60	26.73	14.48	23.74	41.16	11.18
	3	24.49	26.80	17.93	25.22	26.78	5.85
C1-075-08	1	25.94	31.01	18.27	27.93	29.57	9.89
	2	20.85	26.78	16.29	25.27	21.88	5.62
	3	22.82	27.26	16.32	24.44	28.50	10.31
C1-075-09	1	17.99	24.96	13.23	21.56	26.44	13.60
	2	22.57	25.96	15.98	23.47	29.21	9.60
	3	31.95	34.43	24.99	32.74	21.78	4.89
C2-075-02	1	20.32	24.34	13.19	21.44	35.10	11.92
	2	24.80	27.64	18.36	26.08	25.97	5.63
	3	30.22	33.84	25.83	31.41	14.53	7.18
C2-075-04	1	24.43	28.07	17.69	25.10	27.59	10.57
	2	25.15	27.73	20.16	26.09	19.84	5.89
C2-075-05	2	19.41	22.46	10.94	19.10	43.62	14.94
	3	26.16	24.54	14.76	21.19	43.56	13.64
Average		**24.06**	**27.54**	**17.72**	**25.28**	**26.66**	**8.40**

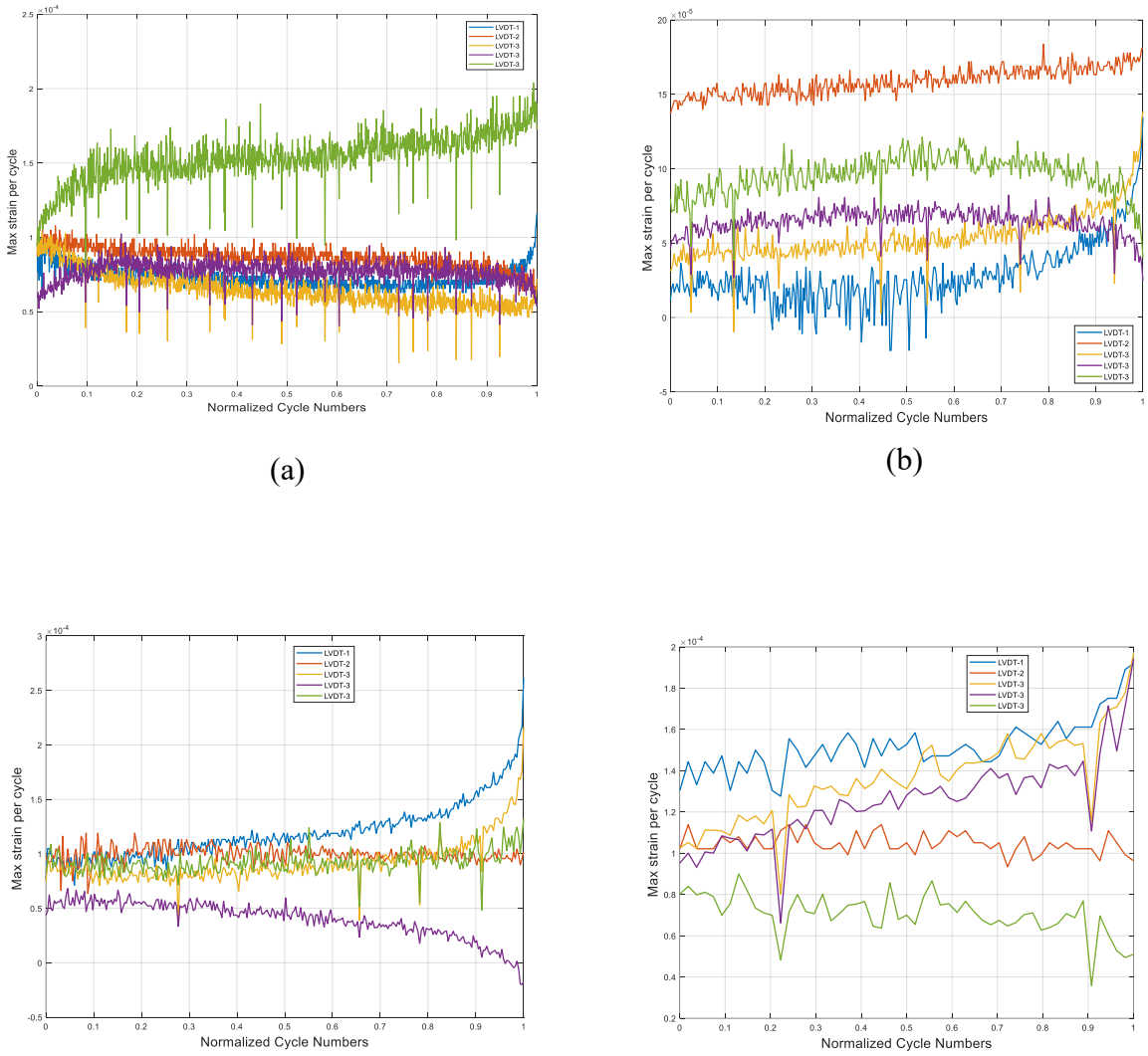

Figure B 1 Maximum strain vs Normalised fatigue cycle test at 0.75 Hz: a) specimen ‘C1-075-02’ b) specimen ‘C1-075-05’ c) specimen ‘C1-075-07’ and d) specimen ‘C1-075-08’

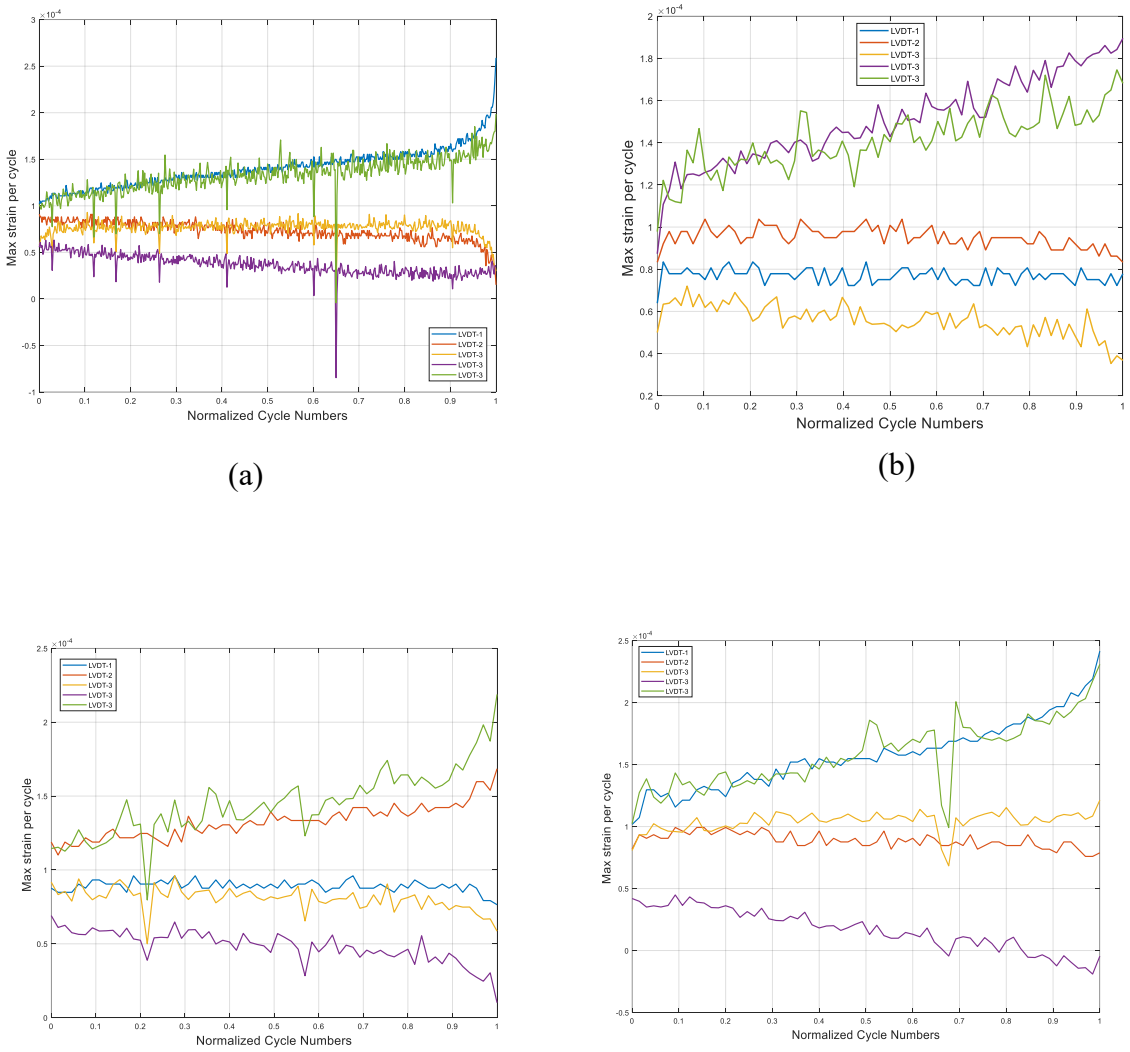

Figure B 2 Maximum strain vs Normalised fatigue cycle test at 0.5 Hz: a) specimen ‘C1-05-04’ b) specimen ‘C1-05-06’ c) specimen ‘C1-05-08’ and d) specimen ‘C1-05-09’.

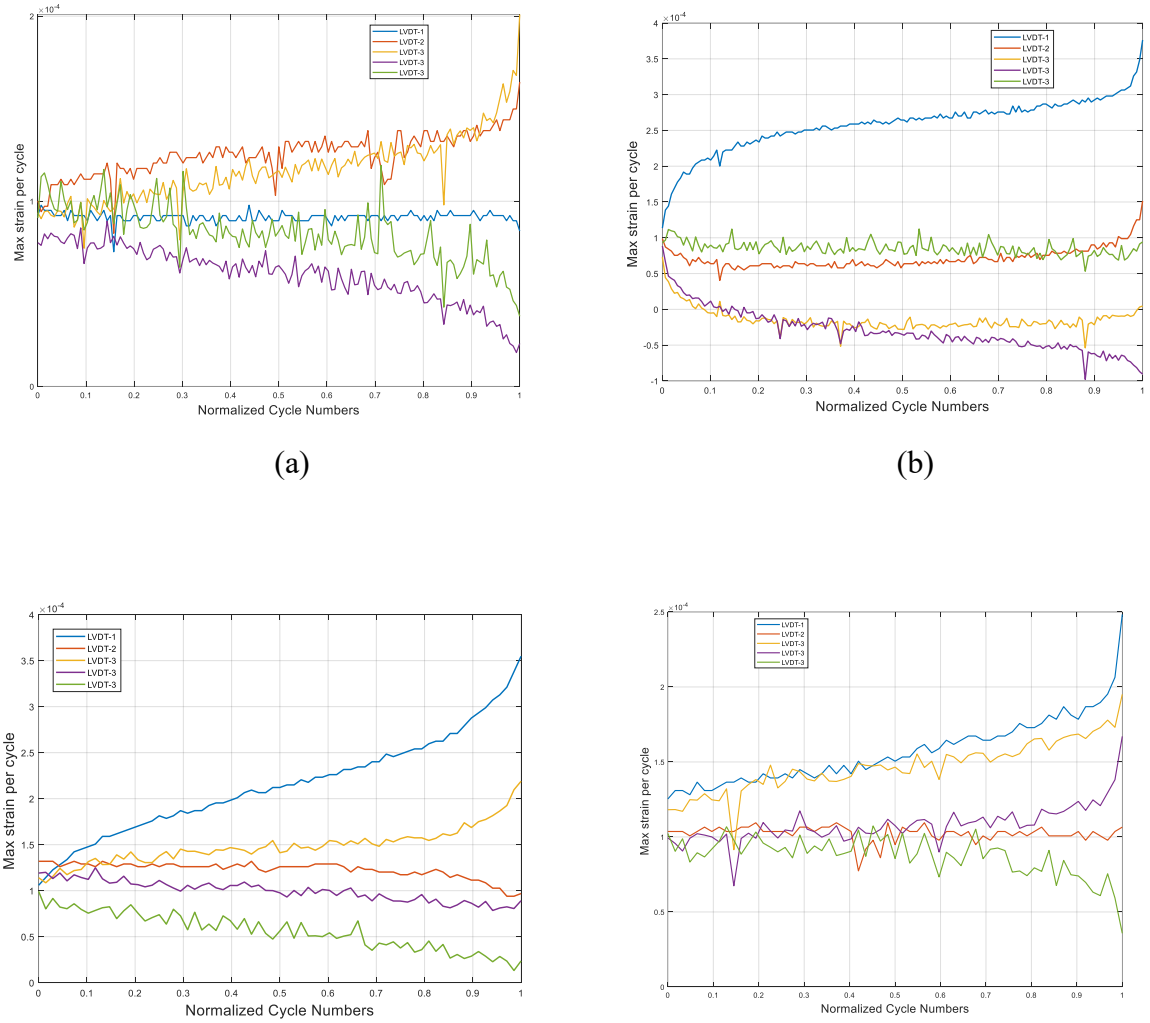

Figure B 3 Maximum strain vs Normalised fatigue cycle test at 0.2 Hz: a) specimen ‘C1-02-02’ b) specimen ‘C2-02-04’ c) specimen ‘C1-02-06’ and d) specimen ‘C1-02-07’.

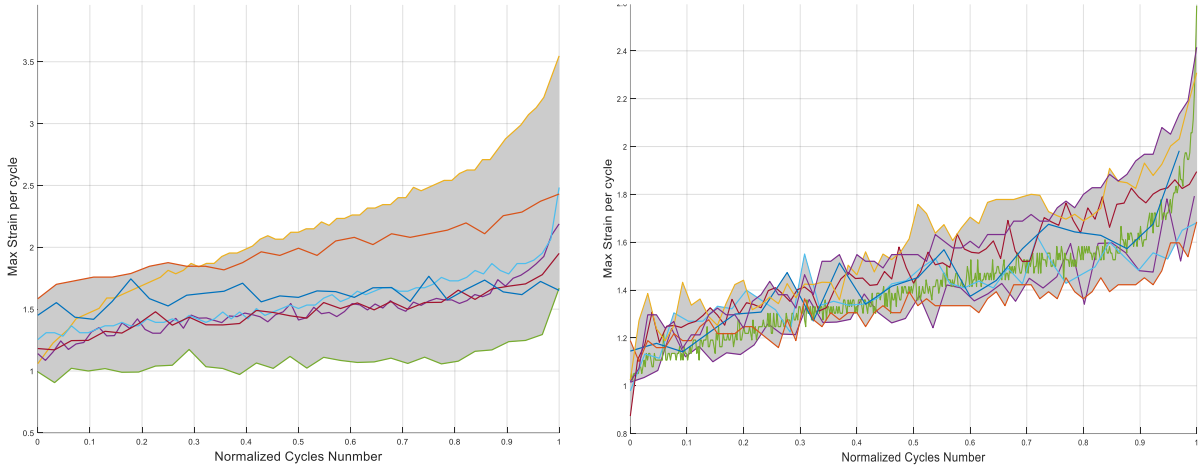

(a) (b)

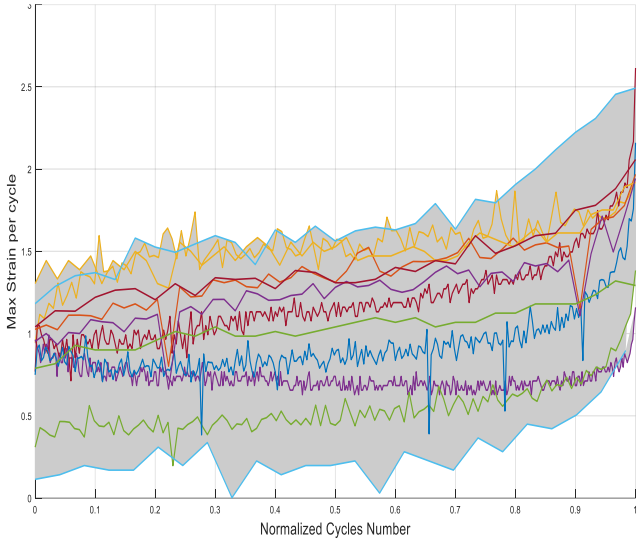

(c)

Figure B 4 The energy bandwidth for maximum strain of LVDTs Vs Normalised fatigue cycles for three different frequencies; a) 0.2 Hz; b) 0.5 Hz; and c) 0.75 Hz.

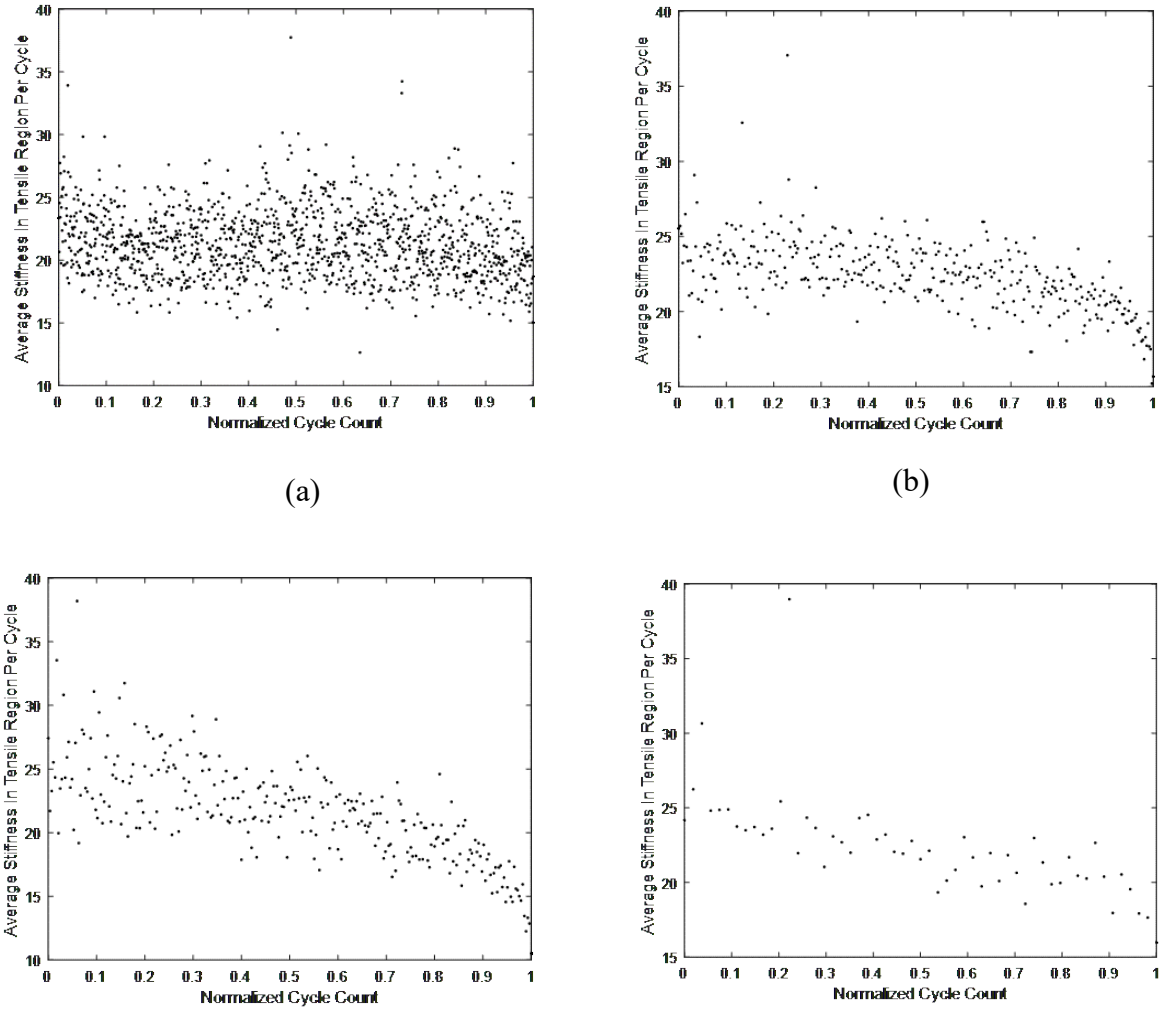

Figure B 5.1 Stiffness degradation of tensile region vs Normalised fatigue cycle test at 0.75 Hz: a) specimen ‘C1-075-02’ b) specimen ‘C1-075-05’ c) specimen ‘C1-075-07’ and d) specimen ‘C1-075-08’.

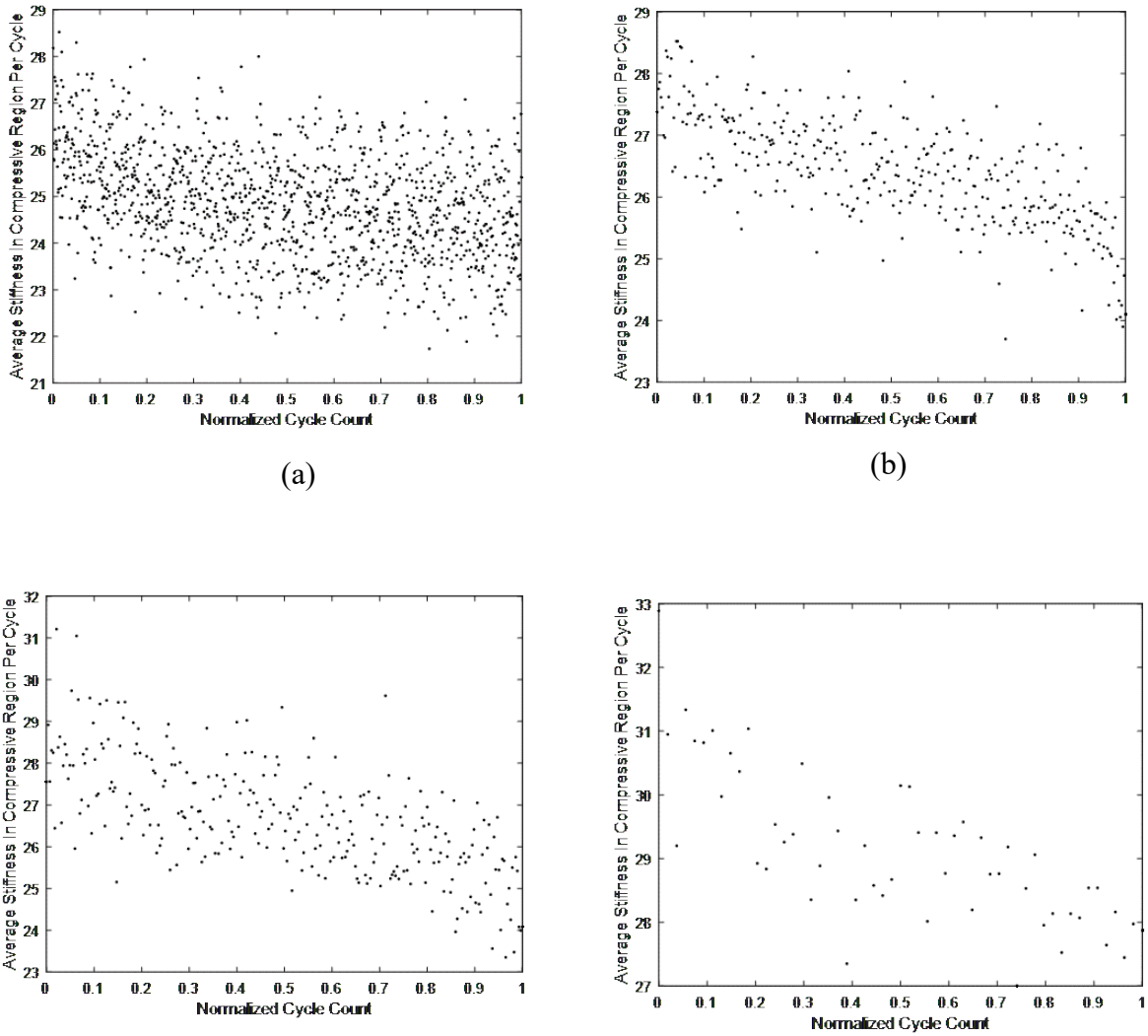

Figure B 5.2 Stiffness degradation compressive region vs Normalised fatigue cycle test at 0.75 Hz: a) specimen ‘C1-075-02’ b) specimen ‘C1-075-05’ c) specimen ‘C1-075-07’ and d) specimen ‘C1-075-08’.

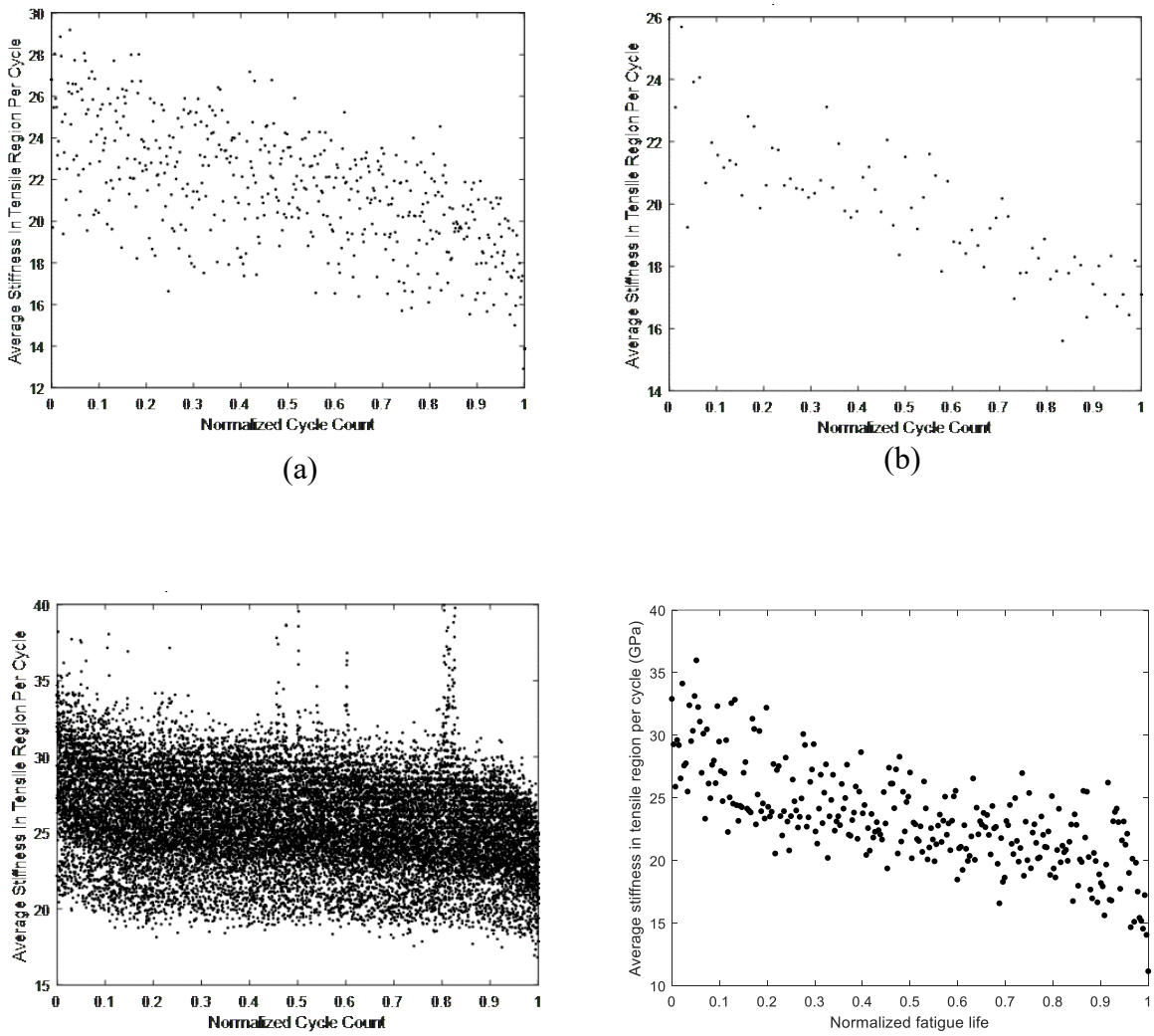

Figure B 6.1 Stiffness degradation of tensile region vs Normalised fatigue cycle test at 0.5 Hz: a) specimen ‘C1-05-04’ b) specimen ‘C1-05-06’ c) specimen ‘C1-05-01’ and d) specimen ‘C2-05-03’.

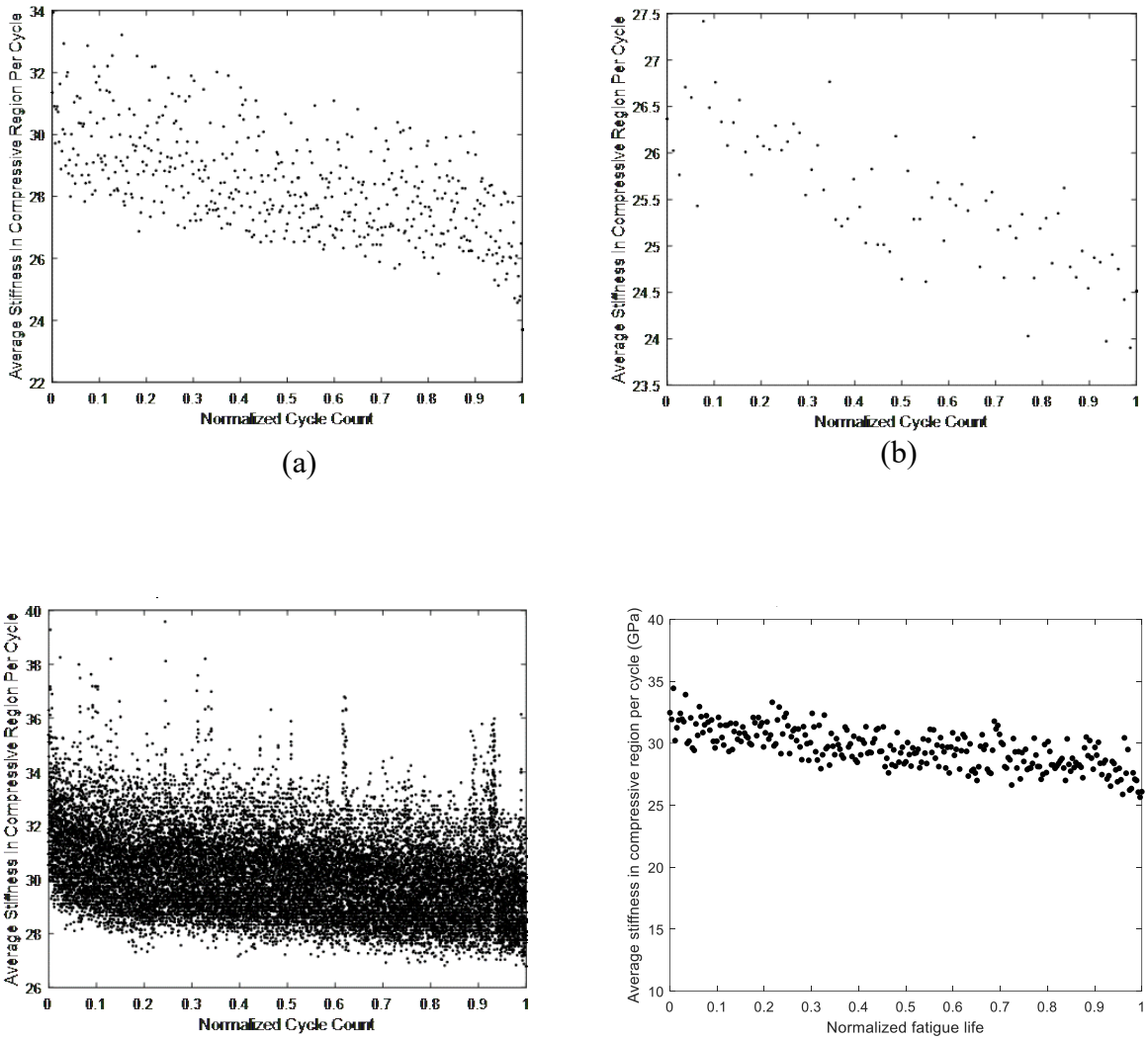

Figure B 6.2 Stiffness degradation of compressive region vs Normalised fatigue cycle test at 0.5 Hz: a) specimen ‘C1-05-04’ b) specimen ‘C1-05-06’ c) specimen ‘C1-05-01’ and d) specimen ‘C2-05-03’.

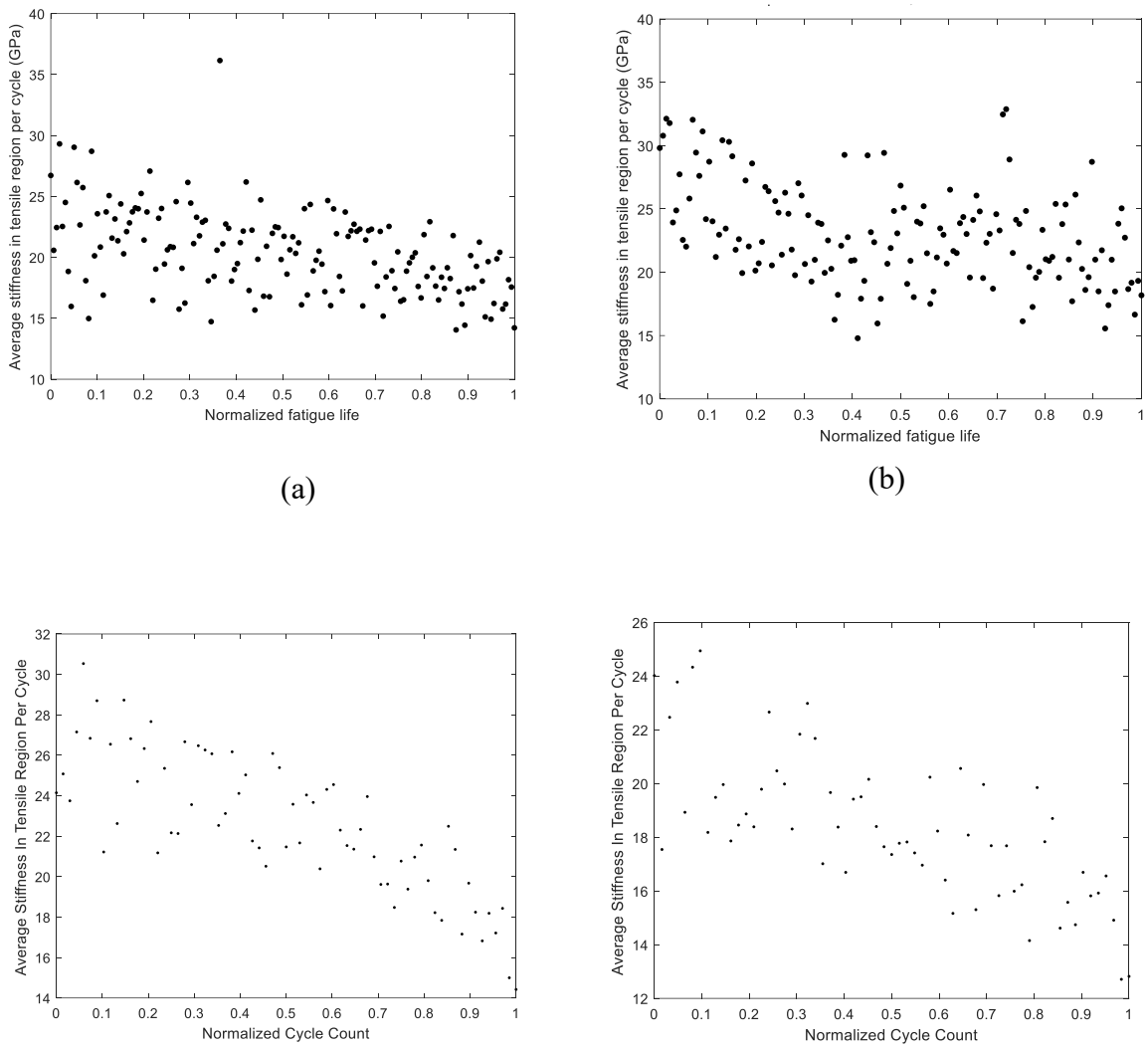

Figure B 7.1 Stiffness degradation tensile region vs Normalised fatigue cycle test at 0.2 Hz: a) specimen ‘C2-02-02’ b) specimen ‘C2-02-04’ c) specimen ‘C1-02-06’ and d) specimen ‘C1-02-07’.

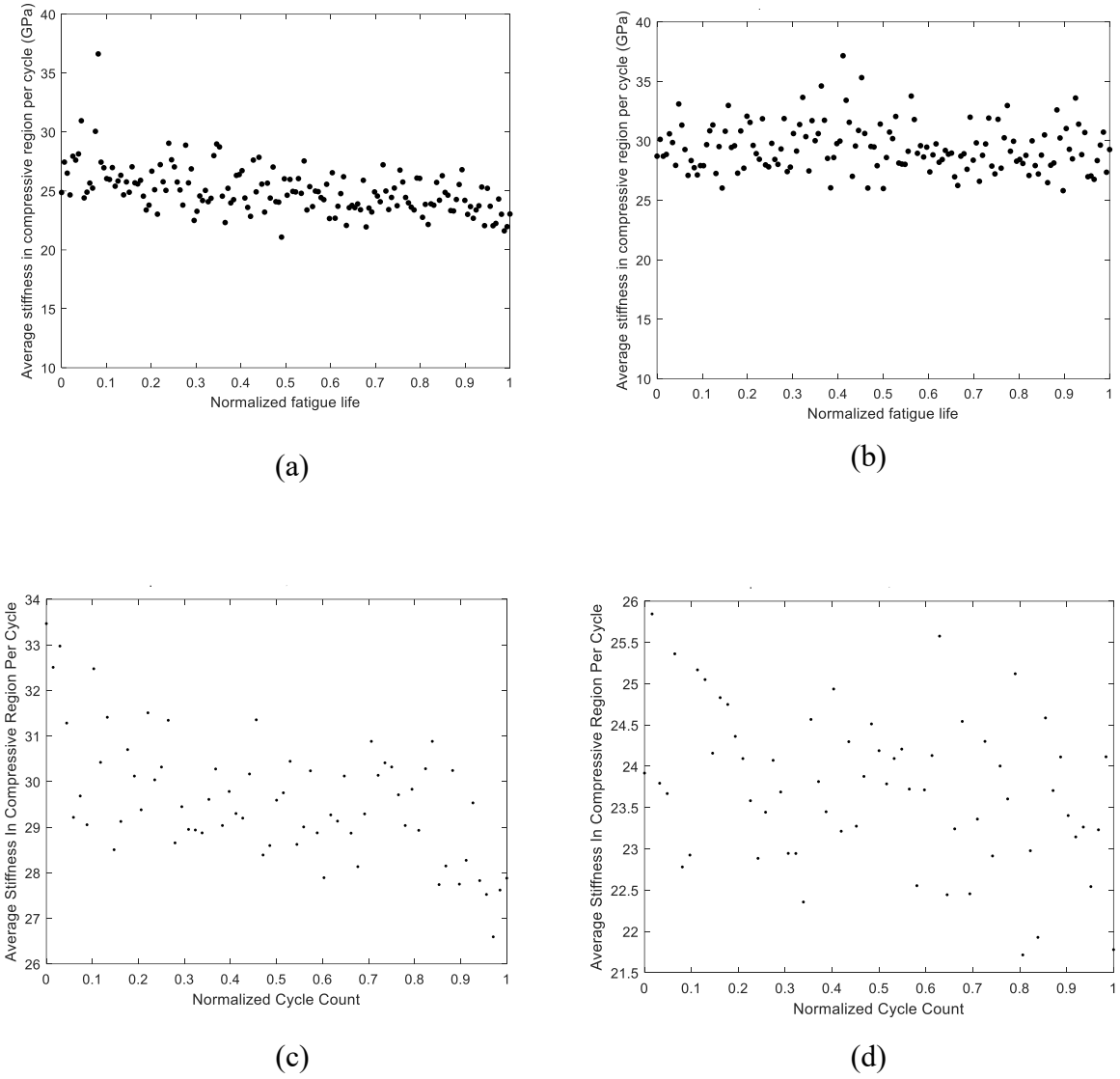

Figure B 7.2 Stiffness degradation compressive region vs Normalised fatigue cycle test at 0.2 Hz: a) specimen ‘C2-02-02’ b) specimen ‘C2-02-04’ c) specimen ‘C1-02-06’ and d) specimen ‘C1-02-07’.